MONASH University

ENSO in a changing climate simulations

Asha Vijayeta

Supervisor: Assoc. Prof. Dietmar Dommenget
Co-supervisor: Dr. Shayne McGregor

A thesis submitted for the degree of
Doctor of Philosophy
At Monash University in June 2020

School of Earth, Atmosphere and Environment
Faculty of Science
Melbourne, Australia

Page left intentionally blank.

Copyright notice

Thesis including published works declaration

I hereby declare that this thesis contains no material which has been accepted for the award of any other degree or diploma at any university or equivalent institution and that, to the best of my knowledge and belief, this thesis contains no material previously published or written by another person, except where due reference is made in the text of the thesis.

This thesis includes 2 original papers published in peer reviewed journals. The core theme of the thesis is studying El Niño Southern Oscillation (ENSO) in a changing climate using the linear recharge oscillator model. The ideas, development and writing up of all the papers in the thesis were the principal responsibility of myself, the student, working within the School of Earth, Atmosphere and Environment under the supervision of Assoc. Prof. Dietmar Dommenget. In the case of *Chapters 2* my contribution to the work involved the following:

Thesis Chapter	**Publication Title**	**Status** *(published, in press, accepted or returned for revision, submitted)*	**Nature and % of student contribution**	**Co-author name(s) Nature and % of Co-author's contribution***	**Co-author(s), Monash student Y/N***
2	*An evaluation of ENSO dynamics in CMIP simulations in the framework of the recharge oscillator model*	*Published*	*Methodology, analysis and writing 70%.*	*Dietmar Dommenget, Methodology and writing 30%*	*No*

The original papers constitutes the majority of Chapter 2. However minor modifications have been made in order to generate a consistent presentation within the thesis.

Student name: Asha Vijayeta

Student signature: **Date:**

I hereby certify that the above declaration correctly reflects the nature and extent of the student's and co-authors' contributions to this work. In instances where I am not the responsible author I have consulted with the responsible author to agree on the respective contributions of the authors.

Main Supervisor name: Assoc. Prof. Dietmar Dommenget

Main Supervisor signature: **Date:**

Abstract

The Coupled Model Intercomparison Project (CMIP) model simulations show widespread uncertainties in El Niño Southern Oscillation (ENSO) statistics and dynamics. In the first chapter, we use the concept of the linear recharge oscillator (ReOsc) to diagnose the ENSO-dynamics in CMIP3 and CMIP5 model simulations. The ReOsc model parameters allow us to quantify Sea Surface Temperature (SST) and thermocline (h) damping, SST coupling to h and vice-versa, sensitivity to wind stress and heat flux forcings and separate atmospheric from oceanic processes. Our results show that the ENSO-dynamics and their diversity within the CMIP ensemble are well represented with the ReOsc model diagnostics. We also illustrate that the ENSO dynamics show more significant biases relative to observations and spread within the models than simple large-scale statistics such as SST standard deviation would suggest. The CMIP models underestimate the atmospheric positive and negative feedbacks, and they have compensating atmospheric and oceanic errors, the thermocline damping is too strong, and stochastic noise forcings in models is too weak. The CMIP5 models only show marginal improvements relative to CMIP3, and our analysis gives directions for improvement.

In the second chapter, we investigate the accuracy of using the 20^0C isotherm (Z20) as an h proxy for ENSO studies instead of the maximum gradient of temperature (maxgrad). Our results indicate that the standard deviation of h is larger when maxgrad is used instead of Z20, which manifests in the SST-h phase relationships with the Z20 estimates being more similar to the theoretical recharge oscillator. Using the ReOsc model, we diagnose ENSO dynamics for both cases and find that Z20 estimates have stronger SST damping, stronger h influence on SST, weaker h damping and weaker SST influence on h in comparison to maxgrad. The differences in the dynamical parameters and the change in the atmospheric and ocean parameter compensation indicate substantial differences in the ENSO dynamics diagnosis representation for the two h estimation techniques.

In the third chapter, we analyze the changes in ENSO dynamics of the CMIP5 simulations for the RCP 8.5 scenario relative to the historical control simulation. ReOsc model is used to focus on changes in the growth rate of T and h anomalies, the coupling between the two, and the noise forcing driving the ENSO variability. We further focused on the feedbacks controlling the growth rate of T, namely the Bjerknes wind to SST feedback, the atmospheric net heat flux, and the residual oceanic feedback. We find significant changes in nearly all of these essential elements of the ENSO dynamics, although the ensemble shows minimal changes in the overall ENSO variability. The growth rate of T weakens resulting from a combination of increased negative atmospheric net heat flux feedbacks, increased positive Bjerknes wind-SST feedback, and increased residual oceanic feedbacks. Further notable changes are an increase in the growth rate of h and a stronger coupling of T to h. Sensitivity analysis can explain why these strong dynamical changes lead to effectively no changes in the overall ENSO variability but are likely to affect the predictability of ENSO.

Acknowledgments

I wish to dedicate this thesis to my late mother, who made innumerable sacrifices for me and always endeavoured to make me independent. I wish you were here Maa, to see me complete this long and arduous journey.

Foremost, I would like to express my deepest gratitude to my supervisor Assoc. Prof. Dietmar Dommenget for the continuous support, motivation, constructive feedback and enthusiastic encouragement throughout the years of my PhD. I am grateful to have benefited from his immense knowledge, no question was ever silly or inconsequential. I am especially grateful for your patience with me, believing I would be able to complete the PhD degree even when I didn't think the same. Every time I struggled and thought of giving up, you went out of your way to motivate me and not let me quit. I will always be grateful for the invaluable assistance that you provided during my study.

I shall forever be indebted to Dr. Jamie Rundle for being the father figure I desired, required and much needed. Thank you for being my support system even when it wasn't your obligation. Many thanks to my second supervisor, Dr. Shayne McGregor for providing his invaluable feedback on my work. Advice provided by my PhD project panel, Prof. Michael Reeder, Prof. Christian Jakob and Prof. Steven Siems, to keep my progress on schedule is greatly appreciated.

My special thanks is extended to my colleague Byju Pookandy, my office mates over the years, Micheal Murphy, Eumni Ahn and Mustafa Adamu for all the lunches, laughs and help with my Matlab codes! I would like to acknowledge the continuous support I received from the Faculty of Science office staff, Yuzhou Lin, Silvana Katragadda and Robert Oakley. This research was funded by the Monash International Postgraduate Research Scholarship (MIPRS), the Monash Graduate Scholar-

ship (MGS), and the Australian Research Council's Centre of Excellence for Climate System Science (ARCCSS).

I am very grateful for all the support from my sister Abha, brother in law Suraj, nephew Aarush, cousin Ashish and aunt Reena. My dear friends back in India - Arshia, Swati, Rajtarangini, Priyambada, Prasad, Ruchi and Himadri – thank you for the warm welcome you extended whenever I visited the place I once called home.

My heartfelt thanks go to my friends here in Australia, Monisha and Parijat for truly being a friend in need. I had sought a friend, you both took on the mantle of being a foster parent! Thank you so much for your warm-hearted support throughout my PhD and my stay in Australia. This thesis would not have been possible without all of you. Lastly, thank you very much Alok for being there for me when I needed it the most. I'll forever be grateful.

In loving memory of Maa

Punya Prava Patel

(19th August 1966 - 3rd August 2019)

Contents

List of Figures

List of Tables

Chapter 1

Introduction

1.1 El Niño Southern Oscillation (ENSO)

The term El Niño refers to the large-scale ocean-atmosphere climate phenomenon linked to a periodic warming in sea-surface temperatures across the central and east-central equatorial Pacific (between approximately the date line and 120°W). El Niño represents the warm phase of the El Niño Southern Oscillation (ENSO) cycle, and is sometimes referred to as a Pacific warm episode. El Niño originally referred to an annual warming of sea-surface temperatures along the west coast of tropical South America. Trenberth and Hoar (1997) reviewed the meaning of the term "El Nino" and how it has changed in time with increasing knowledge of the ENSO phenomenon.

ENSO is important to be studied as recent studies indicate that the occurrence of floods, droughts or climate related disasters may be more predictable in the years of El Niño or La Niña. Past El Niño have caused floods and landslides in Peru and California, droughts in Australia and are known to influence the Indian monsoon (Kumar et al. 1999, 2006). ENSO is known to affect ecosystems especially coral reefs (Glynn and De Weerdt 1991; Aronson et al. 2000), agriculture (Hansen et al. 1998; Adams et al. 1999), tropical cyclones, drought (Dilley and Heyman 1995; Schoennagel et al. 2005; Vicente-Serrano et al. 2011), bushfires, floods and other extreme weather events worldwide (Vincent et al. 2011; Cai et al. 2012). Potential future changes in extreme El Niño occurrences could have profound socio-economic consequences.

Fig. 1.1 illustrates the three tropical pacific ENSO patterns for (a) El Niño events (b) La Niña events and (c) neutral conditions. The neutral conditions are depicted by Fig 1.1(c) and we can see the convection associated with rising branches of the Walker Circulation over the Maritime continent, northern South America, and eastern Africa.

El Niño and La Niña are departures from this neutral conditions where the Walker

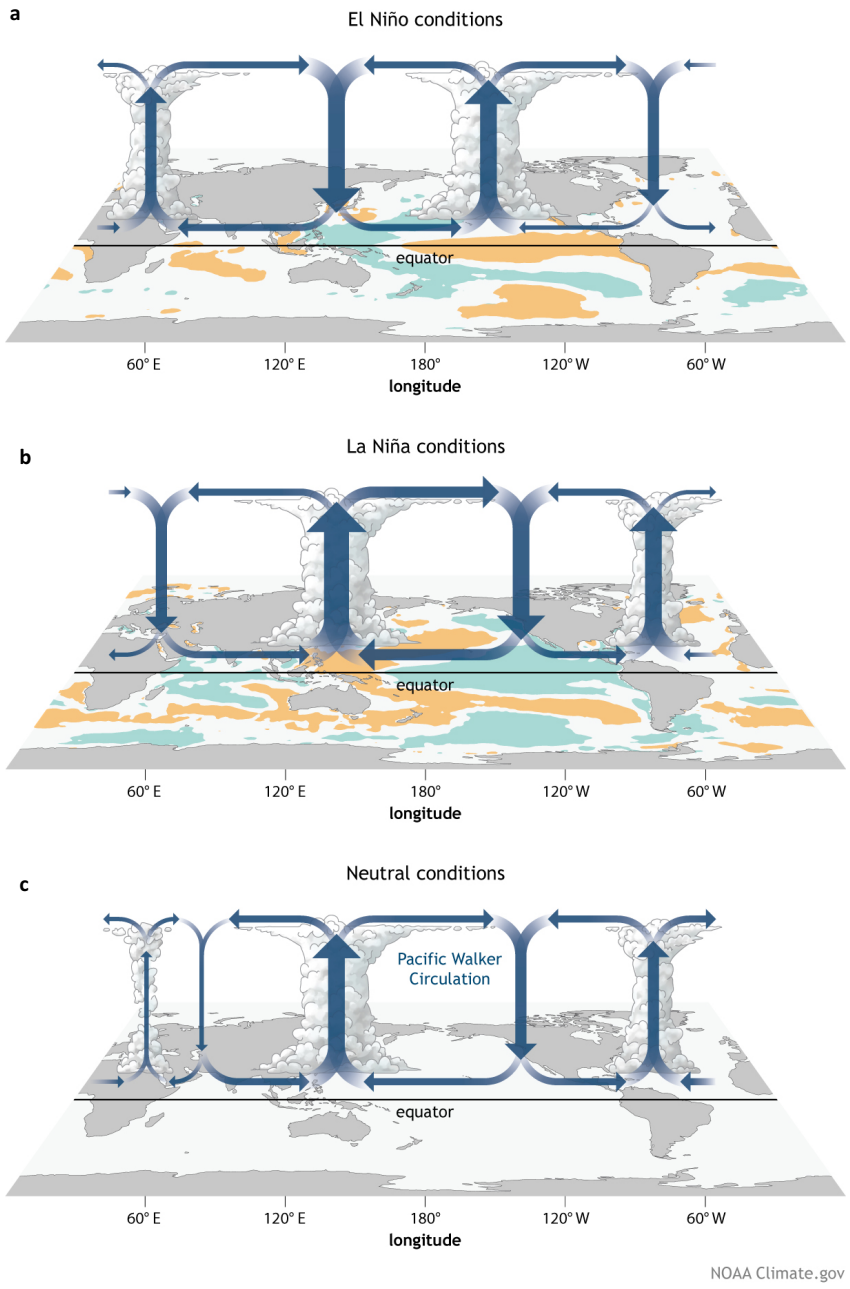

Figure 1.1: Generalized Walker Circulation (December-February) anomaly overlaid on map of average sea surface temperature anomalies during (a) El Niño events, (b) during La Niña events and (c) ENSO-neutral conditions. Illustration sourced from NOAA/Climate.gov, drawing by Fiona Martin.

circulation deviates from neutral conditions. El Niño is characterized by an anomalous warming of the central and eastern equatorial Pacific (Fig. 1.1(a)), which is associated with westerly wind anomalies, an eastward shift of the western Pacific atmospheric deep-convective pattern and a reduced zonal slope of the ocean thermocline along the equator.

During La Niña (Fig. 1.1(c)), central and eastern SST are anomalously low with stronger trade winds and an increased zonal thermocline slope. Bjerknes (1969) discussed the existence of a coupled positive feedback,where an initial eastern equatorial warm sea surface anomaly induces a weakening of the wind field due to a reduced zonal SST gradient. The weakening of the wind field leads to a deepening of the thermocline in the east, which reinforces the initial warm anomaly (vice versa for La Niña).

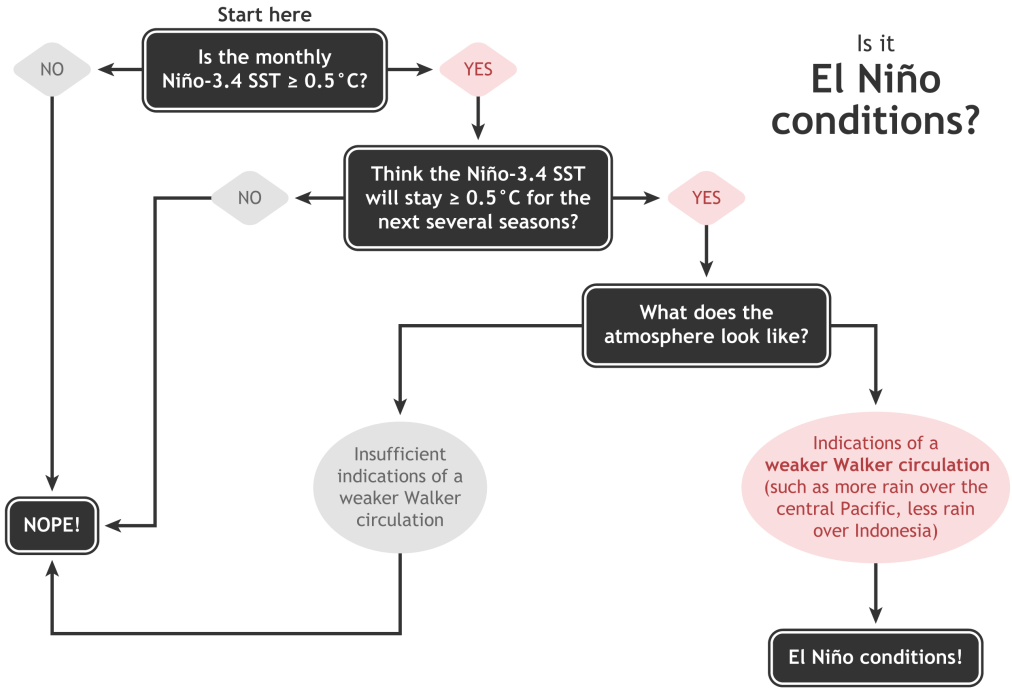

Figure 1.2: Summary of decision process in determining El Niño conditions. Image sourced from NOAA/Climate.gov, illustration by Glen Becker and Fiona Martin.

The decision process usually followed in determining El Niño conditions can be nicely summarized by the decision tree shown in Figure 1.3 sourced from the NOAA Climate.gov

website. NOAA's Climate Prediction Center, which is part of the National Weather Service, declares the onset of an El Niño episode when the 3-month average sea-surface temperature departure exceeds 0.5°C in the east-central equatorial Pacific [between 5°N-5°S and 170°W-120°W].

1.2 ENSO theory and Simple statistical Models for ENSO

Bjerknes (1969) first hypothesized that ENSO is a result of ocean–atmosphere interaction in the tropical Pacific and later Wyrtki (1975, 1985) indicated that the growth and decrease in sea level over the western Pacific Ocean are related to ENSO. The salient cyclic nature of ENSO was later explained by the combined Bjerknes– Wyrtki – Cane– Zebiak hypothesis. This hypothesis emphasized that ENSO is a natural basin-wide tropical Pacific ocean– atmosphere oscillation system and a positive feedback along with subsurface ocean memory of the dynamical system are essential for ENSO. Based on this hypothesis Jin (1997a,b) developed a recharge–discharge oscillator model for ENSO represented by six equations.

The equatorial thermocline depth is one of the main variables for understanding ENSO dynamics, and the upper ocean dynamics can be approximately represented by the following equation,

$$h_E = h_W + \hat{\tau} \tag{1.1}$$

h_W denotes the thermocline depth anomaly in the western Pacific, h_E is the thermocline depth anomaly in the equatorial eastern Pacific; and $\hat{\tau}$ is proportional to the zonally integrated wind stress in this band.

The tropical wind anomaly associated with ENSO is largely over the western to central Pacific , hence the thermocline depth changes averaged over the western equatorial Pacific is approximated as,

$$\frac{dh_W}{dt} = -r(h_W + \alpha\hat{\tau}) \tag{1.2}$$

where r is the collective damping of the upper ocean system through mixing and the equatorial energy loss to the boundary layer currents at the east and west sides of the ocean basin. $\alpha\hat{\tau}$ is the Sverdrup transport across the basin and has a minus sign because a westerly wind stress anomaly will lead to a shallower thermocline over the western Pacific. Equation (1.1) and (1.2) describe the basinwide equatorial oceanic adjustment under anomalous wind stress forcing of low frequencies (Jin 1997a).

The climatological upwelling associated with the climatological trade wind along the equator pumps water into the surface layer which thereby leads to the local thermocline depth to control the SST. This central to east Pacific SST anomaly variations can be approximately depicted as,

$$\frac{dT_E}{dt} = -cT_E + \gamma h_E + \delta_s \tau_E \tag{1.3}$$

where T_E, τ_E are SST and windstress averaged over the central to eastern equatorial Pacific respectively, c is a collective damping rate, γh_E represents the thermocline upwelling process and $\delta_s \tau_E$ is the advective feedback process. γ is the thermocline feedback coeeficient and and $\delta_s$is Ekman pumping feedback coefficient.

The simple approximate relations of the atmospheric response to a warm SST anomaly in the central to eastern Pacific is a local westerly wind response over the same region and

for the east SST anomaly there is an easterly anomaly. These can be represented by the following equations,

$$\hat{\tau} = bT_E, \tau_E = b'T_E \tag{1.4}$$

where b and b' are coupling coefficients.

The two prognostic and two diagnostic equations were presented as an extended recharge oscillator by incorporating the concept of eigen values by (Burgers et al. 2005),

$$\frac{dh_W}{dt} = -r(h_W + \alpha\tau) \tag{1.5}$$

$$\frac{dT_E}{dt} = -\epsilon_1(T_E - \gamma_h h_E) \tag{1.6}$$

$$\tau = bT_E; \tag{1.7}$$

$$\frac{dh_E}{dt} = -\epsilon_2(h_E - h_W - \tau) \tag{1.8}$$

Equation (1.5) elucidates the collective response of the western Pacific to wind stress changes through Kelvin waves, Rossby waves and western boundary reflection. The mismatch between the windstress and thermocline tilt is an important factor for interannual variability according to Neelin et al. (1998). In the context of the above equations the mismatch is caused due to T_E reacting instantaneously to h_E but Kelvin waves takes time to propagate a signal from Central Pacific to the East Pacific.

By making the approximations that h is almost equal to 0.5*($h_E + h_W$) the equations

can be written as,

$$\frac{dT_E}{dt} = a_{11}T_E + a_{12}h \tag{1.9}$$

$$\frac{dh}{dt} = a_{21}T_E + a_{22}h \tag{1.10}$$

the coefficients a_{ij} are estimated by straightforward algebra.

The recharge discharge mechanism can be explained by a schematic diagram, as shown in Fig. 1.3. During the warm phase of ENSO, anomalous westerlies cause an anomalous tilt of the thermocline. The thermocline deepens when SST anomalies are getting too positive in the eastern part of the equatorial Pacific. Westerly wind stress anomaly gets created, the curl of the which is associated with a poleward Sverdrup transport. This divergence of the Sverdrup transport leads to a discharge of equatorial heat content. This phase is the discharge phase of the oscillator.

The divergence of zonally integrated Sverdrup transport eventually results in a discharge of heat content which shallows the entire equatorial Pacific thermocline causes system to move into Phase 2 where eastern Pacific SST leads to a La Niña event. Once SST anomalies are back to normal, the westerly wind stress anomaly disappears. Then, the thermocline becomes more shallow in the eastern part, leading to the appearance of upwelling in the east Pacific. SST anomalies become negative, and easterly wind stress appears. The anomalous cool SST in the eastern Pacific induces anomalous easterlies and causes a recharge of upper ocean heat content due to a convergence of Sverdrup transport. The Sverdrup current is bringing heat content towards the Equatorial region, recharging the system.

The recharge then conditions the system to start a new cycle leading the warm phase of ENSO to the cold phase. The same process but with the opposite sign can lead the cold phase to the warm phase. After that, the system reaches another transition phase, with a deep thermocline due to the previous recharge (Figure 1.3- Phase IV) that would eventually sink in Eastern part leading to a new El Niño phenomenon. Thus, "the recharge–discharge process makes the coupled system oscillate on interannual time scales".

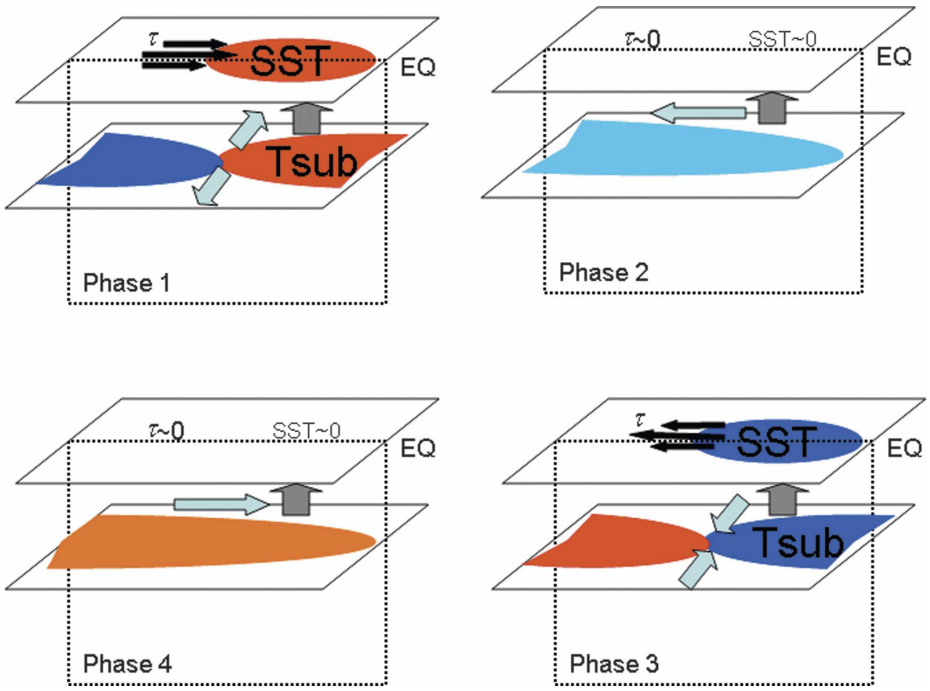

Figure 1.3: Schematic diagram of the recharge–discharge oscillator mechanism for ENSO. Phase 1 is El Niño conditions, Phase 3 is La Niña conditions. Phases 2 and 4 are transition conditions. The red and blue colors indicate the positive and negative SSTAs respectively. The blue thick arrows represent the anomalous Sverdrup transport,black arrows represent the anomalous wind stress, the gray arrows indicate the climatological upwelling across the thermocline.Figure and caption sourced from (Zhang et al. 2007; Meinen and McPhaden 2000)

Although conceptual models provide a computationally efficient way to diagnose ENSO dynamics in complex GCMs, it is also imperative to note their limitations. The non linear nature of ENSO and the expected change in ENSO dynamics due to a warm-

ing future scenario stresses the need for conceptual models to examine and incorporate non-linearities in the model framework. Graham et al. (2015) carried out a reassessment study to highlight deficiencies in linear conceptual models arising from fixed estimated parameters and note that multiplicative noise instead of additive noise is most appropriate. While most of the conceptual models approximate the feedback parameters to be linear, including a non linear atmospheric component to the model leads to improvement in ENSO asymmetry reproduction (Choi et al. 2013).

Applicability of the recharge discharge mechanism to the different types of ENSO was addressed by Ren and Jin (2013) who point out the interference of a strong decadal background signal in case of the Western Pacific ENSO. Eigenmode analysis by Bejarano and Jin (2008) reveals existence of two most important modes quasi-quadrennial (QQ; have periods of around 4 yr) and quasi-biennial (QB; period of 2 years). For QQ mode the phase transition is due to the slow oceanic dynamic adjustment of equatorial heat content, which is consistent with the simple conceptual recharge oscillator. In QB mode the anomalous advection of sea surface temperature by equatorial zonal current anomalies plays a dominant role in phase transition. The simplest recharge oscillator equations may-not encompass all the varied flavours of ENSO.

The thermocline depth (h) is an important variable in the study of ENSO phenomenon and is defined as the depth at which ocean potential temperature gradient is maximum. Most commonly used proxy is the depth of the 20°C isotherm (Z20 henceforth). The accuracy of using the Z20 needs to be investigated as several studies have advocated the use of maximum gradient of temperature instead of Z20 for future ENSO projections and analysis (Zelle et al. 2004; Yang and Wang 2009).

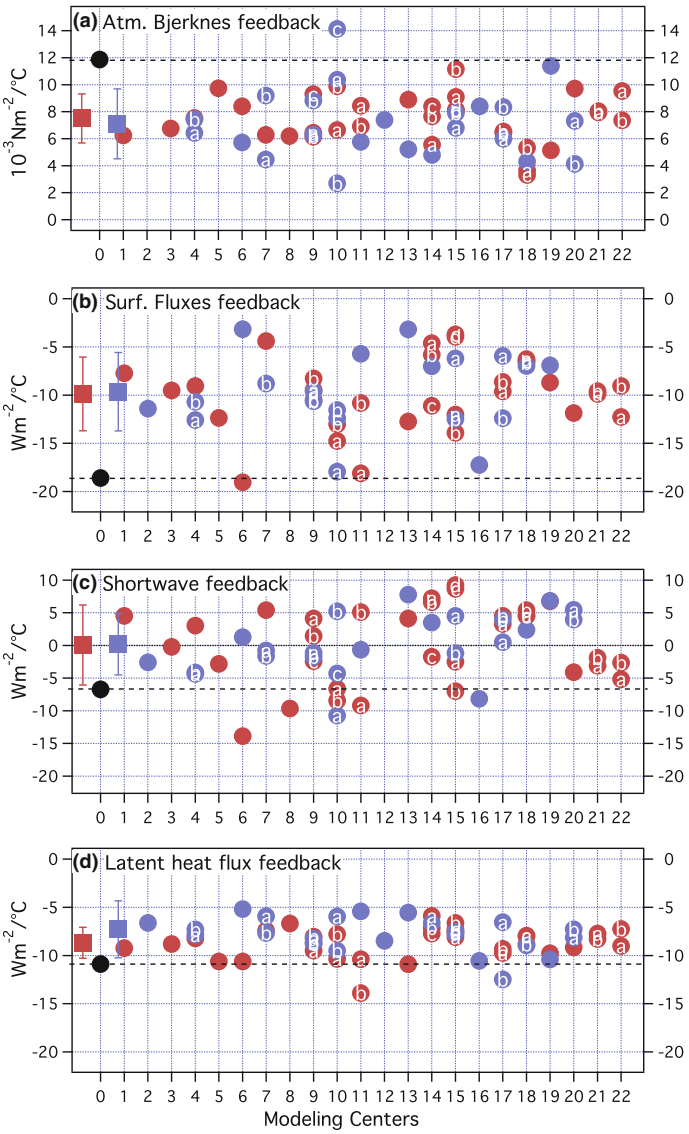

Figure 1.4: Atmosphere feedbacks during ENSO for pre-industrial control simulations–CMIP3 (blue) and CMIP5 (red). (a)Bjerknes feedback(regression of Niño4 wind stress over Niño3 SST(10^{-3} N m^{-2} °C^{-1}); (b) heat flux feedback (regression of total heat flux over SST in Niño3 (W m^{-2} °C^{-1}); (c)Shortwave component of (b); (d) Latent heat flux component of (b). Observations shown as black solid circles and dashed lines, are ERA40 for (a) and OAFlux for (b), (c) and (d). The CMIP3 and CMIP5 multimodel mean are shown as squares on the left of each panel with the whiskers representing the inter-model standard deviation. Figure and caption sourced from Bellenger et al. (2014)

1.3 ENSO in General Circulation Models (GCMs)

Over the last few decades, steady progress has taken place in simulating and predicting ENSO global variability using coupled General Circulation Models (Latif et al. 2001; Davey et al. 2002; Achuta Rao and Sperber 2002). Improvements in Coupled Model Intercomparision Project - Phase 3 (CMIP3) model formulation such as improved parameterized physics and increase in the horizontal and vertical resolutions of atmospheric component models etc. have led to a better spatial representation of the east Pacific SST anomalies (Achuta Rao and Sperber 2006).

Coupled Global Climate Models (CGCMs)are capable of simulating realistic ENSO, albeit with the occurrence of significant biases concerning ENSO characteristics. Systematic errors in simulating both the mean climate and the natural variability persist (Capotondi et al. 2006; Zhang and Jin 2012). Coupled Model Intercomparison Project phase 3 models (CMIP3) underestimate the thermodynamic damping and positive feedbacks, e.g. zonal advective and thermocline feedbacks (Meehl et al. 2007; Kim and Jin 2011; Lloyd et al. 2009). These feedbacks are essential as they are responsible for ENSO variability, and display a large diversity of ENSO amplitude, stability, and teleconnections (Guilyardi 2006; Kim and Jin 2011).

Guilyardi et al. (2009) report that models have difficulty in simulating the correct intensity and spatial structure of the East Pacific cold tongue along the equatorial Pacific (Reichler and Kim 2008), the mean thermocline depth and slope along the equator and the structure of the equatorial currents (Brown and Fedorov 2008). Models fail to correctly simulate the mean zonal equatorial wind stress (Guilyardi 2006; Lin 2007), the meridional extent of the wind variability in the eastern Pacific which is essential for ENSO phase change (Zelle and Dijkstra 2005). The models tend to produce anomalies that extend too far

into the western tropical Pacific, and the simulations typically have diffused thermoclines (Davey et al. 2002). The models also have difficulty in simulating the spatial and temporal structure of the El Niño-La Niña asymmetry (Monahan and Dai, 2004), amplitude and structure of ENSO variability (Davey et al. 2002) and correct phase locking between the annual cycle and ENSO.

The "double Intertropical Convergence Zone (ITCZ)" which is a significant source of model error and is responsible for excessive precipitation over the tropics exists in the models (Lin 2007). Latif et al. (2001) carried out an inter-comparison of an ensemble of twenty-four coupled ocean-atmosphere models in terms of performance of the annual mean state, the seasonal cycle, and the inter-annual variability and almost all models (even those employing flux corrections) showed problems in simulating the SST climatology.

CMIP5 models have shown some improvements over CMIP3 in regards to ENSO simulation. Kim and Jin (2011) suggested that both the heat flux and atmospheric Bjerknes feedbacks contribute to CMIP3 model errors. Bellenger et al. (2014) reviewed ENSO representation in CMIP3 and CMIP5 model and investigated if there has been any progress in the representation of these atmospheric feedbacks in the CMIP5 ensemble. Fig. 1.4 sourced from (Bellenger et al. 2014) shows the atmospheric feedback parameters for CMIP3 and CMIP5 models for the pre-industrial control run. For almost all feedback parameters there is no significant improvement in the model ensemble mean. There is no qualitative change in the multi-model ensemble mean atmospheric Bjerknes feedback (Fig 1.4 (a)). The observed heat flux feedback (Fig. 1.4 (b)), is also underestimated by most CMIP3 and CMIP5 models. CMIP3 and CMIP5 models both poorly reproduce the shortwave feedback (almost zero) as CMIP5 models still struggle to represent convection and cloud processes (Jiang et al. 2012) . There is some improvement in CMIP5 models when comparing the latent heat flux feedback.

Kim and Yu (2012) reported that CMIP5 models simulate more realistically the observed spatial patterns of the two types (or flavours) of ENSO and have a significant reduction of inter-model diversity in their amplitudes of the two types of ENSO. Zhang and Jin (2012) demonstrated a modest improvement in simulating the meridional width of ENSO sea surface temperature (SST) anomaly that generally tends to be narrow, which is attributable to a more realistic simulation of equatorial winds and ENSO periodicity in CMIP5 models.

1.4 ENSO in a greenhouse warming scenario

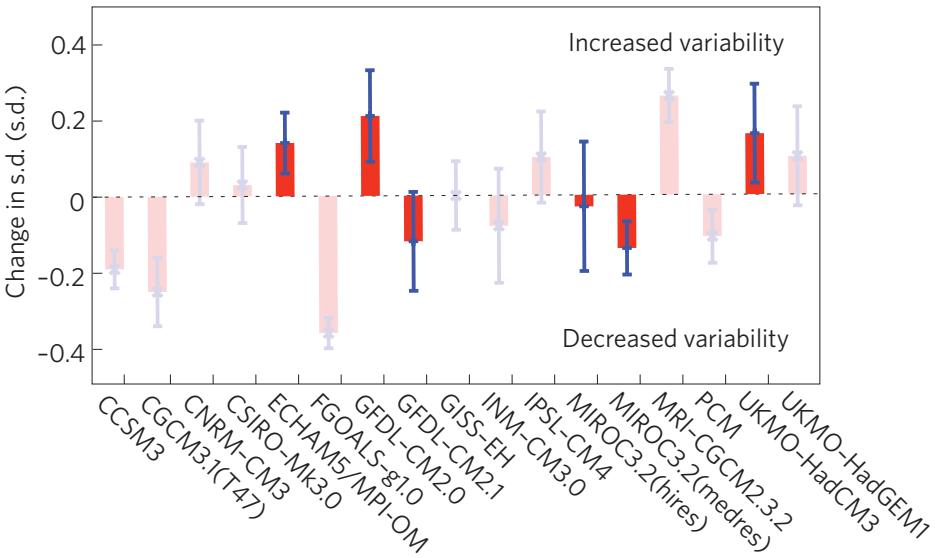

Figure 1.5: Projected changes in ENSO amplitude variability in CMIP3 models as a response to global warming. This figure is sourced from (Collins et al. 2010)

SST and atmospheric pressure instrumental records since the late 19th century allow us to explore changes in some aspects of ENSO (Worley 2005, Smith 2008). For a more extended analysis, paleo-climate data records from oceanic and lake sediments, corals and tree rings have been used to diagnose changes in ENSO many years into the past. NIÑO3 SST records indicate variations in the amplitude and frequency of ENSO and increased

ENSO activity over the past 50–100 years. Vecchi and Wittenberg (2010) used a state-of-the-art global climate model to suggest that ENSO changes similar to those over the past millennium could occur without changes to radiative forcing.

Van Oldenborgh et al. (2005) analyzed the climate model experiments prepared for IPCC AR4 and reported that the amplitude of ENSO variability had large uncertainties and has no statistically significant changes in the future. They estimated very little influence of global warming on ENSO. Collins et al. (2010) report that global warming induced change in the mean climate of the Pacific region, may modify one or more of the physical processes responsible for characteristic amplitude or frequency of ENSO events. Expected changes would be weakening of tropical easterly trade winds, faster warming of ocean surface near the equator and more slowly farther away; shoaling of the equatorial thermocline along with steeper temperature gradients across the thermocline. Change in nonlinear feedbacks like cloud-albedo or thermocline-SST feedback could also lead to different ENSO dynamics. As illustrated in Fig. 1.5 sourced from (Collins et al. 2010), the amplitude of ENSO variability in the future based on CMIP3 models show an increase in some CGCMs, other CGCMs show a decrease, and some show no statistically significant changes.

ENSO amplitude is represented by magnitude of the associated sea surface temperature (SST) variability no consensus on the change in the magnitude of the associated SST variability (Guilyardi 2006; Collins et al. 2010; Stevenson et al. 2012). Kim et al. (2014) attributed this lack of consensus to expectation of unidirectional trend in ENSO amplitude over the entire twenty-first century, and unrealistic model dynamics of tropical Pacific SST variability.

The large uncertainty in the projected change in ENSO amplitude is due to the performance of CGCMs in simulating the feedback processes discussed above and their relative importance varies. Although overall ENSO dynamics are approximately linear (Jin 1997a)

there are non linear aspects which have important implications on ENSO characteristics (An and Jin 2004).

1.5 Research objectives and outline

From the above discussions few major research questions arise that are associated with ENSO in a changing climate. The various questions are as follows:

1. Is the Recharge Oscillator model a good representation of ENSO in CMIP models?
2. Evaluation of ENSO in historical scenario:

   Do the CMIP models exhibit changes in internal dynamics?

   Is there an effect of model biases and model spread on ENSO dynamics?

   Do compensating model parameter errors exist?

   How good are the models in terms of a dynamical skill score?
3. Effect of ENSO thermocline estimation techniques on ENSO

   Is there a difference in the diagnosis of ENSO dynamics representation due to different techniques of estimating thermocline depth.
4. Evaluation of ENSO in climate change scenario:

   Effect of climate change on the ENSO dynamics, statistics and predictability.

This thesis is outlined as follows. Chapter 2 will answer questions 1 and 2 providing proof of concept to illustrate the skill of the linear recharge oscillator model in diagnosing the ENSO behavior in different CMIP model simulations. The chapter will then focus on the characteristics of the CMIP model ensemble utilizing the ReOsc model parameter diagnostics. The ENSO dynamics, ENSO statistical parameters, effect of model biases and

spread on ENSO dynamics, atmospheric and oceanic feedback errors will be investigated and the chapter will be concluded with an inter-comparison of all CMIP models on the basis of a skill score.

Chapter 3 will focus on the third question and evaluate the estimation techniques of thermocline depth anomaly, which is an important variable of ENSO dynamics. We shall investigate the differences in diagnosis of CMIP ENSO dynamics representation in the recharge oscillator model framework when using two definitions of thermocline depth.

Chapter 4 will focus on the fourth question, i.e. ENSO dynamics climate change simulations with respect to historical scenario using the ReOsc model. We will carry out sensitivity analysis to analyze effect of probable ENSO dynamic changes on ENSO variability and predictability.

The thesis is concluded with three short summary sections of the main result chapters and with a section on future work.

Chapter 2

An evaluation of ENSO dynamics in CMIP simulations in the framework of the recharge oscillator model

This thesis chapter originally appeared in the literature as

Vijayeta, A., Dommenget, D. , *An evaluation of ENSO dynamics in CMIP simulations in the framework of the recharge oscillator model. Climate Dynamics, 51(5-6), 1753-1771 (2018). https://doi.org/10.1007/s00382-017-3981-6*

2.1 Introduction

El-Niño Southern Oscillation (ENSO) is the dominant mode of interannual climate variability in the tropical Pacific. ENSO has its origins in the tropical Pacific but it is known to influence the weather all over the world. The dynamics that control ENSO are important for global seasonal climate predictions, but are also important for long-term global climate change. ENSO being a result of complicated dynamical processes encompasses several atmospheric and oceanic feedbacks. The main linear atmospheric feedbacks are the Bjerknes feedbacks (Bjerknes 1969) and the net atmospheric heat flux feedback (Zebiak and Cane 1987). The Bjerknes feedbacks are essentially a positive feedback loop leading to ENSO growth and the net atmospheric heat flux feedback is a negative feedback. Several conceptual models have been proposed which condense the dynamics of ENSO into simple theoretical frame works like the delayed action oscillator (Suarez and Schopf 1988) the recharge oscillator(Jin 1997a,b) and the further simplified recharge oscillator (Burgers et al. 2005). For our analysis, we use the latter and refer to it as the ReOsc model henceforth.

State-of-the-art coupled general circulation models (CGCMs) are capable of simulating the ENSO dynamics albeit with some biases with respect to the observed ENSO characteristics. Latif et al. (2001) carried out an intercomparison of an ensemble of twenty-four CGCMs in terms of performance of the annual mean state, the seasonal cycle and the interannual variability and almost all models (even those employing flux corrections) exhibited problems in simulating the sea surface temperature (SST) climatology. Although our understanding of ENSO has improved over the last decades CGCM simulations of the phase 3 and 5 of the Coupled Model Intercomparison Project (CMIP3 and CMIP5) still have difficulties in simulating the climatology of the tropical Pacific, this includes the correct intensity and spatial structure of the East Pacific cold tongue along the equatorial Pacific(Bellenger et al. 2014; Reichler and Kim 2008), mean thermocline depth and slope

along the equator and the structure of the equatorial currents (Brown and Fedorov 2008), mean zonal equatorial wind stress (Guilyardi 2006) and meridional extent of the wind variability which is important for ENSO phase change (Zelle and Dijkstra 2005).

Because of the scale of ENSO effects on the weather all over the world, changes in dynamics of ENSO in the future is an important scientific question that needs to be answered. Van Oldenborgh et al. (2005) showed no statistically significant changes in amplitude of ENSO variability in the future. Uncertainties in the variability being large, they estimated very little influence of global warming on ENSO. On the other hand, Collins et al. (2010) report that global warming may change mean climate of the Pacific region, which in turn may modify one or more of the physical processes responsible for determining the characteristics of ENSO. Expected changes would be weakening of tropical easterly trade winds, faster warming of ocean surface near the equator and more slowly farther away; shoaling of the equatorial thermocline along with steeper temperature gradients across the thermocline. Change in non-linear feedbacks like cloud-albedo or thermocline-SST feedback could also lead to different ENSO dynamics. However, confidence in these findings is undermined by the diversity in the model projections. Simulations from different CGCMs result into very different future projections of ENSO (Collins et al. 2010). Here again the uncertainty in the GCGM simulation of the ENSO dynamics is a limiting factor. The relative importance of different processes contributing to the ENSO dynamics is different from model to model and different to those observed.

The aim of this study is to evaluate the CGCM simulation of the CMIP 3 and 5 databases in their performance of ENSO dynamics. We will base our analysis on the ReOsc model, which has been used in many studies to analyze ENSO dynamics in different ways (Burgers et al. 2005; Frauen and Dommenget 2010; Jansen et al. 2009; Levine and McPhaden 2015; Yu et al. 2016). The ReOsc model being a simplified representation of ENSO dynamics, allows us to diagnose the dynamical parameters of the ENSO variability

from the statistics of the model simulations or observations. The advantage of this approach in comparison to simple statistical parameters (e.g. SST standard deviation, SST pattern) or heat budget analysis (e.g. the BJ-index from Jin et al. (2006)) is that it defines a dynamical framework with only a small numbers of parameters. The dynamical framework allows us to determine the sensitivity of ENSO statistics to different dynamical parameters. Further, the simplicity of the model allows for a large reduction of complexity in the ENSO dynamics. This approach will help us to get from model evaluations towards direct model developments by linking error in large-scale statistics with dynamical processes that are closer to the processes that are simulated in CGCMs.

This chapter is organized as follows. The data sets, model and methods used are described in Section 2.2. The statistical analysis and test of the ReOsc model skill to represent ENSO dynamics is presented in Section 2.3. The main results of this study are presented in Section 2.4. It addresses the CMIP model ENSO dynamics in terms of ReOsc model parameters along with the effect of CMIP model parameter distributions and biases on ENSO dynamics. Section 2.5 presents a dynamical skill (bias) score of each CMIP model based on the results of the previous sections. The study is concluded with a summary and discussion in Section 2.6.

2.2 Data, models and methods

For observational data we use the 1950–2014 HadISST1.1 data (Rayner et al. 2003) for SST and the 1982–2002 BMRC 20 °C isotherm depths of (Smith 1995) as an estimate for the thermocline depth. Since the BMRC 20 °C isotherm depths record is much shorter than the SST record we restrict our analysis of SST and thermocline depth co-variability to 1982–2002. The 1979–2014 ERA Interim data set is used for estimates of zonal surface wind stress (Dee et al. 2011) and the 1984–2004 OA Flux for estimates of surface heat

fuxes (Yu and Weller 2007).

We analyze model simulations from the CMIP3 and CMIP5 databases (Meehl et al. 2007; Taylor et al. 2012). For the CMIP3 models we use the "20 cm3" simulations and the "historical" scenario for the CMIP5 models for the years 1900–1999. Only one ensemble members have been used from each model. We used all available models that provide all climate variables needed for the following analysis. These are 10 CMIP3 and 29 CMIP5 models; see Table 2.1.

Table 2.1:: CMIP3 and CMIP5 models with the corresponding model numbers

No.	CMIP3 model	No.	CMIP3 model
1	CGCM3.1	6	GISS-ER
2	CGCM3.1.T63	7	IPSL-CM4
3	CNRM-CM3	8	MPI-ECHAM5
4	GFDL-CM2.0	9	MRI-CGCM2.3.2
5	GISS-AOM	10	UKMO-HADCM3
No.	CMIP5 model	No.	CMIP5 model
1	ACCESS1-0	16	GISS-E2-R
2	ACCESS1-3	17	GISS-E2-R-CC
3	CCSM4	18	HadCM3
4	CESM1-BGC	19	HadGEM2-CC
5	CESM1-CAM5	20	HadGEM2-ES
6	CESM1-FASTCHEM	21	IPSL-CM5A-MR
7	CESM1-WACCM	22	IPSL-CM5B-LR
8	CNRM-CM5	23	MPI-ESM-LR
9	CSIRO-Mk3-6-0	24	MPI-ESM-MR
10	CanESM2	25	MRI-ESM1
11	FGOALS-g2	26	NorESM1-M
12	GFDL-ESM2G	27	NorESM1-ME
13	GFDL-ESM2M	28	bcc-csm1-1-m
14	GISS-E2-H	29	CMCC-CM
15	GISS-E2-H-CC		

All analysis is based on monthly mean anomaly time series for thermocline depth averaged over the equatorial Pacific (130°E–80°W, 5°S–5°N) and NINO3 (150°W–90°W, 5°S–5°N) SST index and net heat flux, and central Pacific (160°E – 140°W, 6°S–6°N) zonal surface wind stress. Monthly anomalies are computed by subtracting the mean seasonal cycle for each dataset.

The ReOsc model from (Burgers et al. 2005) is given by two tendency equations of the NINO3 region SST anomalies, T, and equatorial Pacific mean thermocline depth anomalies, h:

$$\frac{dT(t)}{dt} = a_{11}T(t) + a_{12}h(t) + \zeta_T \tag{2.1}$$

$$\frac{dh(t)}{dt} = a_{21}T(t) + a_{22}h(t) + \zeta_h \tag{2.2}$$

The model parameters a_{11} and a_{22} represent the damping (or growth rate) of T and h, and the parameters a_{12} and a_{21} the coupling between T and h. The two equations are forced by stochastic noise terms ζ_T and ζ_h. The parameters of the 2-dimensional model Equation (2.1) and (2.2) are estimated for observations and also for each CMIP model simulation by multivariate linear regressing the monthly mean tendencies of T and h against monthly mean T and h, respectively following the approach in previous studies (Burgers et al. 2005; Frauen and Dommenget 2012; Jansen et al. 2009). The residual of the linear regression fit can be interpreted, as the random noise forcings with the standard deviation (stdv) of the residuals being the stdv of the noise forcings for the T and h equations (ζ_T and ζ_h).

The ReOsc model strongly simplifes the ENSO dynamics and each of the 4 parameters and the two noise forcing terms can be a result of many different physical processes in the atmosphere and oceans. To further untangle the complexity the parameters, a_{11} and a_{21} can be split up into an atmospheric, $a_{11A}$and a_{21A}, and oceanic part, a_{11O} and a_{21O} following the approach of Frauen and Dommenget (2010) and Yu et al. (2016) :

$$a_{11} = a_{11A} + a_{11O} \tag{2.3}$$

$$a_{21} = a_{21A} + a_{21O} \tag{2.4}$$

The atmospheric damping (or growth rate) of T, a_{11A}, is effectively a coupling to wind stress and net heat flux(Frauen and Dommenget 2010):

$$a_{11A} = a_{12}\lambda C_{\tau T} + \frac{C_{fT}}{\gamma} \tag{2.5}$$

The coefficient $C_{\tau T}$ is the linear regression of zonal wind stress, τ_x, in the central Pacific box and NINO3 SST. This essentially represents one of the three Bjerknes feedbacks. C_{fT} is a linear regression between net atmospheric heat flux and SST in the NINO3 region. λ is a positive free coupling parameter and γ the ocean mixed layer depth following the approach of Frauen and Dommenget (2010), which is based on the study of Jin (1997a). The atmospheric part of the coupling of h to T, a_{21A}, can be expressed as:

$$a_{21A} = \frac{a_{22}}{2}\lambda C_{\tau T} \tag{2.6}$$

The oceanic parts of the couplings to T, a_{11O} and a_{21O}, in Equations (2.3) and (2.4) can be estimated as the residuals of a_{11} and a_{21} in Equations (2.3) and (2.4) when a_{11A} and a_{21A} are estimated from Equations (2.5) and (2.6). All parameters values as estimated from observations or calculated are listed in Table 2.2 for an overview. In the analysis part the parameters $C_{\tau T}$, C_{fT}, a_{11O} and a_{21O} will be estimated for the CMIP simulations in the same way as for the observations. To reduce the complexity in the analysis we assumed γ to be the same for all models. The coupling parameter λ is fixed for all analysis, as it was estimated in (Frauen and Dommenget 2010) from running CGCM sensitivity studies. Even though the ocean components are by definition residuals of the feedback parameters after subtracting the atmospheric components, they are a combination of the of thermocline feedback, zonal advection feedback and Eckman pumping feedback. It is beyond the scope of this thesis to formulate the ocean feedbacks individually, there are other methods of

estimating the ocean feedback processses individually namely the BJ index.

It should be noted here that in model simulations the regions of wind-SST or other interactions may be shifted in location (e.g. east–west shift), but be otherwise similar to observations. This would lead to changes in the estimated parameters. We will not discuss such variations due to regional shifts, but leave this to future studies.

The ReOsc model Equations $(2.1)$and (2.2) can be integrated with stochastic noise forcing terms ζ_T and ζ_h to generate stochastic time series of T and h. We therefore integrated the equations with a time step of 24 h and red noise forcing terms ζ_T and ζ_h. The decorrelation time of ζ_T and ζ_h is set to 3 days to mimic weather fluctuations that effectively results into white noise for monthly mean data. Monthly mean stdv of the noise forcings is the stdv as observed or estimated from the CMIP simulations in Equations (2.1) and (2.2) as described above.

Table 2.2:: All model parameters values as estimated from observations or calculated otherwise

a_{11} (T damping/growth rate)	− 0.074 [1/month]
a_{12} (T coupling to h)	0.021 [C/m/month]
a_{22} (h damping/growth rate)	− 0.022 [1/month]
a_{21} (h coupling to T)	− 1.23 [m/C/month]
stdv (ζ_1) (amplitude of T noise)	0.25 [C/month]
stdv (ζ_2) (amplitude of h noise)	2.22 [m/month]
$C_{\tau T}$ (wind-SST feedback)	0.011 [N/m^2/C]
C_{fT} (atmos. heat–SST feedback)	− 16.9 [W/m^2/C]
λ (free coupling parameter)	2100 [m^3/N]
γ (scaled ocean mixed layer depth)	79.0 [C m^2/W/month]

2.3 Proof of concept

Before we apply the ReOsc model to diagnose the ENSO dynamics in the CMIP model simulations we first like to start with a proof of concept. We therefore do a number of different analyses to illustrate the skill of the ReOsc model in diagnosing the ENSO behavior in different model simulations.

We start the analysis by evaluating the observed time series of T and h, see Fig. 2.1a. In addition to the standard deviations of T and h, the power spectrum of T and the laglead correlation between T and h are two important statistical characteristics describing the ENSO behavior; see Fig. 2.1c, d. The observed time evolution of h leads that of T by about 5–6 months (peak of cross-correlation), which is indicative of the ENSO recharge and discharge mechanism, which is the fundament of the ReOsc model.

The stochastic integration of the ReOsc model with the observed parameters (see Table 2.2) shows very similar stochastic behavior. Figure 2.1b shows a 20 years sample from the 1000 years long integration. The statistical properties stdv(T), stdv(h), power spectrum of T and the cross correlation between T and h based on the 1000 years integration of the ReOsc model are all similar to observed. The stdv(h), spectral slope and the cross-correlation are, however, slightly overestimated (Table 2.3). In summary, we conclude that the ReOsc model does replicate the main stochastic characteristic of T and h and their interaction fairly well.

Figure 2.2 shows the power spectrum and cross correlation between T and h for four CMIP5 models. Here we highlighted four CMIP simulations that have fairly different ENSO behaviors. They differ in the shape of the power spectrum, the overall variance and in the cross correlation between T and h. The stochastic integrations of the ReOsc model

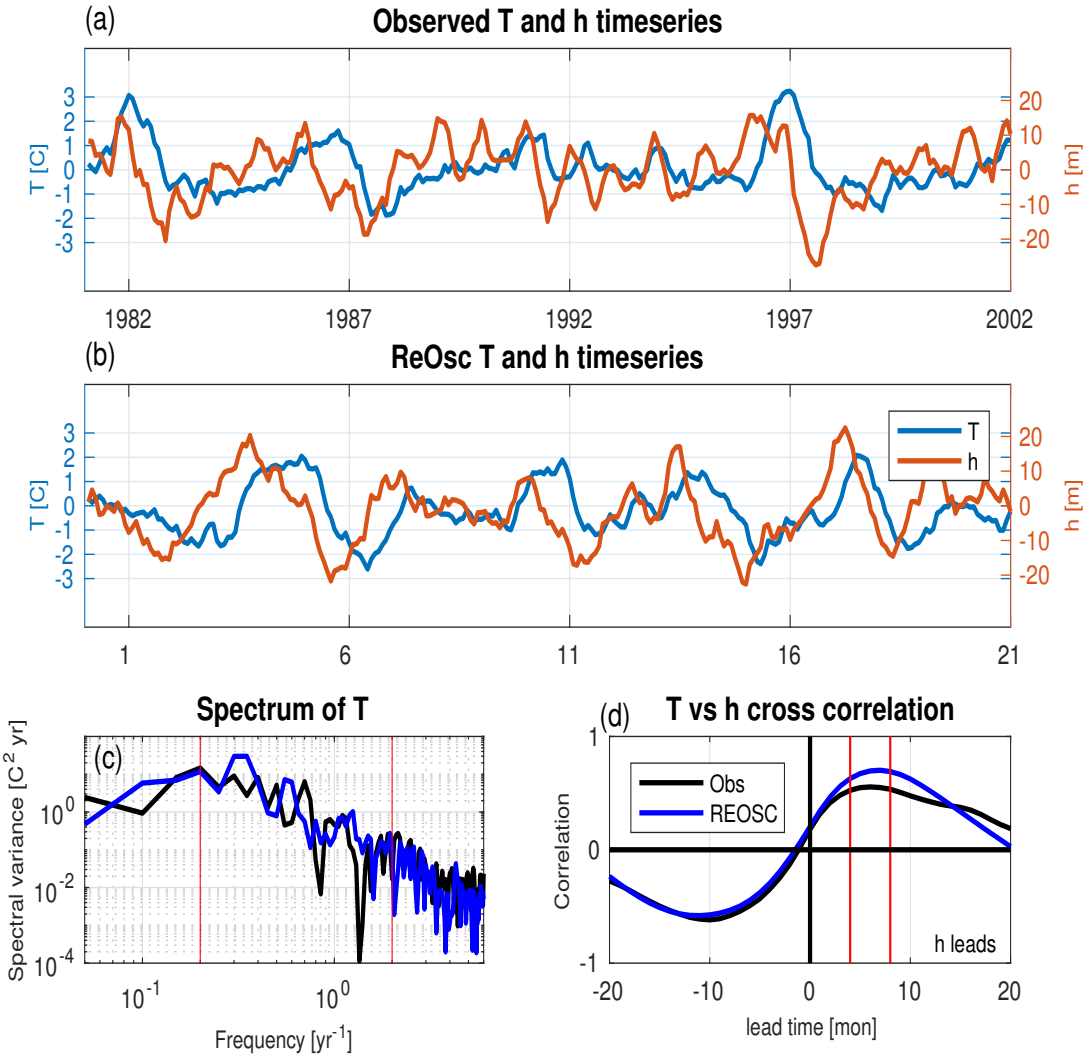

Figure 2.1: (a) Time series of observed NINO3 SST anomaly (T) and mean Equatorial Pacific thermocline depth (h) anomaly. (b) Time series of ReOsc toy model T and h. (c) Power spectra of T. The red vertical lines mark the 5 years and 0.5 years periods, which mark the period range used to estimate the spectral slopes in the analysis sections. (d) Cross correlation between T and h. The solid vertical red lines are the 4 and 8 month lead, which mark the lag range used in the analysis sections.

with the parameter from the four CMIP model simulations (see Sect. 2.2 for details) do replicate the differences in these main statistical characteristics fairly well. For instance, the ReOsc integration mimicking the bcc-csm1-1-m simulation has a much stronger peak

Table 2.3:: Comparison of observational data and REOSC toy model estimates

	stdv of T	stdv of h	Spectral slope	Mean correlation (4–8 months lead)
Observation (1982–2002)	1.0	6.8	– 2.5	0.61
Recharge oscillator toy model	0.99	7.8	– 3.1	0.71

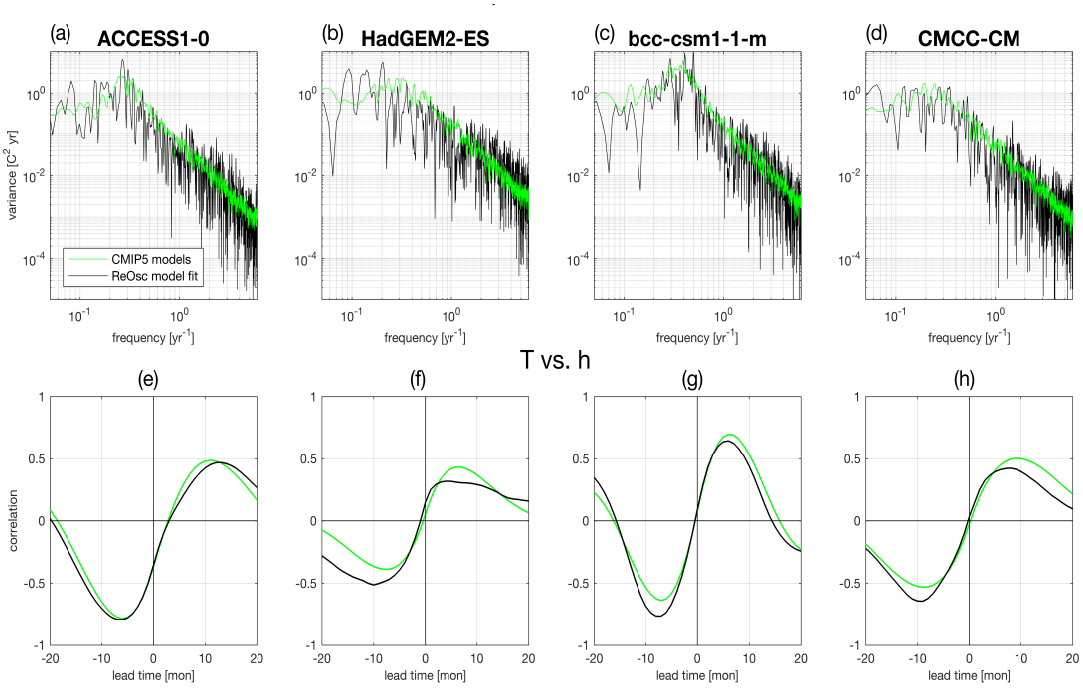

Figure 2.2: Power spectra of T (upper) and cross correlations between T and h (lower) for some example CMIP5 models (black) and the ReOsc model regenerated data (green) for the same model. Positive lead times in the cross-correlations indicate h leading T.

in the power spectrum than the one for the CMCC-CM, replicating the same difference seen in the original CMIP simulations of bcc-csm1-1-m and CMCC-CM. Similarly, the weak cross correlation between T and h in the CMCC-CM simulation is well captured by the ReOsc integration. These preliminary results suggest that the ReOsc model is capable

of capturing the most important characteristics of ENSO behavior in CMIP simulations.

We now compare four main statistical properties [stdv(T), stdv(h), power spectrum slope and cross correlation between T and h] of all CMIP simulations against the ReOsc integration mimicking the CMIP models, see Fig. 2.3. Here we first of all focus on the proof of concept, but we will in the next sections discuss the results further. The ReOsc model is able to replicate the stdv(T) and stdv(h) with very high correlations for both CMIP3 and 5 (see Fig. 2.3). It may, however, be argued that this is not totally unexpected, as we have fitted the model parameters to the T and h tendency Eqs. (2.1),(2.2) for each model. This essentially enforces a close match in stdv(T) and stdv(h) if the ReOsc model has any value in presenting the main dynamics of the CMIP simulations. However, the fact that we closely reproduce the stdv(T) and stdv(h) does suggest that the ReOsc is capturing some essential elements of the ENSO dynamics in the CMIP simulations. It should be pointed out here that this model does not consider seasonal difference in the parameters (all parameters are constants) neither does it consider non-linearities. Thus, to first order these are not essential to understand the main ENSO statistics presented in this study.

The ReOsc model also has some skill in reproducing the variations in the power spectrum. To captures the difference in the power spectrum we estimated the slope (in log-scale) of the power spectrum for each model and observations for periods from 6 months to 5 years (see Fig. 2.3c). This marks the range of the power spectrum in which the variance is strongly increasing with period length (e.g. see Fig. 2.2c). The ReOsc model estimates are closely following the variations in the CMIP models suggesting that the ReOsc model describes much of the large-scale variations in the power spectra shape.

The mean cross correlation between T and h for 4–8 months lag (h leading T) is also fairly well captured by the ReOsc model (Fig. 2.3d). However, the ReOsc model tends to overestimate the cross correlation between T and h, suggesting that T and h are more tightly

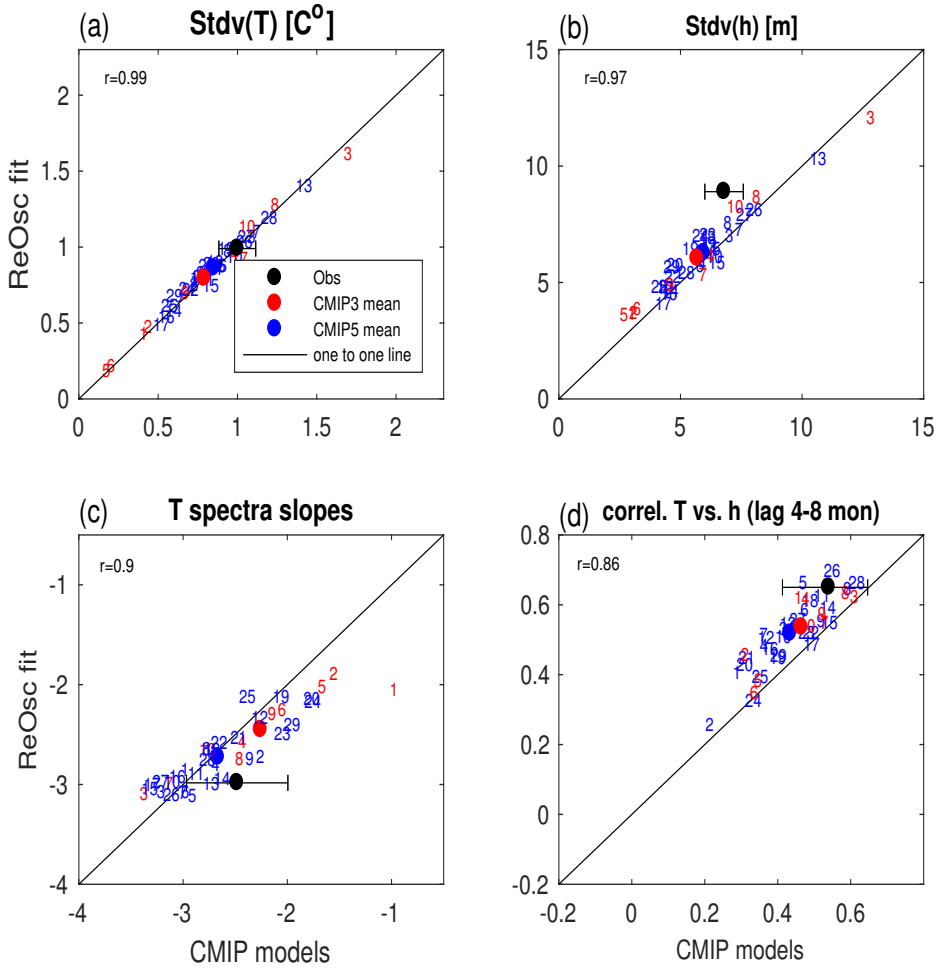

Figure 2.3: Scatter plots of observed (black), CMIP3 (red) and CMIP5 (blue) data on x-axis and ReOsc toy model regenerated data on y axis for (a) Standard deviation of T [°C]; (b) Standard deviation of of h [m]; (c) Spectral slope of T (log-scale) estimated from 5 years to 0.5 years periods [$\log(°C^2)/\log(\text{year}^{-1})$]; (d) mean of the cross correlation between T and h for lags 4 to 8 mon. (h leading T). Observed error bars are the 90% confidence intervals. The r value marks the correlation between the x-axis vs. the y-axis of CMIP data points. Supplemental Table S2.1 lists all model values shown in this figure.

related in the ReOsc model than they are in the CMIP simulations. Given the simplicity of the ReOsc model this is not entirely unexpected.

Another way of testing the ReOsc model is to evaluate the tendencies of T and h. According to the ReOsc model Eqs. (2.1), (2.2) the tendencies of T and h should be

related to T and h themselves [first two terms on the rhs of Eqs. (2.1), (2.2)] and to the noise terms ζ_T and ζ_h. Given the estimated parameters we can evaluate what the correlation between the sum of the two T and h terms in Eqs. (2.1), (2.2) and the tendencies of T and h for all CMIP simulations, see Fig. 2.4a, b. The correlations for the tendencies of T in the ReOsc model are distributed somewhere between 0.2 and 0.8 with a mean of about 0.5. The spread in this distribution reflects the different ReOsc model parameters in the CMIP5 simulations. The distribution is similar for h, but the correlation for the h tendencies tend to be larger, indicating that h is more strongly forced by the two T and h terms than by the noise term [last terms in Eqs. (2.1),(2.2)]. We can estimate what distributions of correlations we should expect from the ReOsc model, by doing Monte Carlo integrations of the ReOsc model with the same CMIP parameters.

We therefore integrated a 1000 years long time series of the ReOsc model for each CMIP model parameter set and computed the correlation values. We did these 100 times for each model. The ReOsc model distributions are very similar to those of the CMIP models, see red lines in Fig. 2.4a and b. Spread, mean values and even more detailed variations in the distributions are similar to those of the CMIP5 simulations, suggesting that the ReOsc model Eqs. ((2.1), (2.2)) does give a good approximation of the T and h tendencies and their relations to T and h themselves.

Finally, we test the noise estimates of the ReOsc model tendencies Eqs. ((2.1), (2.2)). The assumption of the ReOsc model is that the noise forcings ζ_T and ζ_h have a low lag-1 auto correlations. Thus, essentially being white noise. The distribution of the lag-1 auto correlations for ζ_T and ζ_h in the ReOsc model integrations are shown in Fig. 2.4c, d. The distributions have nearly no spread and have a mean of about 0.2, which is close to what is expected for white noise. The estimates of the residual noise for the CMIP5 simulations show a much wider spread and for ζ_h(for h tendencies) the mean of the distribution is higher ($\sim$ 0.4).

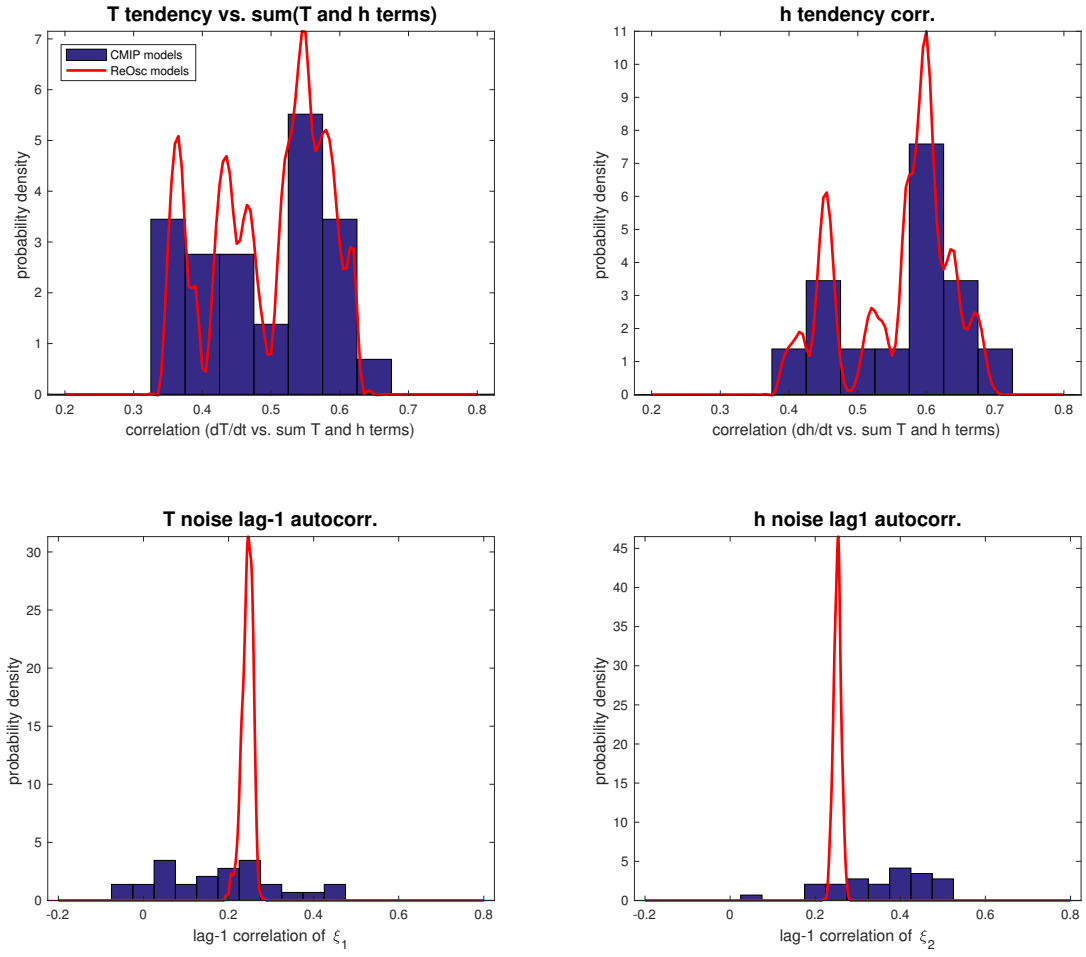

Figure 2.4: Statistics of the T and h tendencies for proof of concept. Probability density of: (a) the correlation between dT/dt and the sum of the T and h term of eqs. (2.1),(2.2); (b) the correlation between dh/dt and the sum of the T and h term of eqs. (2.1),(2.2); (c) the lag-1 auto-correlation of ζ_T, (d) the lag-1 auto-correlation of ζ_h. Blue bars are CMIP model data and the red lines are based on the ReOsc model stochastic integrations using parameter sets from the CMIP models. See text for details.

This indicates that the residual noise forcing estimates in the CMIP model show some deviations from the white noise estimate, in particular for the h tendencies. It illustrates some limitation of the ReOsc model in describing the fully complex CMIP simulations. However, in summary we conclude from this section that the ReOsc model gives a good first order representation of the main ENSO behaviors in the CIMP simulations and that the

ReOsc model parameter estimates therefore are a good diagnostic to describe the ENSO behavior in these model simulations.

2.4 CMIP model ENSO dynamics

After establishing the efficiency of the ReOsc model in replicating the CMIP representation of ENSO, we now focus on the characteristics of the CMIP model simulations ensemble utilizing the ReOsc model parameter diagnostics in combination with other statistical parameters. We start with a comparison of the CMIP models against observations in Sect. 2.4.1. This will be followed by an analysis of the atmospheric and oceanic contributions to the diversity in the dynamics of ENSO in Sect. 2.4.2 and a closer look at the CMIP model ensemble spread in Sect. 2.4.3. This will be followed by an analysis of the sensitivity of the ENSO dynamics to the different model parameters in Sect. 2.4.4, which will be utilized to develop a dynamical bias score for the models in Sect. 2.5 and to summarize the CMIP model parameter spread.

2.4.1 Comparison towards observations

The main statistical properties [stdv(T), stdv(h), spectral slope and lag cross correlation between T and h] of the CMIP3 and CMIP5 ensemble means are fairly close to the observations (Fig. 2.3). The results of Bellenger et al. (2014) for the observed stdv(T) agree fairly well with our findings. The stdv(T), stdv(h) and the cross correlation between T and h for 4–8 months. lag (h leading T) are all on average slightly underestimated by the CMIP3 and CMIP5 ensembles. However, more remarkable are the quite large spreads in the CMIP3 and CMIP5 ensembles in stdv(T) and stdv(h). They are clearly inconsistent with the observed uncertainties. The spread within the models will be discussed in more detail in Sect. 2.4.3.

We now focus on the ReOsc model parameters; see Fig. 2.5. Here we combined the two parameters that influence the T tendency equation in Fig. 2.5a. Both T damping (a_{11}) and coupling to h (a_{12}) are very close to the uncertainties boundary of the observed values for the CMIP3 and CMIP5 ensemble means. However, the spread of these parameters is again larger than expected from statistical uncertainties, suggesting that many CMIP3 and CMIP5 simulations have T damping (a_{11}) and coupling to h (a_{12}) significantly different from that observed.

The parameters influencing the h tendency equation are shown in Fig. 2.5b. The coupling to T is within the observed uncertainties for the CMIP3 and CMIP5 ensemble means suggesting a fairly good agreement of the models with observations in this parameter in average. The h damping (a_{22}) is in most model simulations clearly over estimated (more negative). This has even increased slightly from the CMIP3 to the CMIP5 ensemble (Fig. 2.5b). The strength of the noise forcing estimates for T and h (stdv (ζ_T) and stdv (ζ_h)) are shown in Fig. 2.5c. The mean T noise forcing is very similar to observed, but the strength of the h noise forcing is underestimated in most CMIP3 and CMIP5 simulations. There is also a very large spread within the model ensembles with some models having stronger noise forcings than observed. In particular, the noise forcing of the T tendencies (ζ_T) are much more widely spread within the models than would be expected from statistical uncertainties. Some models have less than half as much stdv(ζ_T) than observed. Here it is interesting to note that despite underestimating the forcing strengths and overestimating the damping of h (a_{22}) the overall variability of T (stdv(T)) is not strongly underestimated, but is in the ensemble mean close to observed.

An alternative way of evaluating the ReOsc model is to look at the relative contribution of the three forcing terms in rhs of Eqs. ((2.1),(2.2)). We estimated the relative contribution of each term by building the mean fraction that each of the three terms contribute to the sum of the absolute values of each term of each monthly mean, see Fig. 2.6. The largest ($\sim 50\%$)

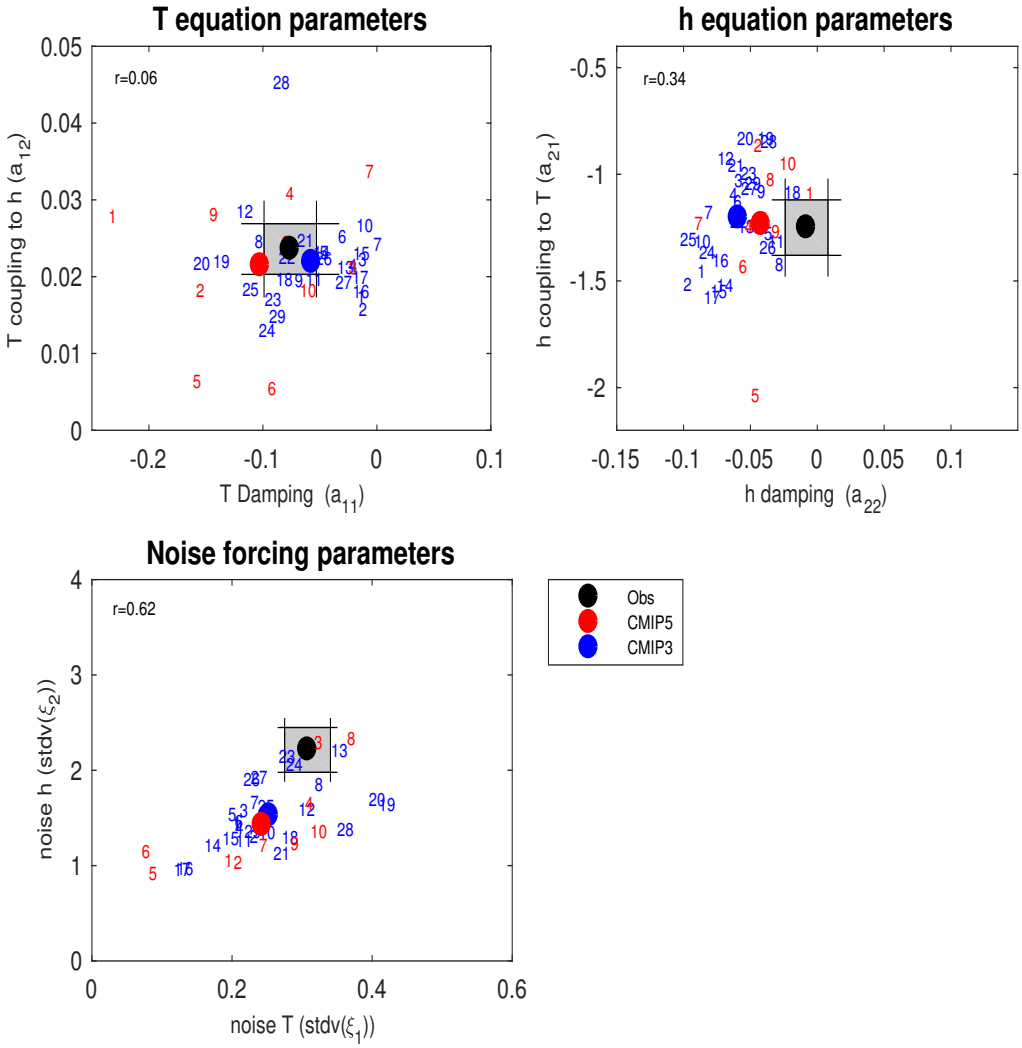

Figure 2.5: Equation (2.1) and (2.2) parameters of the ReOsc model for observed (black), CMIP3 (red) and CMIP5 (blue) models. (a) T damping (a_{11}) vs. T coupling to h (a_{12}); (b) h damping (a_{22}) vs. h coupling to T (a_{21}); (c) noise forcing for T (stdv(ζ_T)) vs. noise forcing h (stdv(ζ_h)). The r value marks the correlation between the x-axis vs. the y-axis of CMIP data points. See models and corresponding numbers in Table 2.1. Supplemental Table S2.2 lists all model values shown in this figure.

contribution to the observed T and h tendencies comes in average from the noise forcings, illustrating that ENSO is a strongly noise driven process. The second largest contribution ($\sim$ 36%) to the observed T tendencies comes from the coupling to h indicating the strong influence of the thermocline variability onto the SST variability. This coupling is even

stronger than the direct effect of T ($\sim 17\%$). Similarly, the tendencies of h are also more strongly forced by the coupling to T ($\sim 36\%$) and less so by h itself ($\sim 7\%$).

The ensemble means of CMIP3 and CMIP5 are very similar to the observed contributions to the T tendencies. However, both ensembles tend to underestimate the relative contribution of the noise forcings to the h tendencies. This is consistent with the above finding that the strength of the h noise forcing (stdv(ζ_h)) was underestimated by the CMIP models and that the h damping was too strong. The relative contribution of h to the tendencies of T is also slightly underestimated.

Individual models show a fairly wide spread in the relative contributions of the different terms to the T and h tendencies. These can in general be linked to the variations in the model parameters (Fig. 2.5).

CMIP5 model 20, for instance, has a strong contribution of T to the tendencies of T (Fig. 2.6a), which is consistent with the strong damping (a_{11}) in this model (Fig. 2.5a). In turn, CMIP5 model 7 with a near zero a_{11} value has almost no contribution of T to the tendencies of T. However, here we have to consider that the relative contributions cannot always be related to the absolute values of the parameters. Low forcing strengths in the CMIP models (Fig. 2.5c), for instance, do not necessarily imply low relative contributions to the tendencies, because the relative contributions of the forcings also result from the integrations with the other parameters of the model. For instance, CMIP5 model 14 does have a relative contribution of the forcings to the T tendency close to those observed, but at the same time it has much weaker noise forcing (stdv(ζ_T); see Fig. 2.5c) and weaker over all T variability (Fig. 2.3a). Biases in the other parameters of the model also contribute to the relative contribution of the forcings.

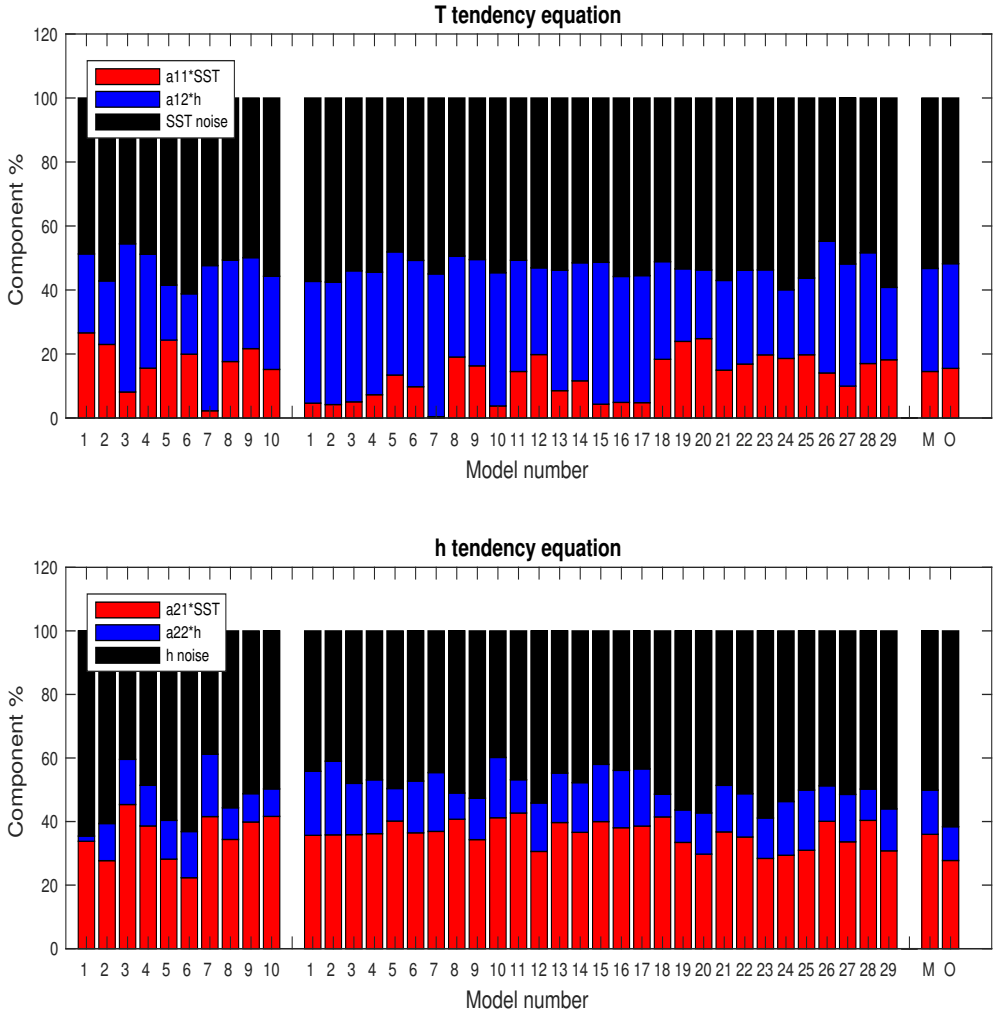

Figure 2.6: Mean percentage contributions of the three rhs terms of Equation (2.1) and (2.2) of the ReOsc model to (a) the monthly mean dT/dt and (b) the monthly mean dh/dt for observations (last bar), CMIP3 (first 10 bars), CMIP5 models (second rows of bars) and all model mean (second last bar).

2.4.2 Contribution from atmospheric and oceanic dynamics

The ReOsc model parameters a_{11} and a_{21} can be split into an atmospheric and a residual oceanic part following the approach of Frauen and Dommenget (2010) (see Sect. 2.2). We will use this approach to get some further separation between atmospheric and oceanic processes.

We start the discussion with the atmospheric processes contributing to the T damping (a_{11A}), which are the wind- SST Bjerknes feedback ($C_{\tau T}$) and the atmospheric net heat flux (C_{fT}), see Fig. 2.7a. The observed $C_{\tau T}$ is positive representing a positive feedback and C_{fT} is negative representing a negative feedback for a_{11} (see Eqs. (2.5),(2.6)). The combined observed atmospheric feedback on T is a positive growth rate a_{11A} (Fig. 2.7b), which is dominated by the positive Bjerknes feedback ($C_{\tau T}$).

The CMIP models ensemble means and indeed almost all model simulations underestimate both Bjerknes ($C_{\tau T}$) and the atmospheric net heat flux (C_{fT}), feedbacks. $C_{\tau T}$ is in ensemble mean only half as strong as observed and similarly C_{fT} is only half as strong as observed. This is qualitatively similar to the finding of Bellenger et al. (2014) and Lloyd et al. (2009). The combined atmospheric growth rate a_{11A} is in the ensemble mean still positive, but weaker than observed and some models have even negative atmospheric growth rates (damping). Even though the two biases in $C_{\tau T}$ and C_{fT} do compensate each other a little bit, as we have a positive and a negative feedback underestimated, they do not compensate each other completely, because the $C_{\tau T}$ term is much stronger for a_{11A} than the C_{fT} term.

The oceanic contribution to the growth rate of T (a_{11O}) is estimated as the residual of a_{11} after considering the atmospheric part (see Eq. (2.3)). The observed oceanic feedback to T is a strong damping (Fig. 2.7b, c) that counter acts the positive atmospheric growth rates leading to the much weaker total damping of a_{11}. Thus, the weak total T damping (a_{11} in Fig. 2.5a) is a result of strong positive atmospheric growth rate and strong oceanic damping. Again, nearly all CMIP5 model simulations underestimate the oceanic damping and the ensemble means are significantly smaller than the observed value. The coupling of h to T (a_{21}) can also be split into an atmospheric and oceanic part (see Eqs. (2.5) and (2.6)). Here the observed a_{21} is dominated by the oceanic part (a_{21O}) with a smaller contribution from the atmospheric part (a_{21A}; Fig. 2.7c, d). This is similar in the CMIP ensembles, but

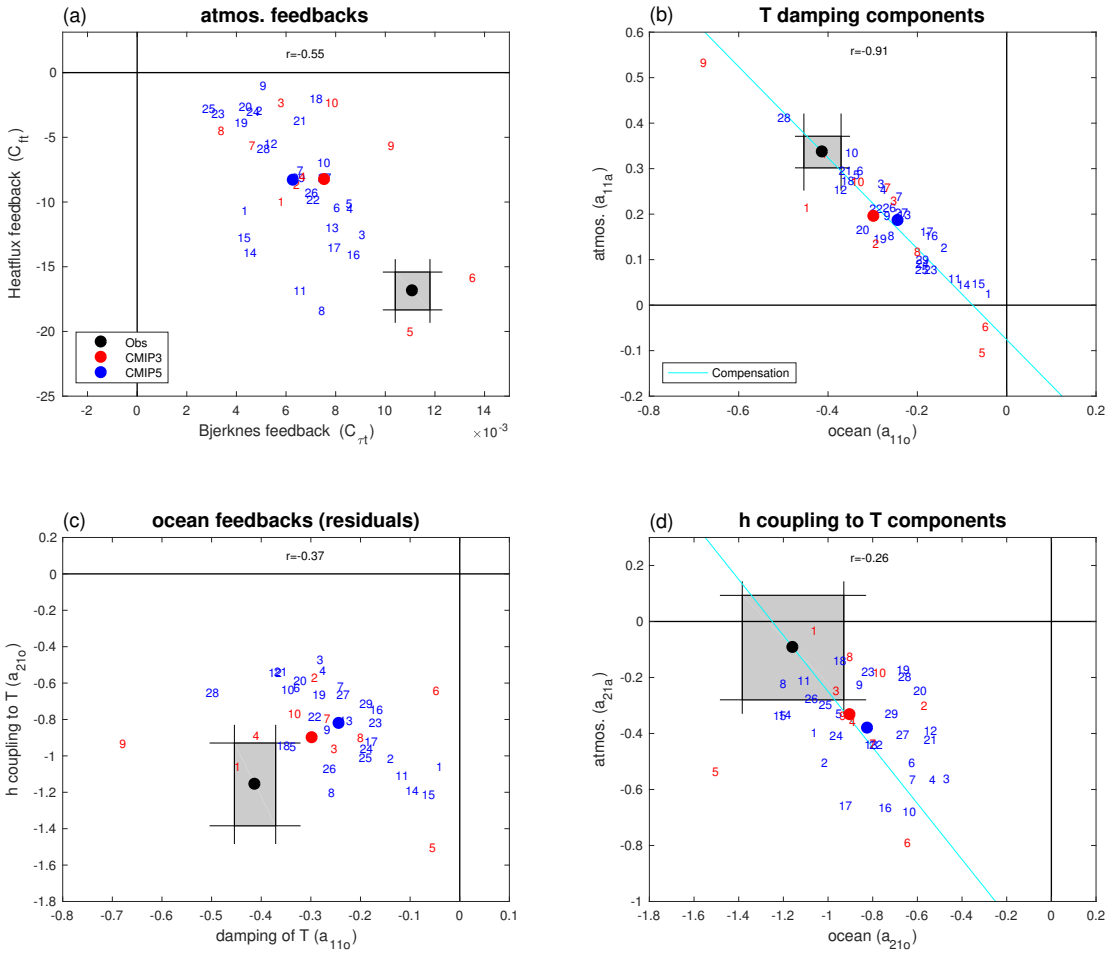

Figure 2.7: Atmospheric and oceanic parameter components for observed (black), CMIP3 (red) and CMIP5 (blue) models. (a) Atmospheric Bjerknes feedback ($C_{\tau T}$) [N/m^2/°C] vs. atmospheric heat flux feedback [W/m^2/°C]; (b) oceanic (a_{11O}) and atmospheric (a_{11A}) components of T damping [1/mon]; (c) oceanic feedbacks of T damping (a_{11O}) [1/month] vs. h coupling to T (a_{21O}) [m/°C/month]; (d) oceanic (a_{21O}) and atmospheric (a_{21A}) components of h coupling to T [m/°C/month]. The cyan line in (b) and (c) marks the compensation line at which atmospheric and oceanic components add up to the observed total values of a_{11} and a_{21}, respectively. The r value marks the correlation between the x-axis vs. the y-axis of CMIP data points. See models and corresponding numbers in Table 2.1.

the models tend to underestimate the oceanic part and overestimate the atmospheric part. The overestimation of a_{21A} results mostly from the too strong h damping (a_{21A}; see Eq. (2.5) and Fig. 2.5b).

2.4.3 Spread within the model ensembles

In addition to how the models compare to the observations we can consider the spread within the model ensemble. If the models are consistent with each other within the statistical uncertainties of the data, then they should have a spread similar to the statistical uncertainties of the observations (Figs. 2.3, 2.5, 2.7). However, the CMIP3 and CMIP5 model ensembles show much larger spreads in all statistics and parameters shown. In particular, the ENSO statistics stdv(T), stdv(h) and the cross-correlation between h and T show large spread. Also, the spread in a_{11}, stdv(ζ_T) and stdv(ζ_h), $C_{\tau T}$, C_{fT}, a_{11A} and a_{11O} are very large. This highlights large diversity in the model simulations with models not only having very different ENSO statistic, but also having very different process parameters, suggesting that the processes controlling ENSO in the different model simulations can be very different from model to model.

The variation in the parameters within the CMIP model ensemble have many interesting cross-correlations. Some of them are shown in Figs. 2.5 and 2.7 and all cross-correlations are listed in Table 2.4. It is beyond this study to discuss all of these cross-relations in the parameters and most of these will be addressed in future further studies. In the following we like to point out a few interesting relations. The ReOsc model parameters (Eq. (2.1), (2.2); a_{11}, a_{12}, a_{22}, a_{21}, stdv(ζ_T) and stdv(ζ_h)) show very little cross correlations within the CMIP ensemble. Only the strength of the noise forcings (stdv(ζ_T) and stdv(ζ_h)) have a stronger positive correlation, suggesting that models that have stronger noise forcing on T also have strong noise forcing on h (see Fig. 2.5c). We can also notice a positive correlation between the strength of the noise forcing on T (stdv(ζ_T)) and the coupling of h to T (a_{21}). A reason for his correlation is unclear to us and would need further future investigations.

If we extend the discussion on all cross-correlation with the atmospheric and oceanic

Table 2.4:: Cross-correlation in the variations of the parameters in CMIP ensembles

Cross correlations in CMIP model parameters

	a_{11}	a_{12}	a_{22}	a_{21}	stdv(ξ_1)	stdv(ξ_2)	a_{11a}	a_{11o}	a_{21a}	a_{21o}	$C_{\tau T}$	C_{fT}
a_{11}		0.06	-0.52	-0.21	-0.18	0.12	0.09	0.33	-0.49	0.14	0.04	-0.07
a_{12}			0.12	0.42	0.47	0.06	0.73	-0.67	0.29	0.23	-0.31	0.22
a_{22}				0.34	0.26	0.08	0.22	-0.42	0.64	-0.11	0.22	-0.03
a_{21}					0.64	0.28	0.48	-0.55	0.44	0.75	-0.31	0.61
stdv(ξ_1)						0.62	0.41	-0.47	0.59	0.26	-0.51	0.61
stdv(ξ_2)							0.04	0.01	0.33	0.05	-0.37	0.36
a_{11a}								-0.91	0.1	0.45	0.1	0.4
a_{11o}									-0.3	-0.37	-0.08	-0.41
a_{21a}										-0.26	-0.57	0.4
a_{21o}											0.09	0.35
$C_{\tau T}$												-0.55

Correlation values with magnitudes < 0.5 are shown in light grey. Values > 0.5 are blue if they are >0.5 in both CMIP3 and CMIP5 ensembles, otherwise they are in dark grey

parameters (a_{11A}, a_{11O}, a_{21A}, a_{21O}, $C_{\tau T}$ and C_{fT},) we see many more significant cross-correlations. The most remarkable cross relation here is that the models tend to underestimate all three elements ($C_{\tau T}$, C_{fT} and a_{11O}) contributing to a_{11} yet the total a_{11} is about the same as observed (Fig. 2.5a). This suggests that the variations of the model simulations relative to the observed atmospheric and oceanic process have strong compensating effects: model simulations that have too strong atmospheric growth rates also have too strong oceanic damping leading to a total T damping close to observed. This is illustrated

in Fig. 2.7b: the models line up closely to the compensation line, which marks the line on which the sum of a_{11A} and a_{11O} adds up to the observed a_{11}. We are not aware of any physical process that could explain this behavior. We will discuss possible implications of this further in the final summary and discussion section.

Some other cross-correlations are quite remarkable too. The atmospheric feedbacks $C_{\tau T}$ and C_{fT}, for instance, are negatively correlated. Thus the variations in these two feedbacks seem to be having compensating effects on a_{11A} (see Eq. (2.5)). Subsequently, variations in a_{11A} are largely unrelated to variations in $C_{\tau T}$ and C_{fT} (Table 2.4) despite a_{11A} being a direct function of both (Eq. (2.4)). Other studies have pointed out a similar relationship between $C_{\tau T}$ and C_{fT}. Bayr et al. (2018) argue that such a negative relationship can result from a shift in the mean state position of the uplifting branch of the walker circulation.

The atmospheric part of the h coupling to T (a_{21A}) is positively correlated to the h damping (a_{22}) as expected from Eq.(2.6). However, the Bjerkness feedback ($C_{\tau T}$) is also expected to be positively correlated following Eq. (2.6), but it has a significant negative cross-correlation. Again, we have no explanation for this unexpected relation.

2.4.4 Sensitivities of ENSO statistics to the ReOsc model biases and spreads

We now focus on the sensitivity of the ENSO statistics to the ReOsc model parameter biases and spreads discussed above. The advantage of using the conceptual framework of the ReOsc model is that we can evaluate the relative importance of different parameters or feedbacks biases by integrating the dynamics ReOsc model and analyzing how the ENSO statistic changes.

We estimate the sensitivity of an ENSO statistic, σ_k, to a parameter, p_i, of the ReOsc

model by integrating the ReOsc model with all other parameters set to the CMIP ensemble mean parameters and perturbing p_i by a small δp_i. The change in the ENSO statistic, $\delta\sigma_k$, relative to the control integration in which all parameters are set to the CMIP ensemble mean parameters gives us an estimate of the sensitivity λ_{ki}:

$$\lambda_{ki} \approx \frac{\delta\sigma_k}{\delta p_i} \tag{2.7}$$

All integrations are done for 500 years using the same white noise forcing. We estimate the sensitivities to $C_{\tau T}$, C_{fT}, a_{11O} and a_{21O} by incorporating them into the ReOsc model Eqs. (2.1),(2.2) replacing a_{11} and a_{21} using Eqs. ((2.3)-(2.6)). By multiplying the sensitivity, estimated with Eq.(2.7), with a difference in a particular parameter, $\triangle p_i$, we can estimate the change in the ENSO statistic $\triangle\sigma_{ki}$:

$$\triangle\sigma_{ki} = \triangle p_i.\lambda_{ki} \tag{2.8}$$

It needs to be noted here that we made a first order linear approximation in this approach. However, the ENSO statistics in the ReOsc model are in general not a linear function of the parameters, but do show some nonlinear behavior (e.g. changing a_{11} = 0.1 by $\triangle a_{11}$ = 0.1 does not have the exact opposite effect of changing it by $\triangle a_{11}$ = +0.1). It also needs to be considered that the sensitivity of the λ_{ki} will in general depend on the values of all other parameters as well.

Figure 2.8a shows the changes in stdv(T) and stdv(h) for the biases of the CMIP ensemble mean (of both CMIP3 and 5) relative to the observed values. First, we can note that the stdv(T) and stdv(h) behave similar: parameter changes that increase the stdv(T) also increase stdv(h). Suggesting that the strength in variability T and h are strongly linked. The largest changes in stdv(T) and stdv(h) result from the biases in the Bjerknes feedback

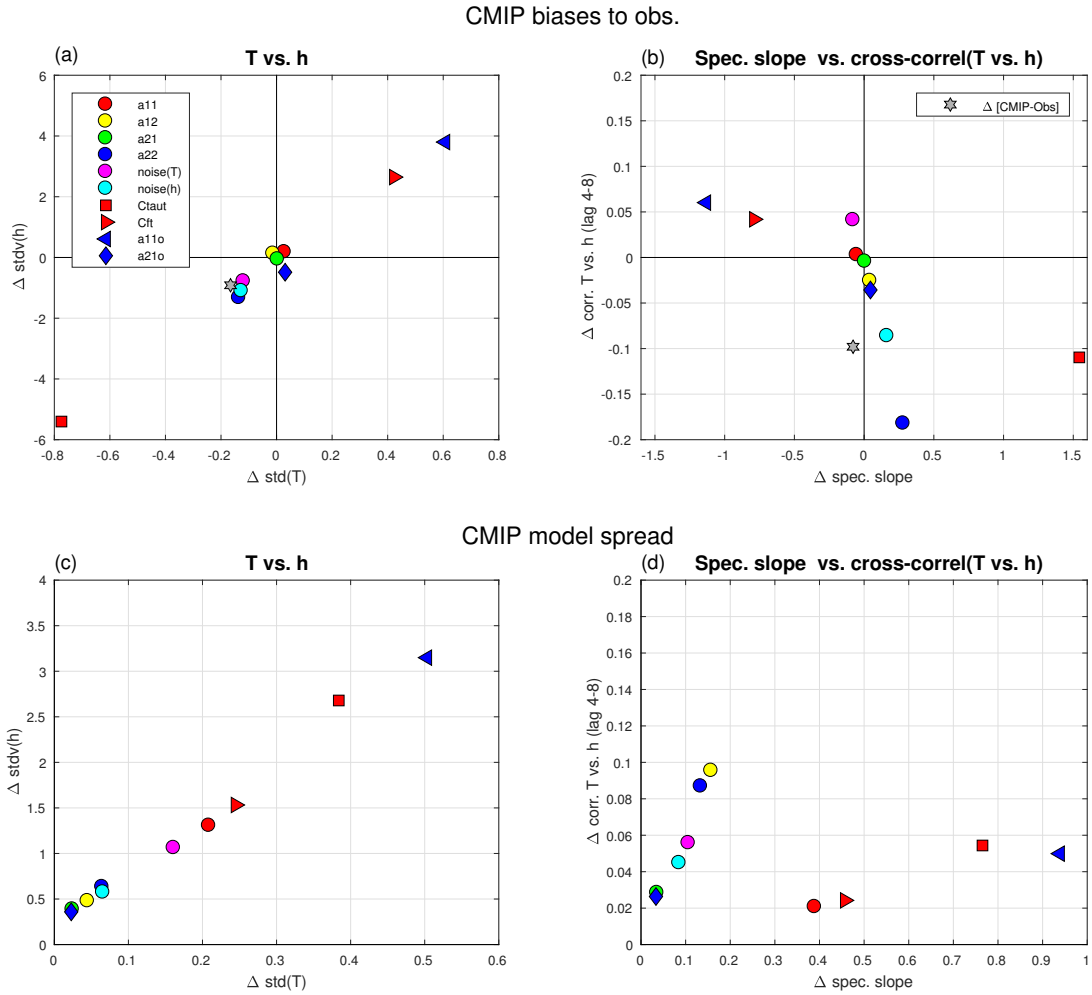

Figure 2.8: Sensitivity of statistical properties to different parameters variations for model biases towards observations using eq. (2.8) (upper) and for the model ensemble internal spread using the absolute values of eq. (2.8) (lower). (a) changes in stdv(T) [°C] and stdv(h) [m] due to biases in the CMIP models relative to the observed; (b) changes in the spectral slope $[\log(°C^2)/\log(year^{-1})]$ and the cross correlation between T and h for lags 4 to 8 mon (h leading T) due to biases in the CMIP models relative to the observed; (c) same as (a) but due to the CMIP model internal spread; (d) same as (b) but due to the CMIP model internal spread. Negative $\triangle$ std(T or h) in (a) and (b) indicate a reduction in the std(T or h) of the ReOsc model. See text for details.

$C_{\tau T}$, the residual oceanic T damping a_{11O} and the atmospheric net heat flux C_{fT}. This reflects that all three have relatively large biases to the observed values (Fig. 2.7a, b) combined with a relatively large sensitivity of the ENSO statistics in the ReOsc model to these

parameters. In turn, the total T damping a_{11} has only a small sensitivity, although it has the same sensitivity (λ_{ki}) as a_{11O}. However, the bias to observed in a_{11} (Fig. 2.5a) is much smaller than in a_{11O} (Fig. 2.7b).

The much too weak $C_{\tau T}$ in the CMIP models would result into a much weaker stdv(T) and stdv(h), and the too weak a_{11O} would result into a stronger stdv(T) and stdv(h). The strongly opposing effects combine (Eqs. (2.3),(2.5)) into the total T damping a_{11}, which has very little bias to observations and therefore has very little effect on stdv(T) and stdv(h). The biases in the strength of the noise forcings and the h damping a_{22} also have some significant influence on stdv(T) and stdv(h), whereas the biases in a_{12}, a_{21} and a_{21O} have very little influence.

The effects of the parameters on the power spectrum slope and the cross-correlation between h and T, (r_{Th}), are shown in Fig. 2.8b. The spectral slope changes are remarkably similar to the changes in stdv(T), but with reversed sign: parameters that increase the spectral slope (thus becoming less negative; see Fig. 2.3c) decrease the stdv(T) (compare with Fig. 2.8a). This suggests that models with stronger SST variability also have a stronger increase in SST variance with increasing periods (more negative spectral slope) and thus have a more pronounce interannual variability. There is indeed a negative correlation of -0.6 between the std(T) and the spectral slopes in the CMIP ensemble (compare Fig. 2.3a, c).

The cross-correlation r_{Th} is most strongly affect by the biases in the h damping (a_{22}), h forcing strength (stdv(ζ_h)) and $C_{\tau T}$. Most other parameters have little effect on r_{Th}. There is a weak indication that changes in the parameters that lead to a stronger r_{Th} also lead to more negative spectral slope. This suggests that models with stronger delayed coupling between h and T have a stronger increase in SST variance with increasing periods (more negative spectral slope) and thus have a more pronounced interannual variability.

The CMIP models have fairly large spread within the ensemble in nearly all parameters. We estimate the sensitivity of the statistics to these parameter variations by using absolute values of Eq. (2.8) (neglecting the signs) with $\triangle p_i$ being the stdv of the parameters within the CMIP ensemble, see Fig. 2.8c, d. The largest changes in statistics of stdv(T) and stdv(h) again result from the spread in $C_{\tau T}$, a_{11O} and C_{fT}. However, the spread in a_{11} and stdv(ζ_T) are now more important than in the bias towards observations. This is due to the fact that a_{11} had little bias towards observations, but have fairly large spread within the CMIP models (see Fig. 2.5a).

The spectral slope again behaves similarly to the stdv(T) with the noticeable difference that the T coupling to h (a_{12}) has stronger influence on the spectral slope than it does on the stdv(T). The T coupling to h (a_{12}) also has the most strongly influence on the cross-correlation r_{Th}. The damping of h (a_{22}) has a similarly strong influence, but most other parameters have weaker effects on r_{Th}.

2.5 Bias score of CMIP models

We can summarize the CMIP model biases relative to the observed ENSO ReOsc model parameters by combining all parameter biases into a normalized bias score, $S\sigma_{ki}$:

$$S\sigma_{ki} = \frac{1}{\sigma_k(obs)} \sqrt{\frac{1}{8}\sum_{n=1}^{8} (\triangle p_n^i . \lambda_{kn})^2} \tag{2.9}$$

with $S\sigma_{ki}$ the bias score for the ENSO statistic σ_k for the model with index i, the model bias in the parameter p_n relative to observed,$\triangle p_n^i$, and the observed ENSO statistic, $\sigma_k(obs)$. This bias score is effectively a root mean square error (RMSE) in the eight model parameters (a_{12}, a_{22}, stdv(ζ_T), stdv(ζ_h), $C_{\tau T}$, C_{fT}, a_{11O} and a_{21O}) scaled by the sensitivity of the ENSO statistics to these parameters (λ_{kn}) in the ReOsc model and normalized by the

absolute value of the observed ENSO statistic, $\sigma_k(obs)$.It thus provides a dynamics- based bias score of ENSO. The higher the bias score the more the model dynamics deviate from the observed dynamics, hence the ideal model should have a bias score close to or within the observed uncertainties.

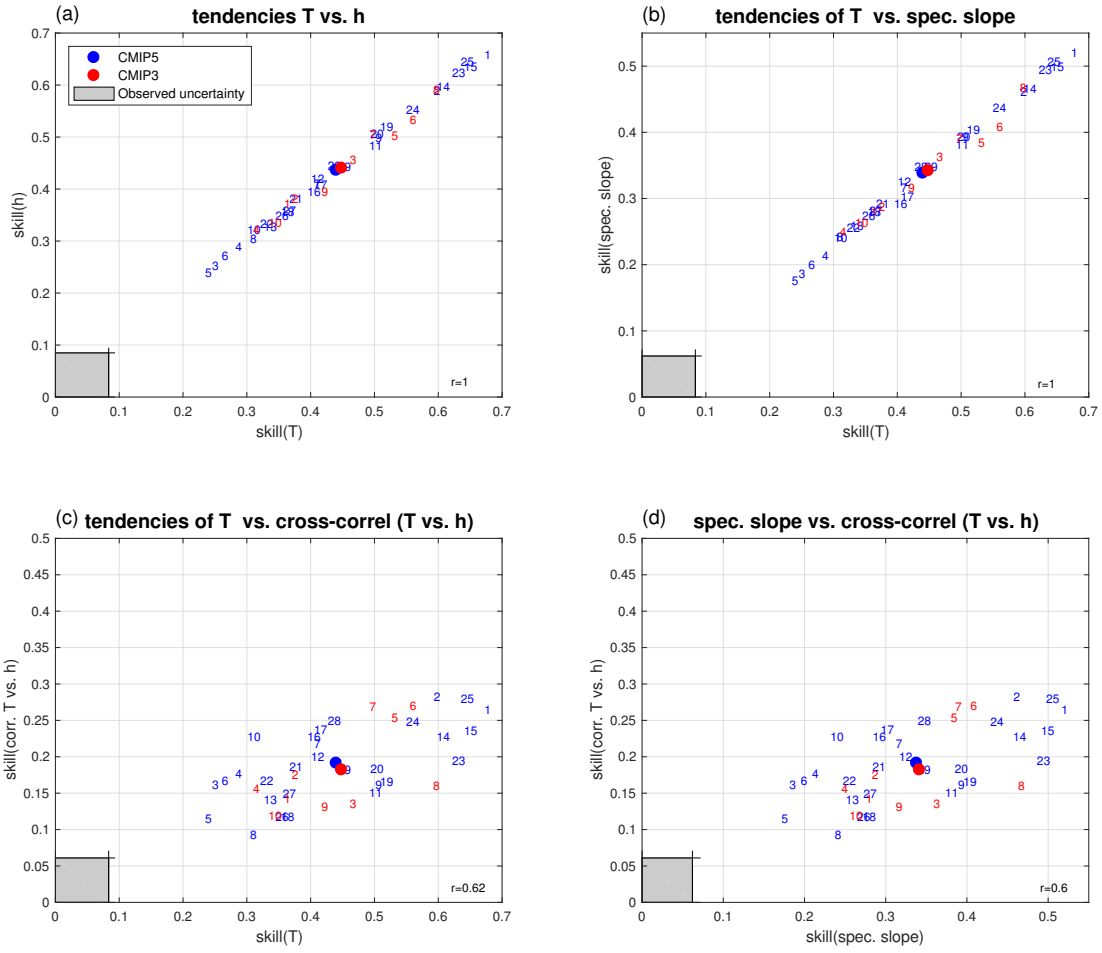

Figure 2.9: Dynamical skill scores of CMIP model for different statistical properties. Skill scores for (a) stdv(T) [°C] vs. stdv(h) [m]; (b) stdv(T) [°C] vs. spectral slope $[\log(°C^2)/\log(year^{-1})]$; (c) stdv(T) [°C] vs. cross correlation between T and h for lags 4 to 8 mon (h leading T); (d) spectral slope $[\log(°C^2)/\log(year^{-1})]$ vs. cross correlation between T and h for lags 4 to 8 mon (h leading T). The r value marks the correlation between the x-axis vs. the y-axis of CMIP data points. See text for details. See models and corresponding numbers in Table 2.1. Supplemental Table S2.3 lists all model values shown in this figure.

Figure 2.9 shows the bias scores for all CMIP models for the ENSO statistics stdv(T), stdv(h), spectral slope and the mean cross-correlation between h and T at lags 4–8 months (r_{Th}). In addition, we show an estimate of the observed uncertainties by replacing $\triangle p_n^i$ in Eq.(2.9) with the 90% uncertainty values of the observed parameters as shown in Figs. 2.5 and 2.7.

There are a number of interesting aspects in the bias score results. Starting with the bias scores in stdv(T) and stdv(h) (Fig. 2.9a) we can first of all notice that all models are relatively far away from the observed uncertainty estimate. Much more than they are from any of the individual parameters (see. Figs. 2.5, 2.7). This is due to the role of compensating errors. In the definition of the bias score (Eq. (2.9)) we have implicitly assumed that the biases are independent. However, some of the parameters with the strongest sensitivities have very strongly compensating biases (see $C_{\tau T}$, C_{fT} and a_{11O} Fig. 2.7a, b). While these compensating errors lead to relatively small biases in the ENSO statistics, they do not lead to small bias values in Eq. (2.9). Thus, the main reason why the models are far away from good bias values is the dominance of compensating errors. This is in particular captured by the bias in a_{11A}, which combines $C_{\tau T}$ and C_{fT}, and by the bias in a_{11O} (Fig. 2.7b). Models that perform well in these have in general small bias scores and vice versa.

Further we can notice that the bias scores in stdv(T) and stdv(h) are nearly identical. Models that perform well in stdv(T) also perform well in stdv(h). This first of all reflects that the correlation between stdv(T) and stdv(h) in the CMIP ensemble is fairly high (r = 0.9). Thus, the strength of the SST variability in the CMIP model simulations is strongly linked to the strength of the thermocline variability. The tight relation in the bias scores also indicates that the sensitivities, λ_{ki}, in the ReOsc model for stdv(T) and stdv(h) are very strongly linked to each other. A parameter change that leads to a change in stdv(T) also leads to an equivalent change in stdv(h).

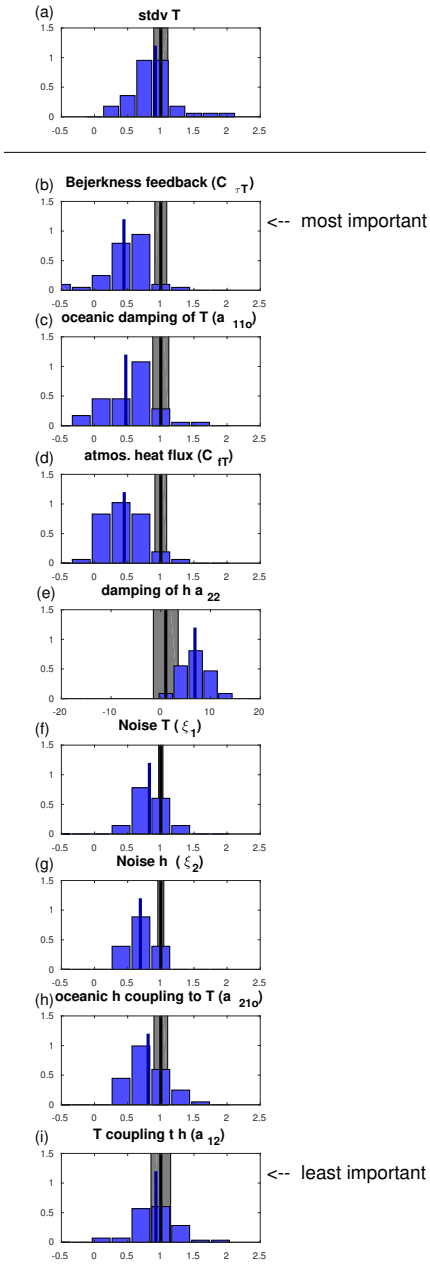

Figure 2.10: Summary of CMIP model parameter biases and spread. Observed values and spread (90% interval) are marked by the black line and grey shaded area. The combined distributions of CMIP3 and CMIP5 models are shown as blue bars with the blue line marking the mean of the distributions. The parameters are sorted by how strongly the CMIP model's parameter biases influence the stdv(T) as shown in Fig. 2.8a. The most influential is the uppermost.

The bias scores of stdv(T) and stdv(h) are also relatively wide spread out with a clear separation between the models. Again, this is much stronger than in any of the individual parameters (see Figs. 2.5, 2.7). It is indicating that the dynamical skills of the CMIP model is indeed very different between the models.

The bias score in the spectral slope behaves very similar to the skill score of the stdv(T) (Fig. 2.9b). Here it has to be noted that the statistical estimate of the spectral slope of the T time series is independent of the stdv(T). The tight relation therefore suggests that the spectral slope and the stdv(T) are dynamically linked. This we already indicated in the discussion of the sensitivities above with the moderate negative correlation between spectral slope and the stdv(T) in the CMIP ensembles (r = -0.57), but here the dynamical skill suggests an even tighter relationship.

The bias score for cross-correlation r_{Th} is more independent from the other bias scores, but also shows less spread within the models and is also closer to the observed uncertainties. In summary of all skill scores we cannot see much difference in the bias scores of the ensembles means of the CMIP3 and CMIP5 simulation, although there is a weak tendency for the CMIP5 ensemble to have slightly smaller biases than the CMIP3 ensemble.

The bias scores of the models as a whole are surprisingly bad considering that the models match observed ENSO statistic much better than the bias scores would suggest. As mentioned above this is due to the fact that the models have compensating biases. A comparison of the CMIP model spread in stdv(T) with the CMIP model spread in the model parameters illustrates this, see Fig. 2.10. We can note that the ensemble mean stdv(T) is very close to the observed with the model distribution wider than the observed uncertainty, but still close to the observed. However, the most important parameters (Fig. 2.10b–e) all have substantial biases towards the observed values and relatively large spread. It is

surprising that the models manage to simulate the observed stdv(T) so well given such large biases in the controlling ENSO dynamics.

2.6 Summary and discussion

In this study, we introduced the linear recharge oscillator model as a diagnostic tool to evaluate the representation of ENSO dynamics in the CMIP model database. We presented a proof of concept analysis that illustrated that ENSO-statistics and their diversity within the CMIP ensemble, can be well represented with the linear recharge oscillator model diagnostics. Although simplified to only represent the first order dynamics, presenting only a linear system, we believe it is an efficient tool to replicate ENSO dynamics in CMIP models. It provides a very effective bridge between simple statistical analysis of ENSO variability and the fully complex dynamical ENSO system with all its feedbacks and processes.

Starting with the simple statistics of the variability in T and h we found that the CMIP ensembles in the mean can present those fairly well, but the model ensemble spread is relatively large suggesting that many models are not consistent with the observed values. Furthermore, as we will point out further below, the good fit in these simple statistics seem to mask bigger problems in the model dynamics of ENSO, as they result from the analysis of the ReOsc model parameters.

The CMIP model simulations present the six parameters of the ReOsc model Equations $((2.1)\,,\,(2.2))$ with different quality. All six parameters show fairly large spread within the CMIP ensemble, with some models being nearly undamped in T tendencies ($a_{11} \approx 0$) and others having more than twice as much damping then the ensemble mean. Other biases of significance are a too strong damping of h and in general too weak stochastic noise forcing on h.

More significant problems in the CMIP ensemble dynamics became apparent when

we split up the growth rate (damping) of T (a_{11}) into atmospheric and oceanic feedbacks. Atmospheric feedbacks (Bjerknes wind–SST feedback, $C_{\tau T}$, and atmos. heat flux feedback, C_{fT}) are largely underestimated, which is consistent with previous studies (Lloyd et al. 2009; Bellenger et al. 2014) and also consistent with the idea of Dommenget et al. (2014) that CGCM simulations are often closer to a slab ocean El Niño dynamics (Dommenget 2010) than to the observed ENSO dynamics. All three elements that make up the growth rate of T (Bjerknes wind-SST feedback, $C_{\tau T}$, atmos. heat flux feedback, C_{fT}, and oceanic damping of T, a_{11O}) are strongly underestimated in the CMIP ensemble, while at the same time the total of T (a_{11}) is essentially unbiased. This is achieved by strongly compensating biases: too weak atmospheric growth rates (a_{11A}) combined with too weak oceanic damping (a_{11O}).

Here it has to be noted that the oceanic damping of T (a_{11O}) was estimated as the residual of a_{11} minus a_{11A} (Eqs.(2.3), (2.4)). A possible explanation for the strong compensation between atmospheric and oceanic feedbacks may therefore be a limitation in the ReOsc model approach used here. The assumption that a_{11A} results from Eq.(2.3) may be limited. However, it is very likely that oceanic processes do contribute to damping of a_{11} and it therefore seems reasonable to assume that the results presented do hold to some degree. It is beyond this study to solve this unexpected result and future study need to address this issue in more detail.

Assuming that there is indeed a compensating effect of atmospheric feedbacks (a_{11A}) and oceanic feedbacks (a_{11O}) in the CMIP ensemble, then we would need to find a reason of why that is. We are not aware of any physical mechanism that could explain such a relationship, but we cannot exclude such a possibility. For instance, Bayr et al. (2018) and partly Kim et al. (2008) argue that $C_{\tau T}$ and C_{fT} are dynamically linked by the position of the Walker circulation. Whether some mechanism like this could explain the link between a_{11A} and a_{11O} is unclear. An alternative possibility is that the CGCM models are tuned to

produce the observed ENSO statistics: by doing so model developers may have, by coincident, tuned errors into the atmospheric and oceanic dynamics that compensate each other nearly completely. Thus, CMIP models may produce apparently good ENSO simulations for the wrong reasons.

The combination of errors we find in the CMIP models suggests that the relative importance of ocean dynamics for the simulated ENSO SST variability is underestimated. This results from underestimated oceanic processes such as noise forcing for h, ocean coupling of h to T(a_{21O}) and too strong damping of h. This is at large consistent with the findings of Kim et al. (2014), who also report an underrepresentation of oceanic processes in ENSO. At the same time CMIP models underestimate atmospheric damping, which allows the models to create ENSO variability with realistic amplitudes. Thus, it appears that the relative importance of atmospheric processes in the CMIP models is larger than observed.

The ReOsc model allowed us to estimate the sensitivity of the ENSO statistics to each model parameter. It illustrated that in terms of model biases towards observed the most important parameter errors are in $C_{\tau T}$, C_{fT}, and a_{11O}, and to a lesser extent in the noise forcing and damping of h. In terms of CMIP ensemble spread the same parameters contribute to the ENSO statistics uncertainty, but in addition the growths rate of T (a_{11}) is important too.

Based on these sensitivities we defined a dynamical bias score that is essentially a normalized root mean squared in the model parameters. All CMIP model have fairly bad bias scores relative to what we could expect from observed uncertainties. These bad bias scores mostly result from the compensating errors in the dynamics as describes above. Even if we would exclude the less clear estimate of a_{11O} the bias scores would remain fairly bad (correlation with original bias score of Eq. (2.9) is still 0.85 if a_{11O} is excluded).

Bias scores that are based on just the ENSO statistics (e.g. stdv(T), etc.) or just the ReOsc model parameters of Eqs. (2.1),(2.2)(not shown) would be much better. However, these would exclude the most important elements of ENSO dynamics ($C_{\tau T}$, C_{fT}, and a_{11O}) and would therefore not present a complete picture. Bellenger et al. (2014) also found little relation between skill scores based on simple ENSO statistical properties vs. those based on dynamics properties. From the bias scores that we estimated we find a fairly clear ranking in the CMIP model performance with no substanital improvement from CMIP3 to CMIP5. The best models in this skill score are the family of models from NCAR/UCAR (CCSM4, CESM1-BGC, CESM1-CAM5, CESM1-FASTCHEM).

The results we found here have some implications for ENSO studies with CGCMs. The fact that the models produce realistic ENSO statistics with compensating errors in dynamics highlights some concerns in the models skill in predicting future SST evolutions. This is relevant not only for seasonal to interannual forecasting, but also for long time climate change projections. Even though models in the ensemble mean project a systematic shift towards El Niño like conditions Collins et al. (2010), this projection is undermined by the CGCM having systematic biases in the dynamics. How ENSO will change in the future strongly depends on the right sensitivity of the tropical Pacific region to the different forcings (e.g. heat fluxes and winds) that drive these changes.

The recent global warming hiatus and the mismatch of the CMIP simulations in predicting tropical Pacific climate trends (e.g. in winds or the Walker Circulation) may be some further indication that the model ENSO dynamics do not have the right balance in feedbacks (England et al. 2014; Kociuba and Power 2014; McGregor et al. 2014). The framework that we have introduced here may help to address such biases. Therefore, the good news from this study is that we can expect that future CGCM simulations will improve in ENSO dynamics, if model developers can use approaches like the one we have introduced here to improve the dynamics of the model.

Supplementary Table S2.1: CMIP3 and CMIP5 model variability statistics.

	stdv(T)	stdv(h)	r_{Th}	Γ_{grad}
CMIP3 #1	0.41	3	0.46	-1
CMIP3 #2	0.44	3.1	0.31	-1.6
CMIP3 #3	1.7	12.8	0.61	-3.4
CMIP3 #4	0.98	6.2	0.48	-2.4
CMIP3 #5	0.17	2.7	0.35	-1.7
CMIP3 #6	0.2	3.2	0.34	-2.1
CMIP3 #7	1.04	5.9	0.53	-3.1
CMIP3 #8	1.24	8.1	0.59	-2.5
CMIP3 #9	0.67	4.6	0.52	-2.1
CMIP3 #10	1.06	7.3	0.48	-2.8

	stdv(T)	stdv(h)	r_{Th}	Γ_{grad}
CMIP5 #1	0.73	6	0.29	-3
CMIP5 #2	0.73	6.3	0.21	-2.3
CMIP5 #3	1.09	7	0.42	-3.2
CMIP5 #4	0.88	5.9	0.36	-2.7
CMIP5 #5	0.9	6.5	0.47	-2.9
CMIP5 #6	0.91	5.8	0.47	-3
CMIP5 #7	1.12	7.4	0.36	-3
CMIP5 #8	0.94	6.9	0.59	-2.8
CMIP5 #9	0.77	5.8	0.52	-2.4
CMIP5 #10	0.98	6.4	0.42	-3.1
CMIP5 #11	0.8	6.2	0.52	-2.9
CMIP5 #12	0.75	4.4	0.37	-2.3
CMIP5 #13	1.42	10.7	0.43	-2.7
CMIP5 #14	0.6	4.6	0.54	-2.6
CMIP5 #15	0.83	6.5	0.54	-3.3
CMIP5 #16	0.55	4.5	0.38	-3.1
CMIP5 #17	0.52	4.3	0.49	-3.3
CMIP5 #18	0.86	6.1	0.49	-2.7
CMIP5 #19	0.93	5.4	0.4	-2.1
CMIP5 #20	0.84	4.8	0.31	-1.8
CMIP5 #21	0.77	4.4	0.32	-2.5
CMIP5 #22	0.71	4.7	0.49	-2.7
CMIP5 #23	0.81	6.1	0.48	-2
CMIP5 #24	0.68	5.8	0.33	-1.8
CMIP5 #25	0.57	4.1	0.35	-2.4
CMIP5 #26	1.05	8	0.55	-3.1
CMIP5 #27	1.06	7.6	0.46	-3.2
CMIP5 #28	1.2	5.3	0.62	-2.8
CMIP5 #29	0.6	4.7	0.4	-2

Supplementary Table S2.2: CMIP3 and CMIP5 model parameters.

	a_{11}	a_{12}	a_{22}	a_{21}	stdv(ξ_1)	stdv(ξ_2)	C_{fT}	$C_{\tau T}$	a_{11a}	a_{11o}	a_{21a}	a_{21o}
CMIP3 #1	-0.23	0.028	-0.005	-1.09	0.2	1.06	-9.9	0.0058	0.21	-0.45	-0.03	-1.06
CMIP3 #2	-0.15	0.018	-0.044	-0.87	0.21	1.03	-8.7	0.0064	0.14	-0.29	-0.3	-0.57
CMIP3 #3	-0.02	0.021	-0.04	-1.21	0.32	2.29	-2.3	0.0058	0.23	-0.25	-0.24	-0.96
CMIP3 #4	-0.08	0.031	-0.051	-1.24	0.31	1.65	-8	0.0067	0.33	-0.41	-0.36	-0.89
CMIP3 #5	-0.16	0.006	-0.046	-2.04	0.09	0.92	-20	0.011	-0.1	-0.05	-0.53	-1.5
CMIP3 #6	-0.09	0.005	-0.055	-1.43	0.08	1.15	-15.8	0.0135	-0.05	-0.05	-0.79	-0.64
CMIP3 #7	-0.01	0.034	-0.089	-1.23	0.25	1.21	-5.6	0.0047	0.26	-0.27	-0.43	-0.8
CMIP3 #8	-0.08	0.024	-0.035	-1.03	0.37	2.34	-4.5	0.0034	0.12	-0.2	-0.13	-0.9
CMIP3 #9	-0.14	0.028	-0.031	-1.27	0.29	1.24	-5.6	0.0103	0.53	-0.68	-0.34	-0.93
CMIP3 #10	-0.06	0.018	-0.022	-0.95	0.32	1.36	-2.3	0.0079	0.27	-0.33	-0.18	-0.77

	a_{11}	a_{12}	a_{22}	a_{21}	stdv(ξ_1)	stdv(ξ_2)	C_{fT}	$C_{\tau T}$	a_{11a}	a_{11o}	a_{21a}	a_{21o}
CMIP5 #1	-0.01	0.018	-0.086	-1.46	0.21	1.45	-10.7	0.0044	0.03	-0.04	-0.4	-1.06
CMIP5 #2	-0.01	0.016	-0.097	-1.52	0.23	1.31	-2.9	0.0049	0.13	-0.14	-0.5	-1.01
CMIP5 #3	-0.01	0.022	-0.059	-1.03	0.22	1.58	-12.5	0.0091	0.27	-0.28	-0.56	-0.47
CMIP5 #4	-0.02	0.021	-0.063	-1.09	0.21	1.4	-10.5	0.0086	0.25	-0.27	-0.56	-0.53
CMIP5 #5	-0.05	0.023	-0.037	-1.28	0.2	1.54	-10.1	0.0086	0.29	-0.33	-0.33	-0.95
CMIP5 #6	-0.03	0.025	-0.059	-1.13	0.21	1.46	-10.4	0.0081	0.3	-0.33	-0.5	-0.62
CMIP5 #7	0	0.024	-0.081	-1.18	0.23	1.67	-7.6	0.0066	0.24	-0.24	-0.56	-0.62
CMIP5 #8	-0.1	0.025	-0.028	-1.42	0.32	1.85	-18.4	0.0075	0.15	-0.26	-0.22	-1.2
CMIP5 #9	-0.07	0.02	-0.042	-1.08	0.24	1.54	-1	0.0051	0.2	-0.27	-0.22	-0.86
CMIP5 #10	-0.01	0.027	-0.086	-1.31	0.25	1.34	-6.9	0.0075	0.33	-0.35	-0.68	-0.63
CMIP5 #11	-0.05	0.02	-0.03	-1.31	0.22	1.26	-16.8	0.0066	0.06	-0.11	-0.21	-1.1
CMIP5 #12	-0.12	0.029	-0.068	-0.93	0.31	1.59	-5.5	0.0054	0.25	-0.37	-0.39	-0.54
CMIP5 #13	-0.03	0.021	-0.053	-1.24	0.35	2.2	-11.9	0.0079	0.2	-0.23	-0.44	-0.8
CMIP5 #14	-0.05	0.023	-0.069	-1.52	0.17	1.21	-13.9	0.0046	0.05	-0.09	-0.33	-1.19
CMIP5 #15	-0.01	0.023	-0.073	-1.55	0.2	1.28	-12.7	0.0043	0.05	-0.06	-0.33	-1.21
CMIP5 #16	-0.01	0.018	-0.072	-1.4	0.13	0.97	-14	0.0087	0.15	-0.17	-0.66	-0.74
CMIP5 #17	-0.01	0.02	-0.078	-1.58	0.13	0.96	-13.5	0.008	0.16	-0.18	-0.66	-0.92
CMIP5 #18	-0.08	0.02	-0.018	-1.08	0.28	1.29	-2	0.0072	0.27	-0.35	-0.14	-0.94
CMIP5 #19	-0.14	0.022	-0.038	-0.83	0.42	1.64	-3.8	0.0042	0.15	-0.28	-0.17	-0.66
CMIP5 #20	-0.15	0.022	-0.054	-0.83	0.41	1.69	-2.6	0.0044	0.17	-0.32	-0.25	-0.59
CMIP5 #21	-0.06	0.025	-0.061	-0.96	0.27	1.13	-3.7	0.0066	0.3	-0.36	-0.42	-0.54
CMIP5 #22	-0.08	0.022	-0.059	-1.22	0.24	1.42	-9.8	0.0071	0.21	-0.29	-0.44	-0.78
CMIP5 #23	-0.09	0.017	-0.051	-0.99	0.28	2.15	-3.2	0.0033	0.08	-0.17	-0.18	-0.82
CMIP5 #24	-0.1	0.013	-0.082	-1.37	0.29	2.07	-3	0.0047	0.09	-0.19	-0.41	-0.96
CMIP5 #25	-0.11	0.018	-0.096	-1.3	0.25	1.62	-2.7	0.0029	0.08	-0.19	-0.29	-1.01
CMIP5 #26	-0.05	0.022	-0.037	-1.34	0.23	1.9	-9.3	0.0071	0.21	-0.26	-0.27	-1.07
CMIP5 #27	-0.03	0.019	-0.051	-1.07	0.24	1.93	-8.1	0.0076	0.2	-0.23	-0.4	-0.66
CMIP5 #28	-0.08	0.045	-0.036	-0.85	0.36	1.38	-5.8	0.0051	0.41	-0.5	-0.19	-0.65
CMIP5 #29	-0.09	0.015	-0.048	-1.04	0.23	1.36	-8.1	0.0065	0.1	-0.19	-0.33	-0.71

Supplementary Table S2.3: CMIP3 and CMIP5 bias-scores for different ENSO statistics as in Fig. 9.

	stdv(T)	stdv(h)	r_{Th}	Γ_{grad}
CMIP3 #1	0.38	0.39	0.13	0.29
CMIP3 #2	0.35	0.36	0.14	0.27
CMIP3 #3	0.44	0.43	0.1	0.34
CMIP3 #4	0.32	0.32	0.12	0.25
CMIP3 #5	0.46	0.44	0.21	0.33
CMIP3 #6	0.49	0.47	0.22	0.36
CMIP3 #7	0.47	0.48	0.21	0.37
CMIP3 #8	0.56	0.56	0.13	0.44
CMIP3 #9	0.49	0.45	0.11	0.37
CMIP3 #10	0.33	0.32	0.1	0.25

	stdv(T)	stdv(h)	r_{Th}	Γ_{grad}
CMIP5 #1	0.62	0.61	0.2	0.48
CMIP5 #2	0.55	0.55	0.22	0.43
CMIP5 #3	0.2	0.2	0.11	0.15
CMIP5 #4	0.24	0.25	0.13	0.18
CMIP5 #5	0.22	0.22	0.08	0.16
CMIP5 #6	0.24	0.25	0.12	0.18
CMIP5 #7	0.37	0.37	0.16	0.29
CMIP5 #8	0.27	0.27	0.07	0.21
CMIP5 #9	0.48	0.48	0.12	0.38
CMIP5 #10	0.29	0.3	0.17	0.23
CMIP5 #11	0.44	0.43	0.12	0.34
CMIP5 #12	0.41	0.41	0.15	0.32
CMIP5 #13	0.28	0.28	0.09	0.22
CMIP5 #14	0.56	0.55	0.18	0.43
CMIP5 #15	0.6	0.59	0.18	0.46
CMIP5 #16	0.34	0.34	0.17	0.24
CMIP5 #17	0.36	0.36	0.18	0.26
CMIP5 #18	0.36	0.35	0.1	0.27
CMIP5 #19	0.5	0.5	0.13	0.39
CMIP5 #20	0.49	0.49	0.14	0.38
CMIP5 #21	0.37	0.37	0.14	0.29
CMIP5 #22	0.3	0.3	0.12	0.23
CMIP5 #23	0.6	0.59	0.15	0.47
CMIP5 #24	0.52	0.52	0.19	0.41
CMIP5 #25	0.61	0.61	0.22	0.48
CMIP5 #26	0.32	0.31	0.08	0.25
CMIP5 #27	0.32	0.31	0.1	0.25
CMIP5 #28	0.46	0.46	0.21	0.37
CMIP5 #29	0.41	0.4	0.14	0.31

Chapter 3

Effects of thermocline estimation techniques on ENSO using the linear recharge oscillator model

3.1 Introduction

The El Niño–Southern Oscillation (ENSO) in the tropical Pacific is the most critical year-to-year climate fluctuation affecting seasonal-to-interannual climate variability globally. It results from the interactions between the equatorial Pacific warm waters and the general atmospheric circulation in the Tropics (Wyrtki 1975; Rasmusson and Carpenter 1982). The dynamics that control ENSO are essential for global seasonal climate predictions but are also crucial for long-term global climate change.

One of the most important variable for ENSO studies is the thermocline depth in equatorial Pacific (h). Fiedler (2010) described thermocline as "a layer of water in which temperature changes more rapidly with depth than it does in the layers above (surface or mixed layer) or below (deep water)". Although the theory of formation and structure of thermocline is still a fundamental problem in physical oceanography (Pedlosky 2006), there are several techniques used for estimating h. Most tropical Pacific ocean studies consider the depth of 20°C isotherm ($Z20$ henceforth) as an optimal proxy for thermocline depth (Meyers 1979; Kessler 1990; Smith 1995; Vecchi and Harrison 2000; Meinen and McPhaden 2000; Fedorov and Philander 2001; Yang and Wang 2009).

Many recent studies have questioned the accuracy of using $Z20$ as a proxy for thermocline depths. Wang et al. (2000) showed that $Z20$ has problems representing the thermocline depth accurately and that it is suitable to represent warm pool but may fail for the cold tongue and coastal upwelling regions as it may surface during the cold seasons. Vecchi et al. (2006) found $Z20$ to be problematic for multi-model climate change analysis as isotherms exhibit inter-model variability and also will change over time in a changing climate. The changes in isotherms were also model dependent as they are a function of other aspects (e.g. climate sensitivity of the model, diapycnal mixing etc.), hence they used

the maximum gradient of temperature (dT/dz; $maxgrad$ henceforth) definition of thermocline depth. Yang and Wang (2009) noted that under a changing climate scenario the trends in the thermocline depth measured as depth of 20°C isotherm and as the depth of maximum dT/dz can be of opposite sign. They wrote that "During the transient period of global warming, the tropical thermocline is usually enhanced because the surface layer warms more and faster than the lower layers. The depth of maximum vertical temperature gradient shoals, which is consistent with the enhanced thermocline. However, the 20°C isotherm depth deepens, which suggests a weakened thermocline."

Analysing and evaluating the thermocline depths estimation techniques are important as the effect of thermocline depth changes on ENSO has been well established. Most ENSO theories like the delayed oscillator (Suarez and Schopf 1988; Battisti and Hirst 1989) the recharge-discharge oscillator (Jin 1997a,b) and the further simplified recharge oscillator (Burgers et al. 2005) have stressed on the role of the upper-oceanic heat content in the ENSO cycle. According to the recharge oscillator theory, the depth of the main thermocline plays an essential dynamic role in ENSO oscillation by controlling temperatures of water upwelled in the eastern equatorial pacific, and deeper main thermocline means upwelling of warmer waters. Thermocline anomalies, in turn, affect the Sea Surface Temperature (SST) anomalies in east equatorial Pacific, which impacts zonal winds. They showed that the $Z20$ for February-March is positively and significantly correlated (0.72) with Niño 3.4 sea surface temperature (SSTs) 10 months after, which suggests that warm water builds up in the tropical Pacific before the onset of El Niño and a substantial heat content anomaly in the Pacific Ocean mixed layer is a necessary condition for El Niño growth. Thermocline depth anomaly also affects the ENSO phase transition while phase lag between zonally averaged thermocline depths in the east pacific produces the SST - h oscillation. McPhaden et al. (2006) showed that in the central-eastern equatorial Pacific, the thermocline fluctuations are transferred to the surface mainly through vertical advection by mean upwelling, a

process called "thermocline feedback". Variations in the equatorial thermocline depth lead ENSO SST anomalies in the eastern Pacific by at least two seasons, and hence variations in the thermocline depths are a significant predictor of ENSO (Meinen and McPhaden 2000; McPhaden et al. 2006).

The relationship between the thermocline depth and SST anomalies in the equatorial Pacific, however, is not straightforward. Harrison and Vecchi (2001) investigated the simultaneous relationship between h and SST in the equatorial Pacific and found significant correlations only in the eastern and east-central Pacific hence concluded it is "inappropriate to attribute SST changes to thermocline depth changes." Zelle et al. (2004) showed that thermocline depth anomalies lead SST anomalies in time, with a longitude-dependent delay ranging from 2 weeks in the eastern Pacific to 1 year in the central Pacific. The growing lag toward the west is linked with the increasing mean depth of the thermocline. In addition to the local advection/mixing the much longer delay in the central Pacific may also be associated with more basin-wide adjustment to thermocline perturbations (Philander 1981).

ENSO cycle also exhibits strong seasonal dependence, with events tending to develop in summer/autumn, peak in winter, and decay in subsequent spring (Rasmusson and Carpenter 1982). Both the SST and the zonal slope of the equatorial thermocline experience a significant annual cycle. Studies based on heat budget analysis of the surface layer (Wang and McPhaden 2000; Kang et al. 2001) also suggested that during the different phases of the ENSO cycle (or different seasons) different budget terms had varying level of contribution. Therefore seasonality may also be a feature in the direct relationship between the thermocline depth and SST anomalies.

This chapter investigates the accuracy of using $Z20$ as a thermocline proxy for ENSO studies as opposed to using $maxgrad$. Assuming that $Z20$ is the best proxy for h, $Z20$ and $maxgrad$ should be equal and make no difference to the ENSO statistics, dynamics,

and predictability. We will base our analysis on the ReOsc model, which has been used in many studies to analyze ENSO dynamics in different ways (Burgers et al. 2005; Jansen et al. 2009; Frauen and Dommenget 2010; Levine and McPhaden 2015). The ReOsc model is a simplified representation of ENSO dynamics, allows us to diagnose the dynamical parameters of the ENSO variability from the statistics of the model simulations or observations.

This chapter is organized as follows. The data sets, models, and methods used are described in Section 3.2. The main results of this study are presented in Section 3.3 where we analyze the effect of thermocline depth estimation techniques on ENSO statistics (differences in annual mean, seasonal mean, field averaged h, standard deviation of h), ENSO dynamics (use the recharge oscillator model to see differences in SST damping, h damping), variability and predictability. The summary and discussion are presented in Section 3.4.

3.2 Model simulation, data and methods

3.2.1 Observational datasets and CMIP Model Simulations

For observations we use data prepared by the Australian Bureau of Meteorology Research Centre (BMRC) using an optimal interpolation technique, which combined data from moored buoys, expendable bathythermographs, and Argo floats (Smith 1995). The BMRC $Z20$ data set covers the tropical Pacific basin on a 1° latitude and 2° longitude grid and is available for the period of January 1980 to January 2011 with monthly resolution. The SST , $Z20$ and $maxgrad$ estimates are calculated from the potential temperature. Since the BMRC 20°C record is much shorter we restrict our analysis of observed SST and thermocline depth co-variability to 1980–2011.

Table 3.1:: CMIP5 models with the corresponding model numbers

01	ACCESS1-0
02	ACCESS1-3
03	CCSM4
04	CESM1-BGC
05	CESM1-CAM5
06	CNRM-CM5
07	CSIRO-Mk3-6-0
08	CanESM2
09	FGOALS-g2
10	GFDL-ESM2G
11	GFDL-ESM2M
12	GISS-E2-H-CC
13	GISS-E2-R
14	GISS-E2-R-CC
15	HadGEM2-CC
16	HadGEM2-ES
17	IPSL-CM5A-MR
18	IPSL-CM5B-LR
19	MPI-ESM-MR
20	NorESM1-M
21	NorESM1-ME
22	bcc-csm1-1-m
23	CMCC-CM
24	GFDL-CM3
25	CMCC-CESM
26	CESM1-FASTCHEM
27	FGOALS-s2
28	IPSL-CM5A-LR
29	CESM1-WACCM
30	HadCM3
31	bcc-csm1-1
32	CNRM-CM5-2
33	CESM1-CAM5-1-FV2
34	CMCC-CMS

The analysis uses CMIP5 model simulation of the historical scenario for the period 1900-1999 (Moss et al. 2010; Taylor et al. 2012) and RCP8.5 for 2048-2100 for the Figure 3.2. We use all model simulations that have all variables available needed for this analysis. These are 34 model simulations, see Table 3.1 out of which we have RCP8.5 data available for 25 models. The historical scenario over the period from 1900 to 1999 is considered as the control climate. All data is linearly detrended and anomalies relative to the mean seasonal cycle are defined. The maxgrad estimate is computed by using spline interpolation

technique, where we fitted a curve to the potential temperature data points at various depth levels with 0.1m scaling. We then find the gradient at each point, and the level of maximum gradient is choosen as the $maxgrad$ estimate. The $Z20$ estimate is calculated as the depth of the 20°C isotherm. $maxgrad$ is computed as dt/dz of the time-mean T instead of the time-mean of the high frequency dt/dz. It is beyond the scope of this chapter to analyse the differences between the two, but we will look at it for future work.

Our analysis is based on monthly mean anomaly time series for SST and thermocline depth averaged over the equatorial Pacific (130°E–80°W, 5°S–5°N) and NINO3 (150°W–90°W, 5°S–5°N) SST index.

3.2.2 The Recharge Oscillator Model

The linear ENSO dynamics are evaluated on the basis of the ReOsc model from (Burgers et al. 2005; Frauen and Dommenget 2012; Vijayeta and Dommenget 2018). This model is given by two tendency equations of the NINO3 region (150°W–90°W, 5°S–°N) SST anomalies, T, and equatorial Pacific (130°E–80°W, 5°S–°N) mean thermocline depth anomalies, h:

$$\frac{dT(t)}{dt} = a_{11}T(t) + a_{12}h(t) + \zeta_T \tag{3.1}$$

$$\frac{dh(t)}{dt} = a_{21}T(t) + a_{22}h(t) + \zeta_h \tag{3.2}$$

The model parameters a_{11} and a_{22} represent the growth rate (or damping) of T and h, and the parameters a_{12} and a_{21} the coupling between T and h. The two equations are forced by stochastic noise terms ζ_T and ζ_h. The parameters of the 2-dimensional model Eqs. (3.1),(3.2) are estimated for each CMIP model simulation by multivariate linear regressing

the monthly mean tendencies of T and h against monthly mean T and h, respectively, following the approach in previous studies (Burgers et al. 2005; Jansen et al. 2009). The residual of the linear regression fit can be interpreted, as the random noise forcings with the standard deviation ($stdv$) of the residuals being the $stdv$ of the noise forcings for the T and h equations (ζ_T and ζ_h). The ReOsc model Eqs.(3.1),(3.2) can be integrated with stochastic noise forcing terms ζ_T and ζ_h to generate stochastic time series of T and h. We therefore integrated the equations with a time step of 24 hours and red noise forcing terms ζ_T and ζ_h. The decorrelation time of ζ_T and ζ_h is set to 3 days to mimic weather fluctuations that effectively results into white noise for monthly mean data.

The ReOsc model strongly simplifes the ENSO dynamics and each of the 4 parameters and the two noise forcing terms can be a result of many different physical processes in the atmosphere and oceans. To further untangle the complexity the parameters, a_{11} and a_{21} can be split up into an atmospheric, $a_{11A}$and a_{21A}, and oceanic part, a_{11O} and a_{21O} following the approach of Frauen and Dommenget (2010) and Yu et al. (2016) :

$$a_{11} = a_{11A} + a_{11O} \tag{3.3}$$

$$a_{21} = a_{21A} + a_{21O} \tag{3.4}$$

The atmospheric damping (or growth rate) of T, a_{11A}, is effectively a coupling to wind stress and net heat flux (Frauen and Dommenget 2010):

$$a_{11A} = a_{12}\lambda C_{\tau T} + \frac{C_{fT}}{\gamma} \tag{3.5}$$

The coefficient $C_{\tau T}$ is the linear regression of zonal wind stress, τ_x, in the central

Pacific box and NINO3 SST . This essentially represents one of the three Bjerknes feedbacks. C_{fT} is a linear regression between net atmospheric heat flux and$T$ in the NINO3 region. λ is a positive free coupling parameter and γ the ocean mixed layer depth following the approach of Frauen and Dommenget (2010), which is based on the study of Jin (1997a). The atmospheric part of the coupling of h to T, a_{21A}, can be expressed as:

$$a_{21A} = \frac{a_{22}}{2}\lambda C_{\tau T} \tag{3.6}$$

The oceanic parts of the couplings to T, a_{11O} and a_{21O}, in Eqs. (3.3) and (3.4) can be estimated as the residuals of a_{11} and a_{21} in Eqs. (3.3) and (3.4) when a_{11A} and a_{21A} are estimated from Eqs. (3.5) and (3.6). In the analysis part the parameters $C_{\tau T}$, C_{fT}, a_{11O} and a_{21O} will be estimated for the CMIP simulations in the same way as for the observations. To reduce the complexity in the analysis we assumed γ to be the same for all models. The coupling parameter λ is fixed for all analysis, as it was estimated in (Frauen and Dommenget 2010) from running CGCM sensitivity studies.

3.3 Results

3.3.1 Mean thermocline depth in the equatorial Pacific

Figure 3.1 shows the idealised temperature profile where the blue curve represents current ocean temperature and the red curve a future warmer ocean temperature profile. The two curves are identical except that the red curve is offset by +3 °C. In this case we are assuming an uniform warming of the ocean at all depth levels. The dashed black line represents the $maxgrad$ estimates, and as the temperature profiles are only offset by a certain amount of uniform warming, the gradient of temperature ($maxgrad$) which represents the thermocline depth doesn't change. But the $Z20$ which represents the 20°C isotherm deepens as there

is now much more surface heat in the upper ocean layers. In such a case the $Z20$ estimate might not be a good proxy for the thermocline depth as it may not coincide with the same.

The effect of future greenhouse warming on the thermocline depths in CMIP5 models is shown in Figure 3.2. The figure shows the mean temperature profiles of the equatorial Pacific (130°E - 280°E, 5°S - 5°N) for the historical and RCP8.5 scenarios of three CMIP5 models. The corresponding right panels shows the East Pacific (210°E - 270°E, 5°S - 5°N) and West Pacific (130°E - 170°E, 5°S - 5°N) temperature profiles with the dashed horizontal lines representing $maxgrad$ estimates. The $Z20$ estimates are not shown in figure, but they are the depths associated with the intersecting point of the black dashed lines and temperature curves. In most models the temperature profile warms on all levels, but the warming is not uniform with depth. The most robust warming is at the surface, and the least amount of warming is very close to the mean thermocline depth although the warming patterns are different for each model. For example, in the CESM1-BGC model the $Z20$ deepens minimally in all three considered regions of the equatorial Pacific but

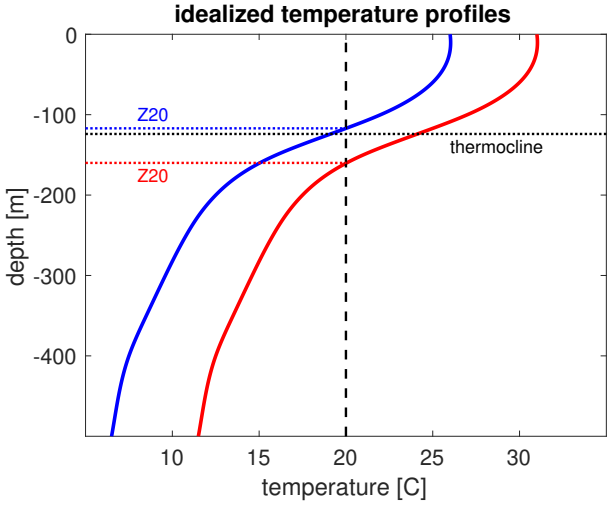

Figure 3.1: Sketch of idealised temperature profiles $Z20$ and $maxgrad$, the profiles are exactly similar with a 3 °C offset. In a warming climate the $Z20$ may change while the $maxgrad$ depths remains the same.

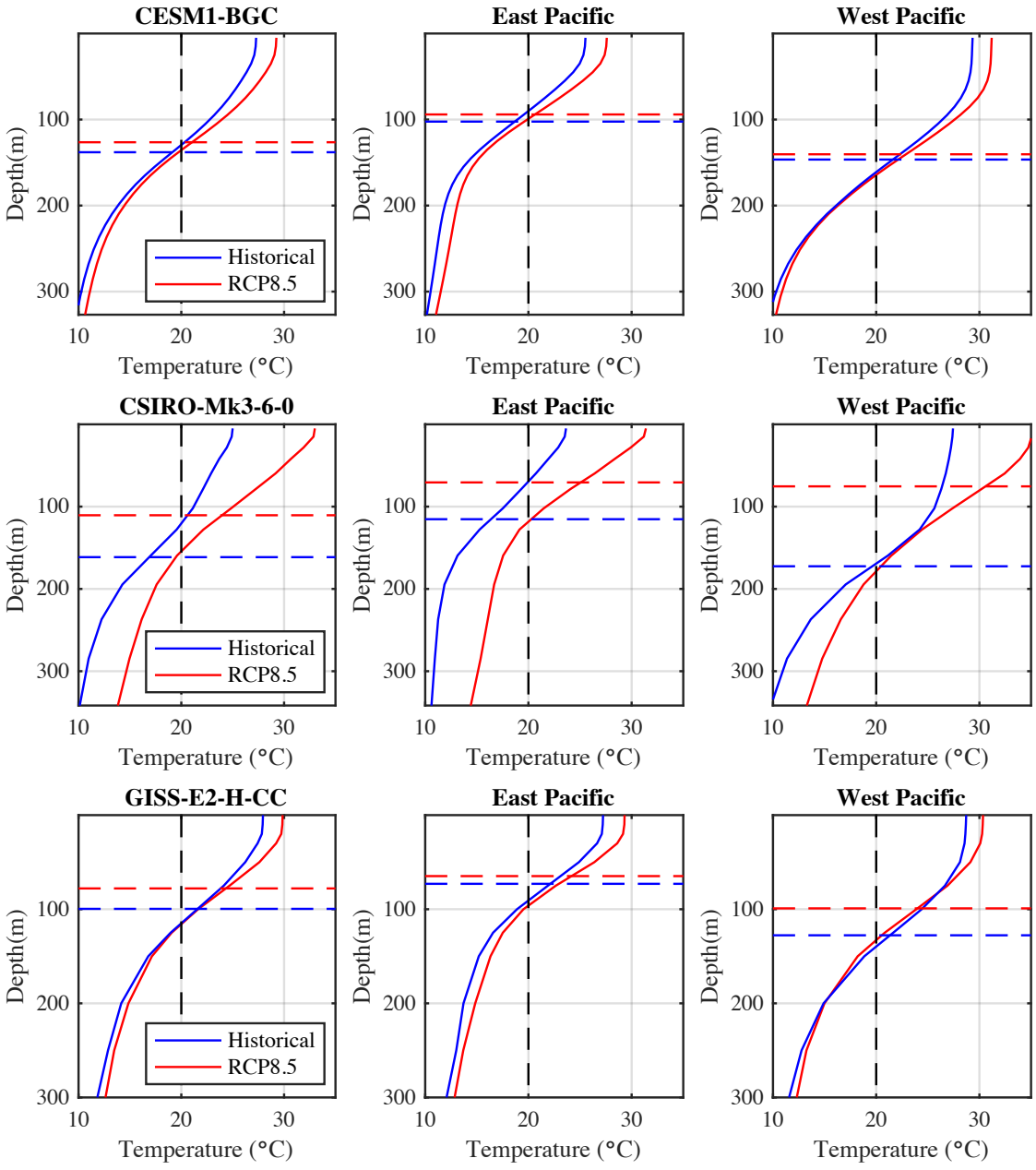

Figure 3.2: The temperature profiles averaged over Equatorial Pacific (130°E - 280°E) for three different models are shown with the corresponding East Equatorial Pacific (210°E - 270°E) and West Equatorial Pacific (130°E - 170°E) in the right panels. The blue curves are for historical data and red curves denotes the RCP8.5 (future) ocean temperatures. The dashed red and blue lines represent the *maxgrad* estimates for historical and RCP8.5 scenario data, $Z20$ is the depth where the black dashed line intersects the temperature curves (not shown).

the $maxgrad$ becomes shallower. In the CSIRO-Mk3-6-0 model the warming in ocean temperatures is quite substantial, $Z20$ deepens but $maxgrad$ shallows. The shallowing of $maxgrad$ is greater than the deepening of $Z20$, especially in the West Pacific region for the model. In the GISS-E2-H-CC model the historical and future temperature profiles are nearly identical except the top 100m, $Z20$ is not changing and the $maxgrad$ becomes shallower. The $Z20$ cannot capture the changes in thermocline depths as $Z20$ estimates are at same depth levels, but in reality the thermocline becomes shallower in the future ocean warming scenario. In all the three above mentioned examples and other CMIP5 models that are not shown, we see the same discrepancies of $Z20$ either not changing or deepening while the actual thermocline shoals. in In such cases the feasibility of using $Z20$ estimates to represent the thermocline depths comes under question as it is incapable of capturing the effect of ocean warming on thermocline depths.

Figure 3.3(a) shows the annual climatological mean observed values of $maxgrad$ and $Z20$ in the equatorial Pacific (upper 300m) plotted against the upper equatorial ocean temperature averaged over 5°N and 5°S. Both thermocline depth estimates generally coincide with each other, except in the West Pacific warm pool region where the $maxgrad$ is shallower than the $Z20$ by about 20–40 m. Figure 3.3(b) shows the CMIP5 multi-model ensemble (MME) mean values of temperature in the upper upper equatorial ocean along with the $maxgrad$ and $Z20$ and it is consistent with observations. Figure 3.3(c) and 3.3(d) show the annual mean differences between $Z20$ and $maxgrad$ for observations and CMIP5 MME, respectively. In the eastern Pacific, where the thermocline dynamics is vital to the$T$ and coupled variabilities, the $Z20$ can adequately represent the $maxgrad$. The thermocline is deep in the western Pacific, hence the discrepancy between the $Z20$ and $maxgrad$ does not matter as the surface is hardly affected by the thermocline locally. Therefore, for a steady-state mean climate, the $maxgrad$ can be adequately represented by $Z20$, and it will not be inconsistent, which has been shown by several studies (Zelle et al. 2004; Zhu et al.

2015). The problem would arise in a changing climate scenario where the surface warms and hence the isotherms shift upwards due to which the thermocline and $Z20$ may or may not coincide.

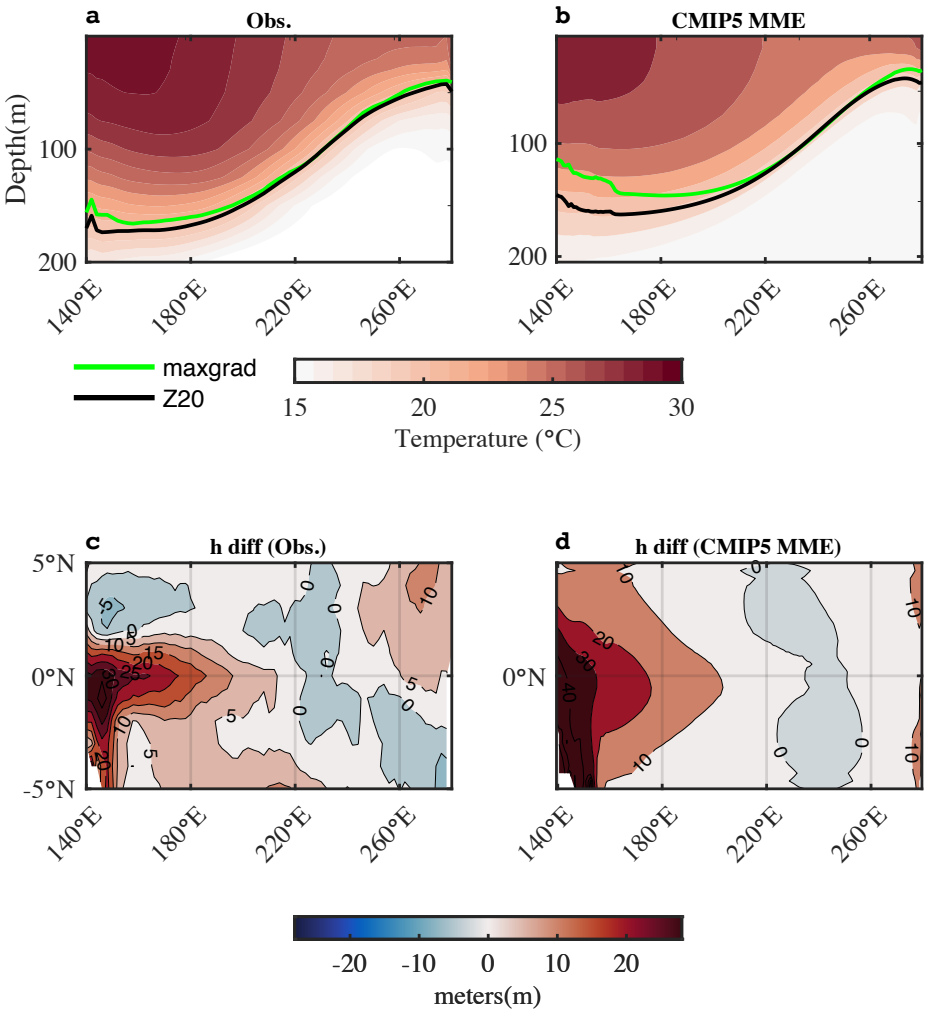

Figure 3.3: Climatological annual mean of equatorial Pacific ocean temperature (the upper 300 m; °C) averaged between 5°S to 5°N for **(a)** Observed BMRC data (1980-2011) and **(b)** CMIP5 multi model mean ensemble historical data (1900-1999). The black lines show the location of the 20°C isotherm ($Z20$) and green lines show the location of maximum vertical temperature gradient($maxgrad$). Climatological annual mean difference between maximum vertical temperature gradient ($maxgrad$) and 20°C isotherm ($Z20$) for **(c)** Observed BMRC data (1980-2011) and **(d)** CMIP5 multi model mean ensemble historical data(1900-1999).

3.3.2 Thermocline depth variability in the context of ENSO dynamics

Figure 3.4 shows the thermocline depth anomaly time series of the Equatorial Pacific (130°E - 280°E, 5°S - 5°N), East Equatorial Pacific (210°E - 270°E, 5°S - 5°N) and West Equatorial Pacific (130°E - 170°E, 5°S - 5°N) for observations and one CMIP5 model (ACCESS1-3). The correlation values are indicated on the northwest side in the panels. For both the observations and CMIP5 models, the standard deviation is higher for West Pacific. Also in this region the depth of $maxgrad$ is a lot shallower than $Z20$. The higher correlation in the CMIP5 models between the two time series as compared to observations is due to the fact that observations are prone to having a number of errors. The CMIP5 models in comparison do not have inconsistencies between the$T$ and thermocline depth data.

Figure 3.5(a),(b) shows the power spectrum of the thermocline depth anomaly for observation and CMIP5 MME respectively, $Z20$ and $maxgrad$ estimates are shown in red and blue curves. While for ENSO studies the$T$ A power spectrum is a more important statistical parameter it is imperative to look at the changes in the h power spectrum. For longer timescales the $Z20$ and $maxgrad$ estimates evolve similarly with $maxgrad$ extimates having higher variance for both observations and individual CMIP5 models. For shorter time scales the $maxgrad$ estimates have greater variance which means they are more noisier and this correlates with the higher standard deviation of $maxgrad$ estimates. In conclusion the importance of higher frequencies of thermocline depth anomalies is relatively greater in case of $maxgrad$ estimates. It is beyond the scope of this study to investigate reason for the differences in the variance distribution at different time scales, it certainly supports the fact that the different h anomaly estimation techniques leads to differences in the representation of ENSO dynamics.

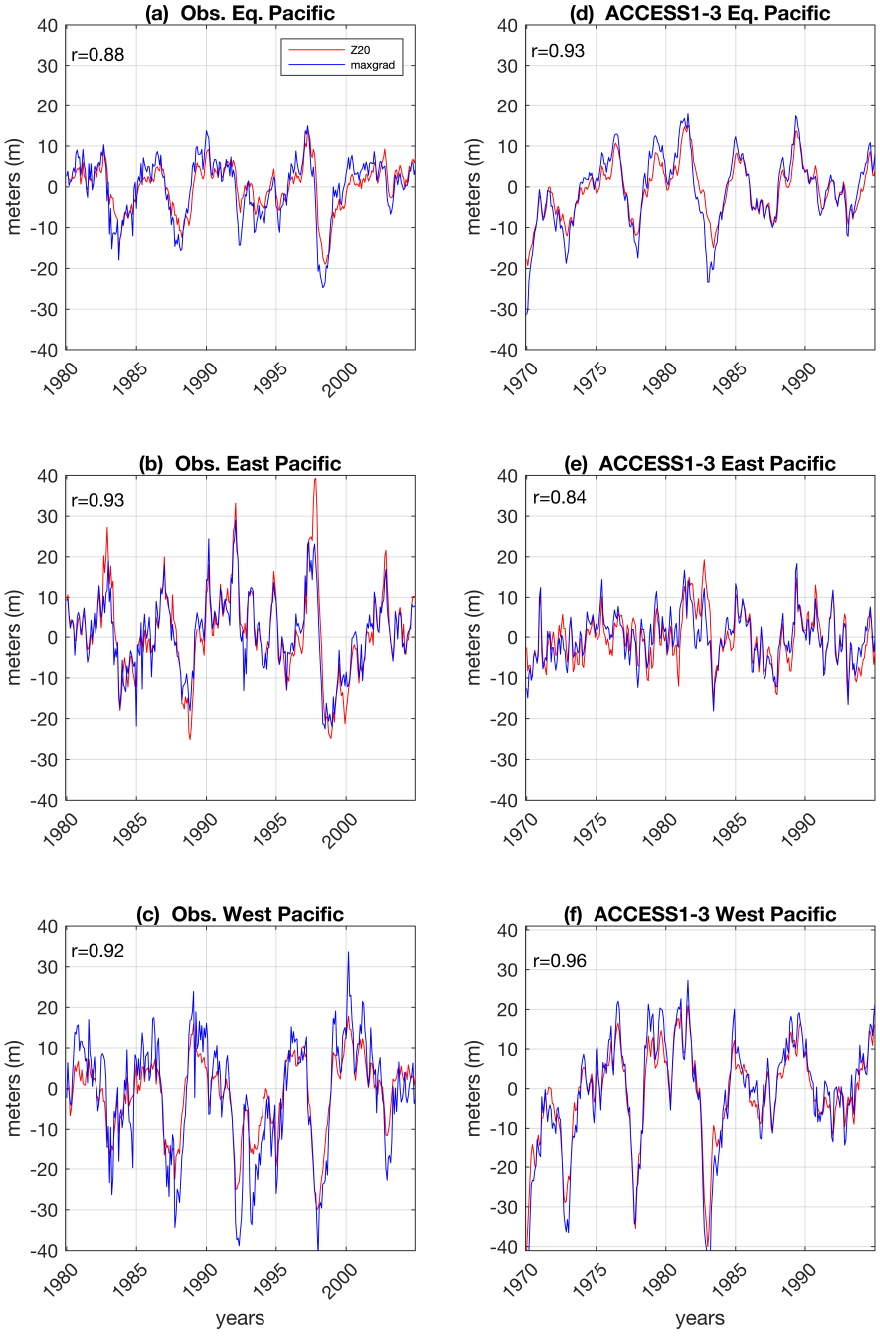

Figure 3.4: The thermocline depth anomaly time series for (a) Equatorial Pacific (130°E - 280°E) (b) East Equatorial Pacific (210°E - 270°E) (c) West Equatorial Pacific (130°E - 170°E). (d), (e), (f) are the corresponding time series for one CMIP5 model:ACCESS1-3 for the same regions as (a), (b), (c) respectively.

Figure 3.6(a) shows the observed correlation between$T$ and h. The observed time evolution of h leads that of T by about 5–6 months (peak of cross-correlation) for the $Z20$ estimates and about 7-8 months for the $maxgrad$ estimates. This is indicative of the ENSO recharge and discharge mechanism diagnosis differences between the two estimation techniques, which is the fundamental basis of the ReOsc model. The observed T and h ($Z20$) correlation have a more pronounced out of phase relationship as compared to the observed T and h ($maxgrad$) correlation. This is evident in the historical CMIP5 simulations as

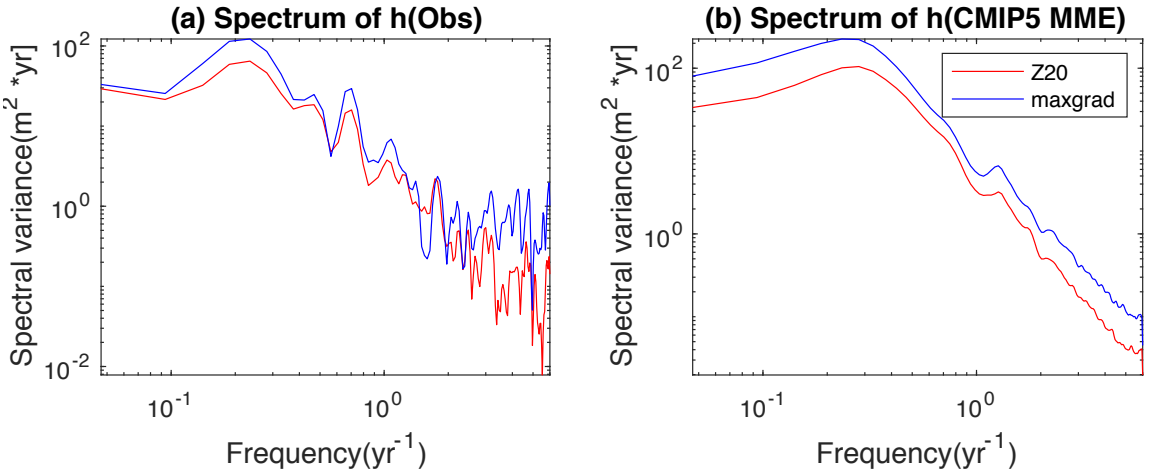

Figure 3.5: Power Spectrum of **(a)** Observed thermocline depth anomaly **(b)** CMIP5 MME thermocline depth anomalies.

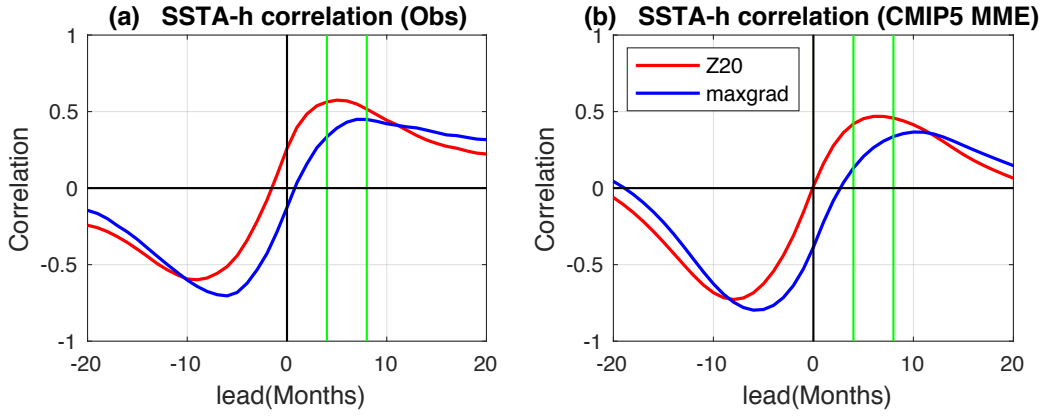

Figure 3.6: The Cross-correlation o fT vs h for **(a)** Observed BMRC data **(b)** CMIP5 multi model mean ensemble historical data (1900-1999). The blue lines are $maxgrad$ estimates and red lines are $Z20$.

well as shown in Figure 3.6(b), where T and h ($Z20$) have a very clear out-of- phase relation, with a strong positive correlation when h leads T and a roughly equally strong negative correlation when T leads h at about the same lead time of 5–8 months overall increase in correlation at the peak. These changes are qualitatively similar in the $maxgrad$ estimates, but are shifted further downwards indicating differences in the correlation patterns at different lead/lag months. The $maxgrad$ estimates has a quite significant negative instantaneous (lag = 0) cross-correlation and the cross-correlation peak for negative lead times (T leads h) is much larger than the one for positive lead times. The different characteristics of the thermocline depth estimates as discussed in this subsection indicate that they can potentially affect the ReOsc model parameters and therefore the representation of ENSO dynamics and its diagnosis in the ReOsc model.

Figure 3.7 shows the statistics of h variability. The standard deviation of h (stdv(h)) and mean cross correlation between$T$ and h for 4–8 months lag (h leading$T$) have been shown for observation and CMIP5 models. The stdv(h) slightly increases while the mean 4-

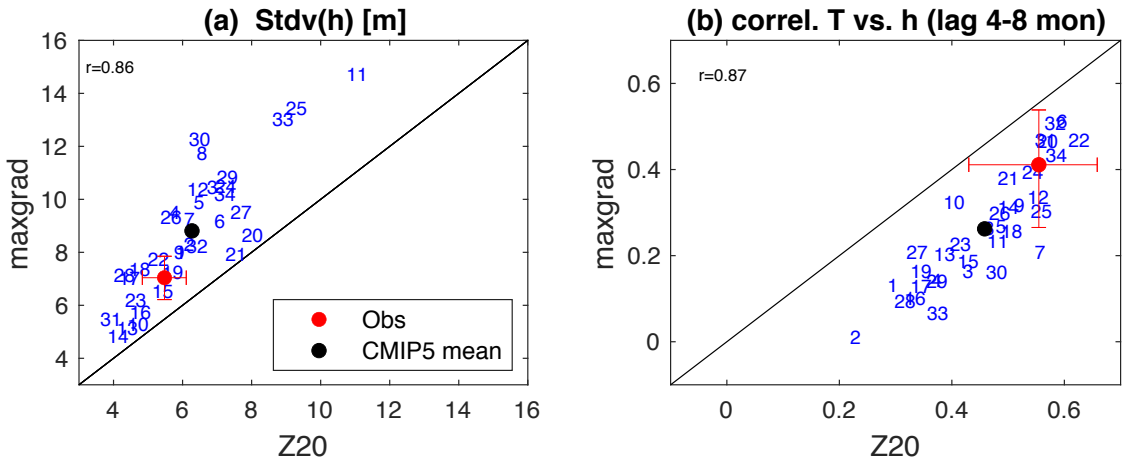

Figure 3.7: Statistics of ENSO variability: Scatter plot of **(a)** Standard deviation of h ($Stdv(h)$) for CMIP5 model historical data (1900-1999), **(b)** 4-8 month mean T - h correlation, for CMIP5 model historical data (1900-1999), with 20°C isotherm ($Z20$) data on x-axis and maximum vertical temperature gradient($maxgrad$) on y-axis.

8 months correlation decreases for $maxgrad$ estimates as opposed to $Z20$ estimates in both observations and all CMIP5 models. The stdv(h) difference within the CMIP5 ensemble between the $Z20$ and $maxgrad$ estimates is quite significant in few individual models. Also the 4-8 mean correlation for four models is significantly lower. Overall, the variability statistics for CMIP5 model ensemble mean show significant changes in the ensemble mean and almost twice the value of $Z20$ for some individual models. We can conclude that the two different h estimation techniques influence the representation of ENSO dynamics. Substantial changes are being reflected in the diagnosis of ENSO dynamics and we will further illustrate the same in the following subsections.

Figure 3.8(a), (b) shows the correlation between $Z20$ and $maxgrad$ estimations of the thermocline depths across the equatorial Pacific for observations and CMIP5 model mean respectively. Both models and observations have similar correlation patterns over the equatorial Pacific. Higher correlation exists between $Z20$ and $maxgrad$ in the Central Pacific regions off equator for both datasets. The west and east pacific have less than 0.6 correlation which indicates substantial differences in the thermocline depth estimation techniques. Figure 3.8(c), (d) shows the difference in standard deviation of thermocline depth anomaly between $maxgrad$ and $Z20$ estimations across the equatorial Pacific for observations and CMIP5 model mean respectively. The differences in the East Pacific aren't as substantial as West pacific, where the high differences between the standard deviations of thermocline depth anomaly suggests higher variability in case of $maxgrad$ estimates.

Figure 3.9(a) presents the lead-lag correlations between the latitude averaged BMRC $Z20$ anomalies and the BMRC T anomalies. This depicts the local T and h relationship, where the correlation between h and T anomalies are plotted as a function of longitude and lag. The data sets are averaged over the 5°N and 5°S latitudes. The correlation values are depicted by the contour lines, positive lag denotes h leading T anomalies. This is consistent with the findings shown previously by (Zelle et al. 2004), where they showed

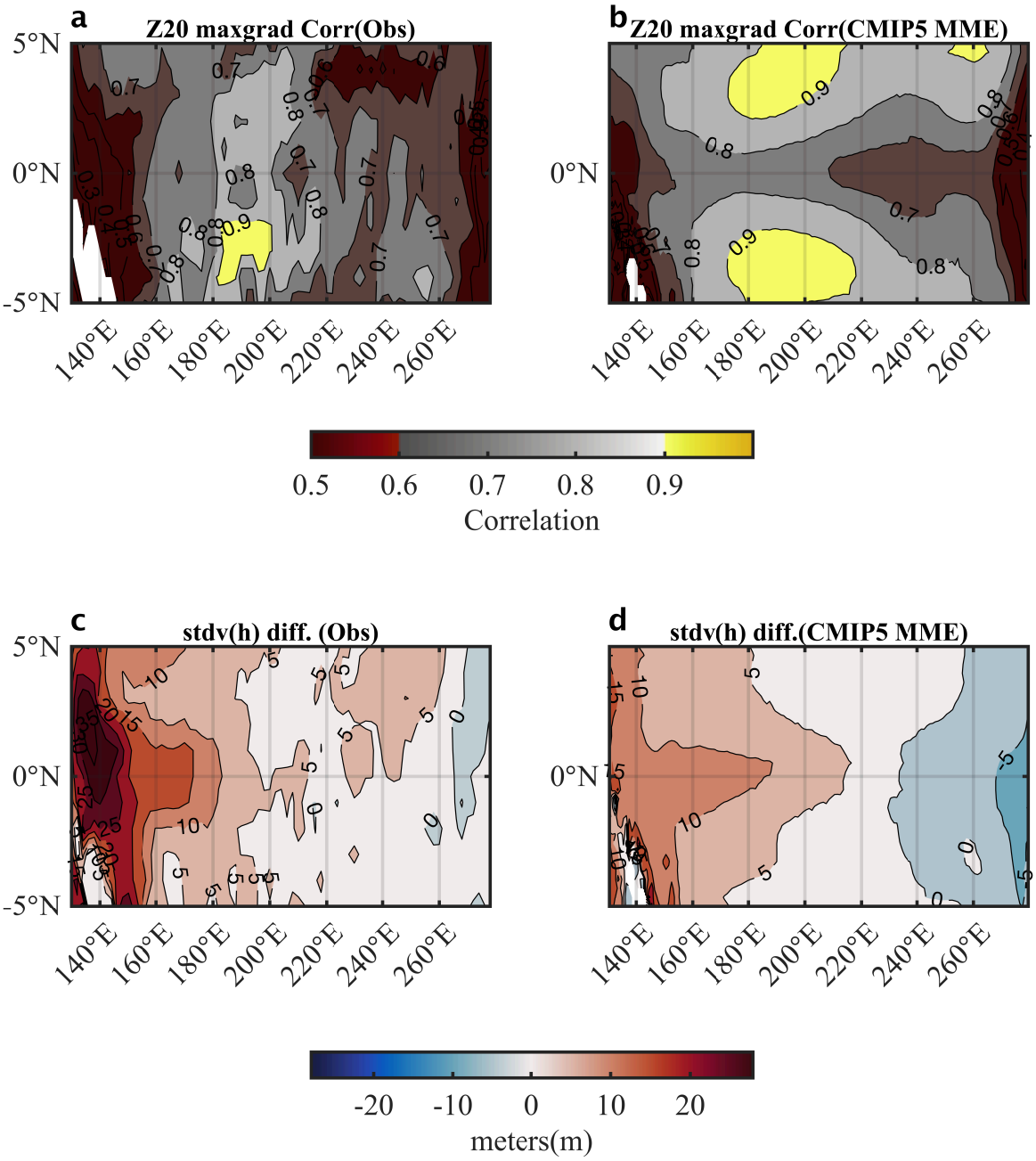

Figure 3.8: Statistics of ENSO variability: Cross correlation between maximum vertical temperature gradient (*maxgrad*) and 20°C isotherm ($Z20$) for **(a)** Observed BMRC data (1980-2011) and **(a)** CMIP5 multi model mean ensemble historical data (1900-1999). Standard deviation of h (stdv(h)) difference between *maxgrad* and $Z20$ for **(c)** Observed BMRC data (1982-2002) and **(d)** CMIP5 multi model mean ensemble historical data(1900-1999).

that thermocline depth anomalies lead$T$ anomalies in time with a longitude dependent delay. Variations in thermocline depth is an important factor for ENSO cycle. Meinen and McPhaden (2000) have shown that the thermocline depth anomalies (related to Warm Water Volume) are precursor to emergence of T anomalies related to ENSO. h and T have less than a month delay (almost in phase) in the eastern Pacific, but in the Central and Western Pacific there is almost 9-10 months delay (significant delay). This h and T correlation structure is also seen with the $maxgrad$ estimates, but the correlation values are significantly lower as compared to $Z20$, indicating different dynamics. The thermocline

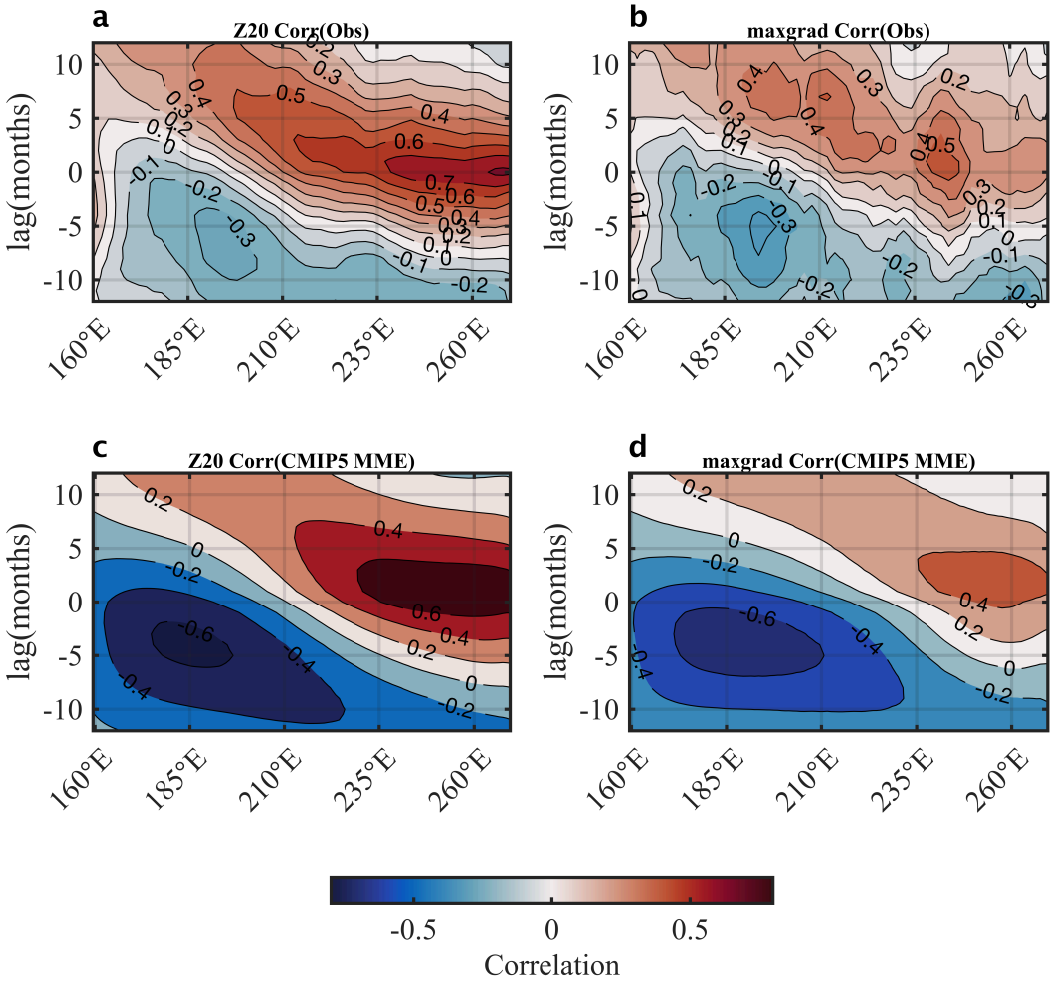

Figure 3.9: **(a)**, **(b)** Lead-lag correlations between observed h and$T$ anomalies for Observed BMRC data (1982-2002) $Z20$ estimates and $maxgrad$ respectively; and CMIP5 multi model mean ensemble historical data(1900-1999).

is shallow in the eastern Pacific hence more substantial correlations than the central Pacific which affects the efficiency of connections between the thermocline and the surface temperature variability.

3.3.3 Dynamical Implications

The linear ENSO dynamics can very well be represented by the ReOsc model parameters (Vijayeta and Dommenget 2018). Hence we can use the model to look for changes in the linear ENSO dynamics due to thermocline depth calculation techniques. Figure 3.10 shows the comparison of the $Z20$ and $maxgrad$ estimates of the ReOsc model parameters and highlights some significant difference in the mean parameters. The $Z20$ estimates of the ReOsc model have a stronger negative growth rate (SST damping; a_{11}) as compared to $maxgrad$ for all models as shown in Figure 3.10(a). The case is different for the h damping (a_{22}), biggest differences can be seen in the h equation parameters. The coupling of$T$ to h (a_{12}) decreases in $maxgrad$ for both models and observations which means that the effect of h ($maxgrad$) on T is weaker than the effect of $Z20$. This could be because the $Z20$ estimates are shallower than the $maxgrad$ hence greater influence on the T . The coupling of h to T (a_{21}) becomes stronger implying the relatively greater influence of T on thermocline depths. The differences in all the four parameters indicates changes in the diagnosis of the ENSO dynamics for the two h estimation techniques. For $maxgrad$ estimates the T damping becomes more positive for some models and h influence on T parameter perhaps contributes to the damping in the T evolution rather than (a_{11}).

In addition, to the ReOsc model parameters, the strength of the noise forcings may change for ζ_h. Figure 3.10 (e), (f) shows changes in stdv(ζ_T) and stdv(ζ_h), the latter changes significantly than the former. This is expected as ζ_T is the T equation residual noise and we use the same T anomaly time series for both sets of parameter estimations. The stdv(ζ_h) is stronger in $maxgrad$ estimates for almost all CMIP5 models and is almost twice the value

for $Z20$ estimates for the observations. This is expected as h residual noise will reflect the same changes as in the h anomaly time series. We have already shown that the standard deviation of h is greater for $maxgrad$ estimates and hence it is reflected in the h noise

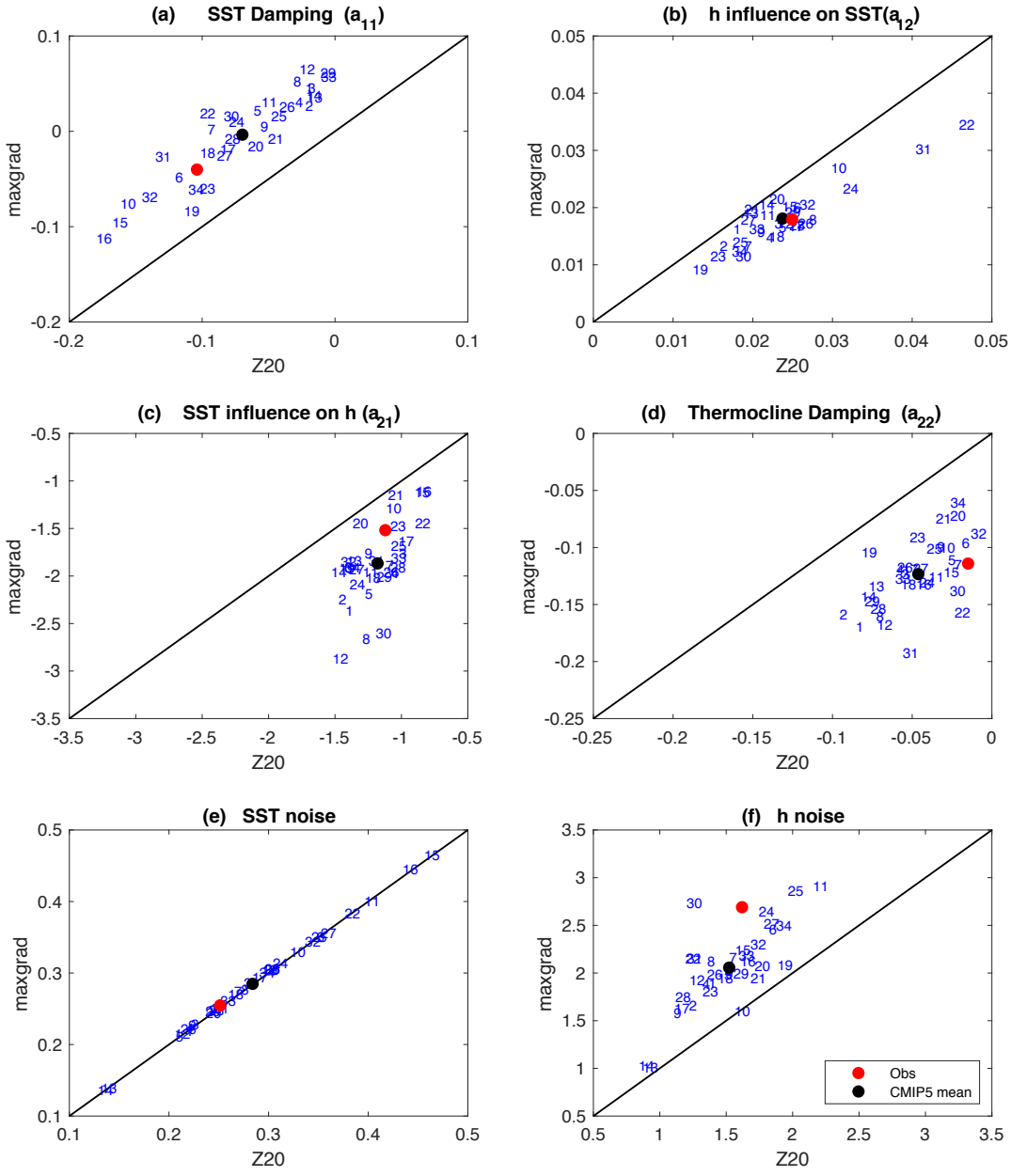

Figure 3.10: Equation (3.1),(3.2) parameters of the ReOsc model for observed CMIP5 models for **(a)**T damping (a_{11}); **(b)**T coupling to h (a_{12}); **(c)** h coupling to$T$ (a_{21}); **(d)** h damping (a_{22}); **(e)** noise forcing for$T$ ($stdv(\zeta_T)$); **(f)** noise forcing h ($stdv(\zeta_h)$). See models and corresponding numbers in Table 3.1

parameter too.

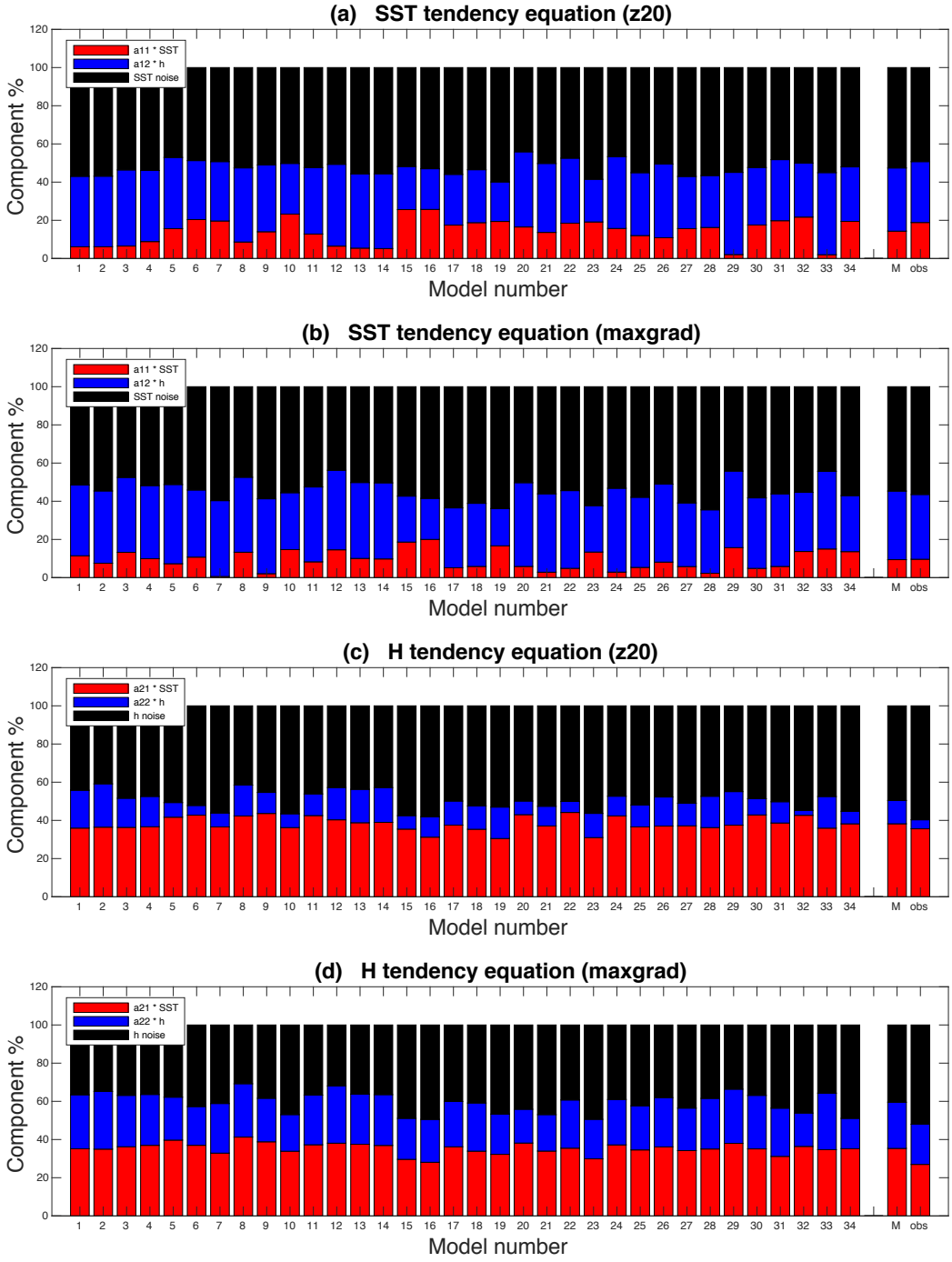

Figure 3.11: Mean percentage contributions of the three rhs terms of Eqs.(3.1),(3.2) of the ReOsc model to (a),(b) the monthly mean dT/dt and (c),(d) the monthly mean dh/dt for CMIP5 models, observations (last bar) and all model mean (second last bar) for $Z20$ and *maxgrad* estimates respectively.

Figure 3.11 provides an alternate way to evaluates the differences in the aforementioned diagnosis of ReOsc ENSO representation when using the $Z20$ and $maxgrad$ estimates respectively. We look at the relative contribution of the three forcing terms in rhs of Eqs. ((3.1),(3.2)). Similar to the analysis in Chapter 2, we estimated the relative contribution of each term by building the mean fraction that each of the three terms contribute to the sum of the absolute values of each monthly mean term. The largest ($\sim 50\%$) contribution to the observed T and h tendencies comes in average from the noise forcings for both $Z20$ and $maxgrad$ estimates, illustrating that ENSO is a strongly noise driven process. The second largest contribution to the observed T tendencies comes from the coupling to h indicating the strong influence of the thermocline variability onto the$T$ variability. This coupling is even stronger than the direct effect of T. For $maxgrad$ estimates the$T$ noise contribution remains more or less same when compared to $Z20$, but instead of the T damping parameter, damping for the oscillatory sytem is dominated by the h influence on T parameter.

Similarly, the tendencies of h are also more strongly forced by the coupling to T and less so by h itself. In this case the thermocline damping contribution to the h evolution equation is stronger, and it comes at the cost of the stochastic noise exciting the system. Interestingly the T influence on h contributions is almost similar for both $maxgrad$ and $Z20$ estimates. The CMIP5 ensemble means are very similar to the observed contributions to the$T$ tendencies.

The ReOsc model parameters a_{11} and a_{21} can be split into an atmospheric and a residual oceanic part following the approach of Frauen and Dommenget (2010). The oceanic contribution to the growth rate of T (a_{11O}) is estimated as the residual of a_{11} after considering the atmospheric part (see Eq. (3.3)). The observed oceanic feedback to T is a strong damping that counter acts the positive atmospheric growth rates leading to the much weaker total damping of a_{11}. Thus, the weak total T damping (a_{11}) is a result of strong positive atmospheric growth rate and strong oceanic damping. The coupling of h to T (a_{21})

can also be split into an atmospheric and oceanic part (see Eqs. (3.5) and (3.6)).

Here in Figure 3.12 the observed a_{21} is dominated by the oceanic part (a_{21O}) with a smaller contribution from the atmospheric part (a_{21A}) for $Z20$ estimates. This is similar in the CMIP ensembles, but the models tend to underestimate the oceanic part and overestimate the atmospheric part. For $maxgrad$ estimates we also see that the atmospheric and oceanic compensation patterns have changed as compared to $Z20$ estimates. This indicates the differences in ENSO dynamics diagnosis, and this dis-similar compensation of error is probably what drives the different contribution of ReOsc model terms in Figure 3.11. From this whole section we can fairly conclude that though the ENSO dynamics are unchanged the diagnosis of ReOSc representation clearly has large differences between the two thermocline depth estimates.

3.3.4 Thermocline depth seasonality

Figure 3.13 (a), (b) shows the seasonality of thermocline feedback which is defined as the correlation between NINO3 T and h anomalies. The red lines are for the $Z20$ estimates and blue lines denote the $maxgrad$ estimates for observations and CMIP5 multi model ensemble mean respectively. The relationship between thermocline depth variability and T is dependent on seasons and is at its lowest during spring. The correlation values for $maxgrad$ estimates are significantly lower for both observations and CMIP5 models, in fact for CMIP5 MME the spring time correlation values are negative. This is consistent with our previous findings that upon using the $maxgrad$ estimates the T - h coupling is weaker which suggests of different ENSO dynamics. Even though the thermocline depth has the strongest persistence during spring, its variations is hard to be communicated to the surface. ENSO prediction skill usually also experiences a significant skill drop during spring (Balmaseda et al. 1994). This is supported by the weakest correlation between T anomalies and $Z20$ anomalies in the Niño3 region during spring (red curve) and for

maxgrad estimates this persistence is stronger (blue curve).

Zhu et al. (2015) showed that the ENSO spring persistence barrier owes its existence not only to the weakest coupling between large-scale T and wind anomalies (Bjerknes feedback) but also to the weakest subsurface-surface connection (thermocline feedback). This study concentrates only on the thermocline feedback, but it has been established that the two feedbacks may partially be dependent upon each other. The T - h seasonal correlation diagnosis is different for both thermocline depth estimation techniques hence will also reflect in the ENSO prediction skill. It should also be noted that the month to month

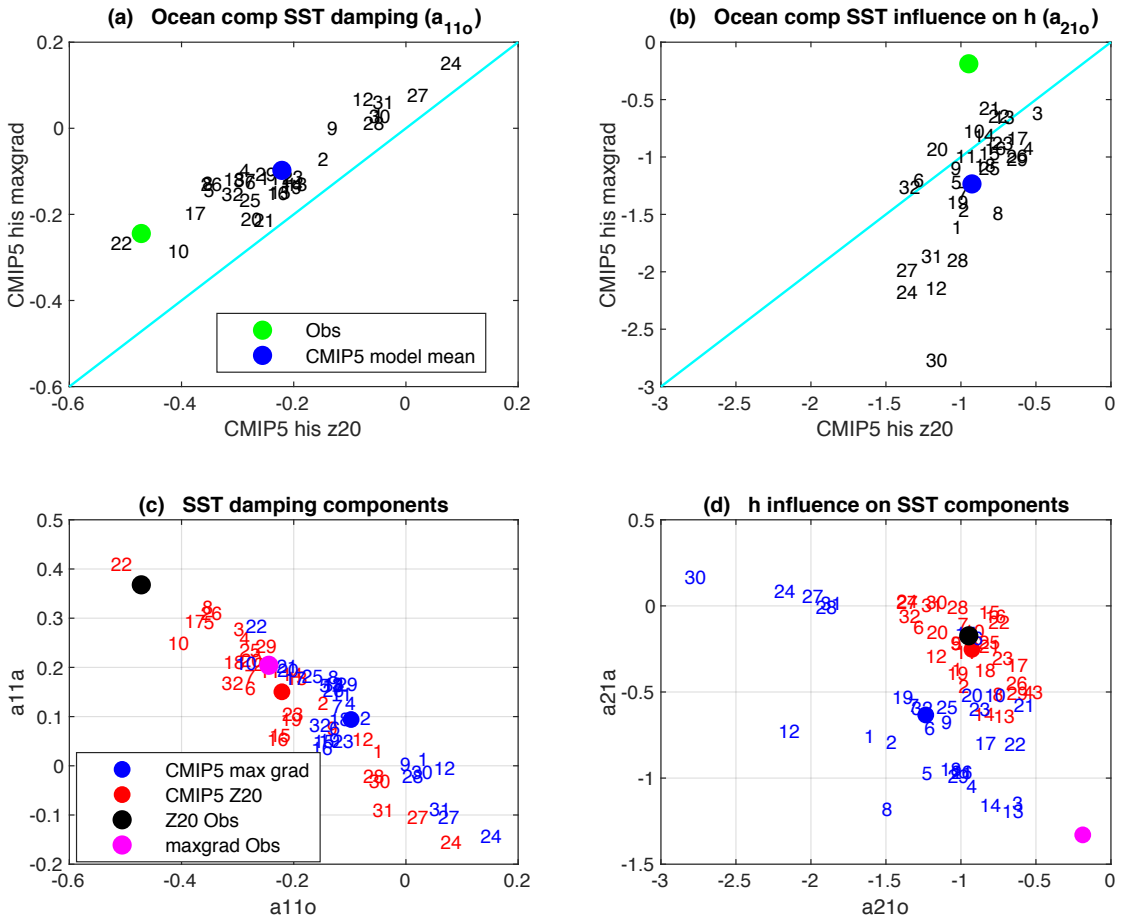

Figure 3.12: ReOsc model parameters of CMIP5 model simulations from Eqs.(3.5),(3.6) for **(a)** Ocean component of T damping (a_{11o}); **(b)** Ocean component of h coupling to T (a_{21o}); **(c)** T damping components (a_{11a}; a_{11o}); **(d)** Components of h coupling to T (a_{21a}; a_{21o}). See models and corresponding numbers in Table 3.1.

change in correlation values are sharper for $maxgrad$ estimates which perhaps is the result of higher standard deviation of thermocline depth.This is more pronounced in the observed values as compared to CMIP5 MME, but also indicated in individual models.The thermocline depth anomalies leading T anomalies have a change in their relationship post 2000 (Meinen and McPhaden 2000) but as this study is limited to 1900-1999 dataset ,it is not investigated here.

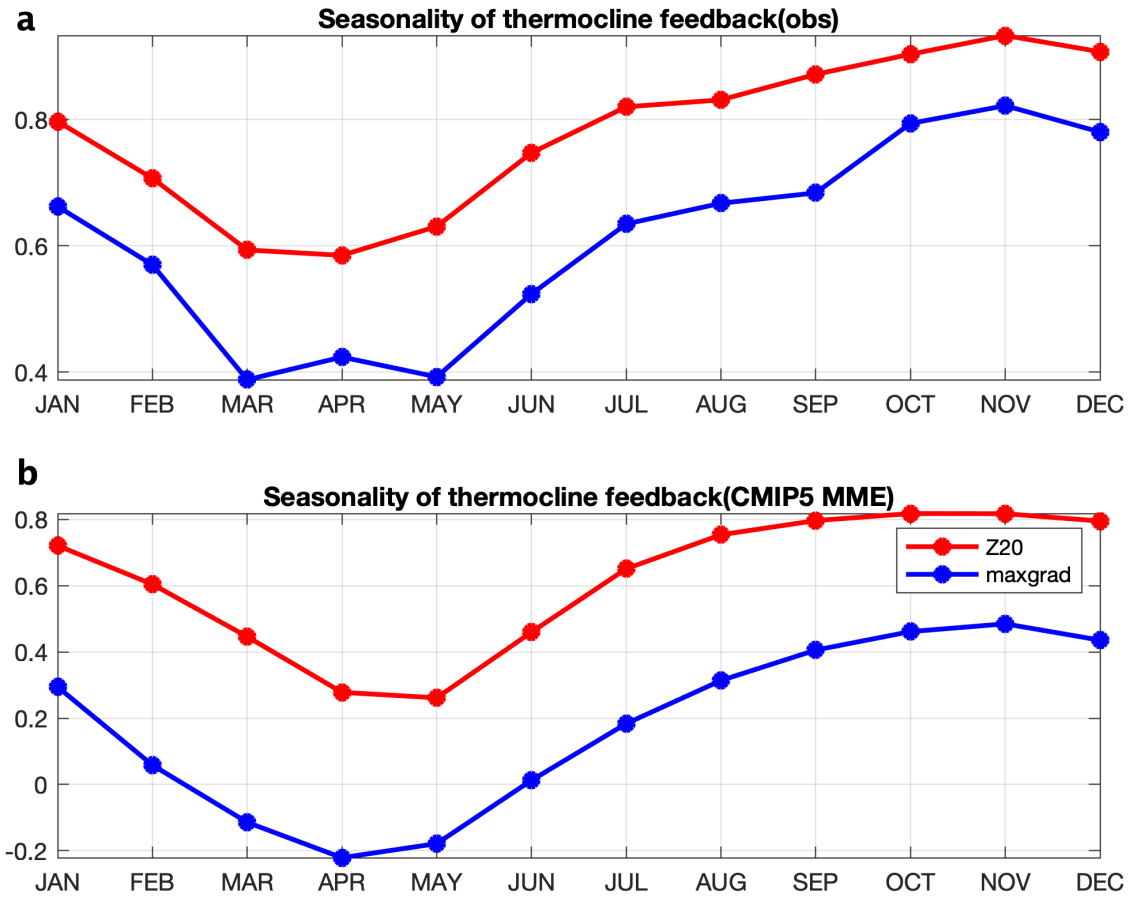

Figure 3.13: Simultaneous correlations as a function of season between h and T anomalies averaged over the Niño3 region for **(a)** Observed BMRC data(Calculations are performed for 1980–2011) and **(b)** CMIP5 MME(1900-1999).The blue lines are for $Z20$ -SST correlation and red lines are for $maxgrad$ estimates.

3.3.5 Sensitivity analysis and Skill score

We analyze the sensitivity of the ENSO statistics to the ReOsc model parameter biases and spreads using the conceptual framework of the ReOsc model. It is computationally efficient to evaluate the relative importance of different parameters or feedbacks biases by integrating the dynamics ReOsc model and analyzing how the ENSO statistic changes. We have already used this approach in Chapter 2 sensitivity analysis. We estimate the sensitivity of an ENSO statistic,σ_k, to a parameter, p_i, of the ReOsc model by integrating

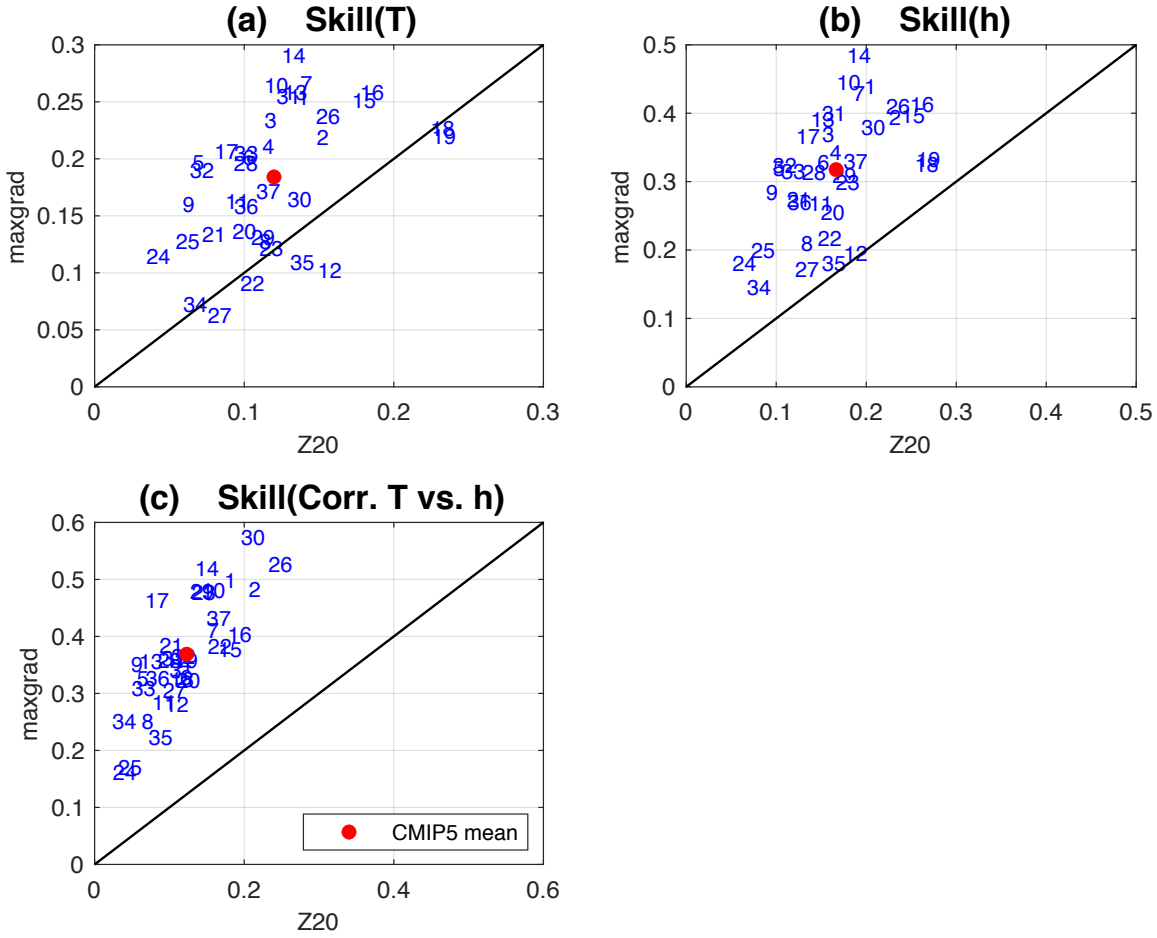

Figure 3.14: Dynamical skill scores of CMIP5 model for different statistical properties. Skill scores for **(a)** stdv(T) (°C) ;**(b)** stdv(h) (m) and **(c)** cross correlation between T and h for lags 4–8 months (h leading T).the values for $Z20$ estimates are on the x-axis and $maxgrad$ estimates on y-axis.

the ReOsc model with all other parameters set to the CMIP ensemble mean parameters and perturbing p_i by a small δp_i. The change in the ENSO statistic, k, relative to the control integration in which all parameters are set to the CMIP ensemble mean parameters gives us an estimate of the sensitivity λ_{ki}:

$$\lambda_{ki} \approx \frac{\delta \sigma_k}{\delta p_i} \tag{3.7}$$

All integrations are done for 1000yrs using the same white noise forcing in all integrations. Here we are estimating the sensitivities to the six parameters from the ReOsc model eq. (3.1),(3.2). By multiplying the sensitivity with a difference in a particular parameter, pi, we can estimate the change in the ENSO statistic ki:

$$\triangle \sigma_{ki} = \triangle p_i . \lambda_{ki} \tag{3.8}$$

It needs to be noted here that we made a first order linear approximation in this approach. However, the ENSO statistics in the ReOsc model are in general not a linear function of the parameters, but do show some non-linear behavior (e.g. changing a11 = 0.1 by $\triangle a_{11}$ = - 0.1 does not have the exact opposite effect of changing it by $\triangle a_{11}$ = + 0.1). It also needs to be considered that the sensitivity of the λ_{ki} will in general depend on the values of all other parameters as well. We can summarize the CMIP model biases relative to the observed ENSO ReOsc model parameters by combining all parameter biases into a normalized skill score, Sσ_{ki}:

$$S\sigma_{ki} = \frac{1}{\sigma_k(obs)} \sqrt{\frac{1}{6} \sum_{n=1}^{6} (\triangle p_n^i . \lambda_{kn})^2} \tag{3.9}$$

with σ_{ki} the skill score for the ENSO statistic σ_k for the model with index i, the model

bias in the parameter p_n relative to observed, $\triangle p_n^i$, and the observed ENSO statistic, σ_k (obs). This skill score is effectively a root mean square error (RMSE) in the six model parameters (a_{11}, a_{12}, a_{21}, a_{22}, stdv(ζ_T), stdv(ζ_h)) scaled by the sensitivity of the ENSO statistics to these parameters (λ_{kn}) in the ReOsc model and normalized by the absolute value of the observed ENSO statistic, σ_k (obs). It thus provides a dynamics-based skill score of ENSO.

We used this skill score approach for evaluating the CMIP3/5 models in chapter 2. Here we use a simpler skill score based on only 6 parameters, from $(3.1)$and (3.2). The main finding from this figure is that when using $maxgrad$ estimates the ReOsc feedback parameters change, and that reflects in the parameters sensitivity to a change. Larger skill score when using $maxgrad$ estimates doesn't mean the models are worse, it simply means while the ENSO dynamics remain same our diagnosis of it's representation in the ReOsc model differs, leading to differences in sensitivity analysis and it gets reflected in a different skill score. We calculate the skill score for the models for all three statistical variables of T, h and T - h cross correlation. For all three properties the $maxgrad$ estimates have worse scores as compared to $Z20$ estimates.

3.3.6 Predictibility

Figure 3.15(a) and (b) shows the plot of NINO3 T anomalies and equatorial Pacific h anomalies for observations and one CMIP5 model respectively. The graphs exhibit an elliptical shaped orbit centered at origin and rotating clockwise. The starting points of the trajectory are marked as a and end points as b, for observations we show 21 years data until 2002 and for the CMIP5 model a snapshot of roughly 16 years is shown. The data has been smoothed using a moving average method, which is equivalent to using a low pass filtering where each datapoint is replaced by average of neighbouring data points. The ellipticity and rotating direction depends on lag between SST and h anomalies, a smaller

lag makes the orbit more elliptical. The recharge discharge mechanism can be explained as follows, an initial positive SST anomaly induces Westerly wind forcing over the central and western Pacific. The thermocline deepens in the Eastern Pacific, which results in a positive feedback amplifying the SST anomaly until oscillation reached a mature phase. At the same time thermocline reduces in the western Pacific which leads to discharge of heat content, reducing eastern Pacific thermocline depth. This transition allows for the upwelling of cold water which in turn enforces negative SST anomaly. As a response to cold SST anomaly western Pacific thermocline deepens and there is recharge of equatorial heat content. The zonal mean equatorial thermocline depth is essential in forming the coupled recharge oscillator and the time delay between h and SST depends on dynamics of the coupled model and noise forcing. For the Figure 3.15 (c) and (d) using the ReOsc model we generate T and h time series while keeping the stochastic noises constant. We generate the $Z20$ and $maxgrad\,T$ - h phase relationships for all models and we have similar characteristics as results. The $Z20$ T - h phase diagrams are more closer to the theoretical recharge discharge oscillator and the $maxgrad\,T$ -h phase diagrams are more asymmetric with T leading thermocline depths. This is again preliminary results and we need to tune and scale our parameters.

In Figure 3.12 (a) it can be seen that when thermocline depth anomalies are estimated using different techniques the diagnosis of ENSO dynamics representation differs from one another. The differences in the $maxgrad$ and $Z20$ estimates are primarily due to thermocline depth variations and not noise forcings as we have already shown in Figure 3.6 that the noise forcings aren't very different for the two estimation techniques. In the case of $Z20$ estimates due to the greater lag the recharge and discharge of heat content is slower as opposed to $maxgrad$ estimates.

Figure 3.16 uses a simple regression equation with thermocline depth anomaly as the predictor and SSTA as the predictand to predict T anomaly upto 24 months. The regres-

sion model is only using h and not T. Therefore when the lag-correlation is zero, then the model will have no skill, as we can see for lag=4 with maxgrad. We are using this only as a preliminary analysis to look for differences in the $Z20$ and $maxgrad$ estimates. The figure has SST anomaly forecasts for each CMIP5 model and the model mean ensemble is highlighted. In this figure the blue line points to $Z20$ and the red line is for the $maxgrad$ estimates. The $maxgrad$ estimates has a lag 0 correlation, so we can use the T - h correlation for predictions for the first two months while $Z20$ has prediction skills beyond two months. The differences in the prediction skill at different lead months for the two estimates allows us to make a choice depending on the lead month we need to forecast.

3.4 Summary and discussions

In this chapter, we investigated the accuracy of using the 20°C isotherm ($Z20$) as a thermocline depth proxy for ENSO studies instead of using the original definition of maximum gradient of temperature ($maxgrad$). We started our analysis by looking at the differences in the mean Pacific thermocline depths when calculated using $Z20$ and $maxgrad$ estimates.

Our results indicated that the $maxgrad$ and $Z20$ estimates have similarity as well as differences while representing the thermocline depths. In some models $Z20$ estimates is incapable of capturing the effect of ocean warming on thermocline depths. The analysis was further focused on the thermocline depth variability and we found that stdv(h) slightly increases while the mean 4-8 months correlation decreases for $maxgrad$ estimates as opposed to $Z20$ estimates in both observations and all CMIP5 models. The thermocline depths estimated using $maxgrad$ approach exhibited more variability than $Z20$ estimates.

For the power spectrum analysis of thermocline depth, we found that for longer timescales the $Z20$ and $maxgrad$ estimates evolve similarly with $maxgrad$ estimates having higher variance for both observations and individual CMIP5 models. For shorter time

scales the $maxgrad$ estimates have greater variance which means they are more noisier and this correlates with the higher standard deviation of $maxgrad$ estimates. We then investigated the correlation between T and h and found that observed time evolution of h leads that of T by about 5–6 months (peak of cross-correlation) for the $Z20$ estimates and about 7-8 months for the $maxgrad$ estimates. The observed T and h ($Z20$) correlation have a more pronounced out of phase relationship as compared to the observed T and h ($maxgrad$) correlation. This is evident in the historical CMIP5 simulations as well where T and h ($Z20$) have a very clear out-of-phase relation, with a strong positive correlation when h leads T and a roughly equally strong negative correlation when T leads h at about the same lead time of 5–8 months and overall increase in correlation at the peak. This indicated that the ENSO recharge and discharge mechanism is different between the two estimation techniques, which is the fundamental basis of the ReOsc model.

Using the ReOsc model, we next diagnosed ENSO dynamics for both cases and found that $Z20$ estimates have stronger T damping, stronger h influence on T , weaker h damping and weaker T influence on h in comparison to $maxgrad$. The differences in the dynamical parameters and the change in the atmospheric and ocean parameter compensation indicated substantial differences in the ENSO dynamics diagnosis representation for the two h estimation techniques. Furthermore, the larger standard deviation of h for $maxgrad$ also manifests in the T - h phase relationships with the $Z20$ estimates being more similar to the theoretical recharge oscillator and the $maxgrad$ T - h phase diagrams are more asymmetric with T leading thermocline depths. The main conclusion was that there is substantial differences in the ENSO dynamics representation diagnosis when using the two thermocline estimation techniques, and when using $maxgrad$ estimates it was clear that thermocline may not have that much of a stronger influence on driving T as suggested by current literature.

This chapter is based on preliminary findings and calls for further analysis. We intend

to address few interesting questions in our future work. The first would be to examine the relationship between maxgrad and other more frequently used measures of upper-ocean heat, such as the heat content (vertically-averaged temperature, say over the top 300 m) and warm water volume. We suspect the warm water volume and upper ocean heat estimates to be similar to maxgrad rather than Z20. We would also need to look closely as to why the spectra in Fig. 3.5 differ between maxgrad and Z20 and the implications about the time scales of variability present at different depths and longitudes. The huge change in zero-lag correlation in Fig. 3.6b is also interesting, and deserves investigation; we intend to look at the recharge/discharge process, and the time scales of conveyance (upwelling/mixing) of subsurface temperature anomalies into the surface layer.

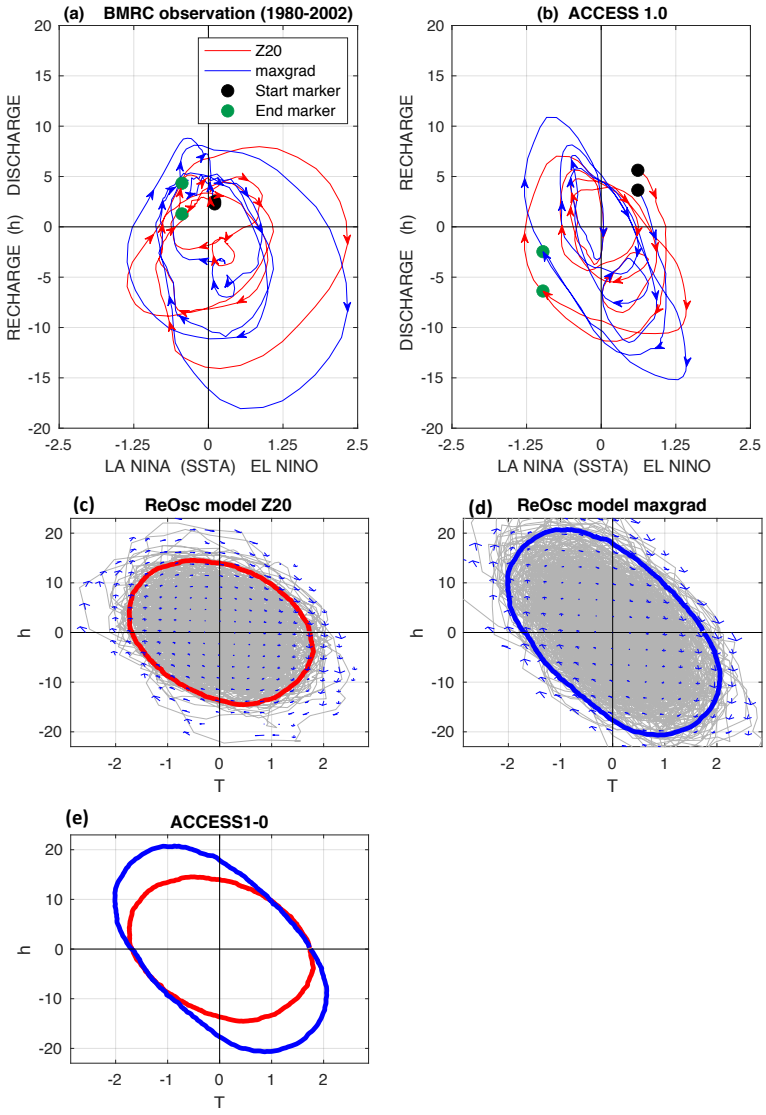

Figure 3.15: Phase orbits of **(a)** Observed data and **(b)** CMIP5 ACCESS1-0 historical data(1900-1999).The T As are plotted on x-axis and h anomalies are plotted on y-axis.a,b denotes the starting and end points respectively. The red lines are for $Z20$ and blue lines represent $maxgrad$ estimates.

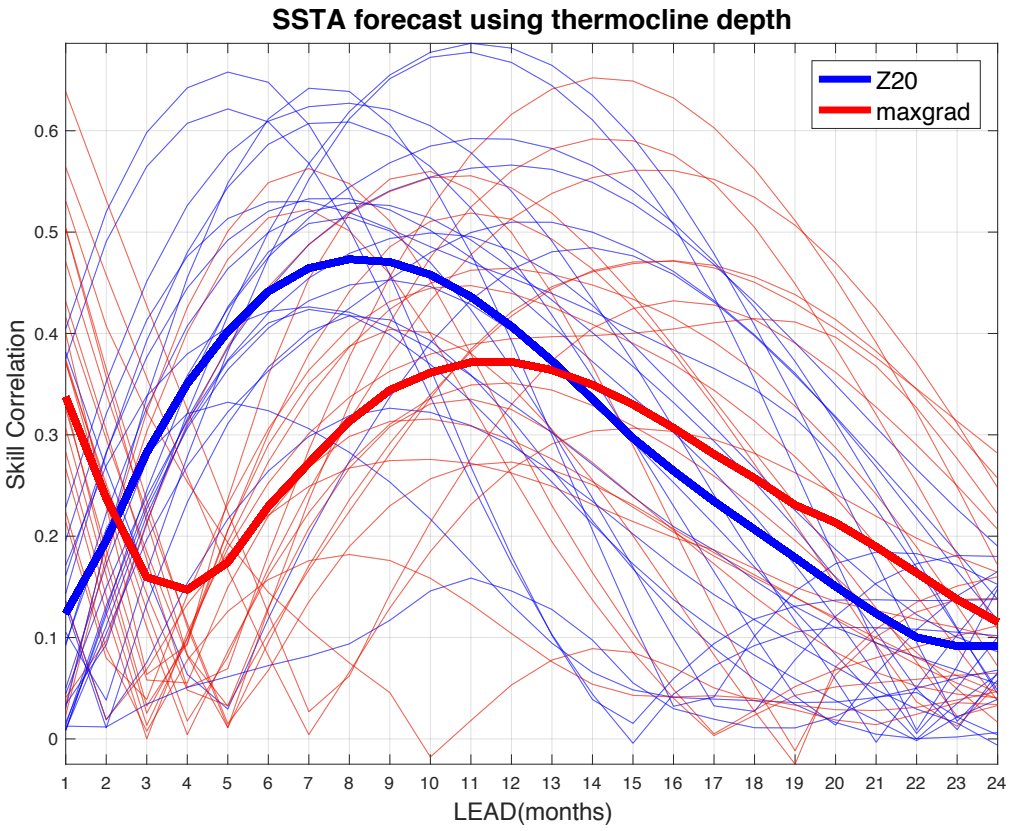

Figure 3.16: SST anomaly predictability using the ReOsc model for CMIP5 multi model mean ensemble historical data(1900-1999).

Chapter 4

Simulated future changes in ENSO dynamics in the framework of the linear recharge oscillator model

This thesis chapter originally appeared in the literature as

Dommenget, D., Vijayeta, A., *Simulated future changes in ENSO dynamics in the framework of the linear recharge oscillator model. Clim Dyn 53, 4233–4248 (2019). https://doi.org/10.1007/s00382-019-04780-7*

4.1 Introduction

Anthropogenic climate change not only alters the mean state climate, but also potentially affects the nature of internal climate variability. How in detail the internal variability will change is an important question of anthropogenic climate change research. In particular, the potential changes in the most important mode of natural climate variability, the El Niño Southern Oscillation (ENSO) mode, are still a subject of current research (Collins et al. 2010; Cai et al. 2015b).

Previous studies on changes in the ENSO variability primarily focussed on changes in ENSO statistics, such as the standard deviation ($stdv$) of the sea surface temperature (SST) variability, the power spectral peak of SST (periodicity) or the changes in the pattern of ENSO SST variability (Van Oldenborgh et al. 2005; Yeh et al. 2009; Collins et al. 2010; Stevenson et al. 2012; Chen et al. 2017). Studies of future climate change with simulations from the couple model intercomparison project (CMIP) found mostly little changes in these statistics. The overall stdv of ENSO in the CMIP ensemble mean is not changing significantly and the periodicity of ENSO is also not changing significantly. However, there is large spread in the CMIP ensemble with individual models showing clear trends in these statistics, but with opposing directions, averaging to a near zero ensemble mean result.

A number of studies have analysed changes in recent observed ENSO variability (Lee and McPhaden 2010; McPhaden et al. 2011; McPhaden 2012; Lübbecke and McPhaden 2013; Guan and McPhaden 2016; Capotondi and Sardeshmukh 2017). These studies suggest that ENSO statistics, dynamics and the pattern have been changing in the recent decades relative to previous decades. A recent study by Zhao et al. (2016) also suggests that the predictability of ENSO is decreasing in recent decades, indicating changes in the dynamics of ENSO. Whether these changes are consistent with the CMIP model projec-

tions is, however, unclear. Here it also needs to be considered that changes in observed ENSO characteristics are typically based on a relatively short time period, which will make it difficult to distinguish such variations from natural internal low-frequency variability (Wittenberg et al. 2014).

Much of these observed changes in ENSO are linked to changes in the tropical Pacific mean state (McPhaden et al. 2011; Zhao et al. 2016). These mean state changes themselves have been analysed in several studies (Liu et al. 2005; Vecchi et al. 2006; DiNezio et al. 2012; England et al. 2014; Bayr et al. 2014; Luo et al. 2015, 2016, 2018; Kohyama et al. 2017). Many of these studies find large differences between observed trends and those project by CMIP simulations. In particular, the changes in the Walker circulation and associated winds, and changes in the equatorial mean SST pattern are inconsistent between recent observations and CMIP model projects. These diverse results are further complicated by the fact the current climate model simulations of ENSO have significant common biases in the underlying processes and dynamics (Bellenger et al. 2014; Vijayeta and Dommenget 2018).

Some studies analysed the dynamical changes of ENSO in CMIP3 and CMIP5 model simulations (Kim and Jin 2011; Chen et al. 2015). Both studies analysed heat budget terms of tropical Pacific SST. Kim and Jin (2011) found significant change in elements of ENSO dynamics, that due to competing effects lead to no changes in the stability of ENSO. Chen et al. (2015) explored the dynamical elements that lead to changes in ENSO amplitude. They found that change in the thermocline and zonal advection feedback are the main drivers in ENSO amplitude changes.

The combination of the above-mentioned studies on changes in ENSO variability, we find a fairly diverse picture, with inconsistencies between recent observations and models, between different model simulations and significant model biases in the ENSO dynam-

ics. Given these uncertainties, it is instructive to gain a better dynamical understanding of the changes in the ENSO variability. We therefore focus in this study on the changes in dynamics of the ENSO mode in future climate change simulations.

The analysis of the ENSO dynamics presented in this study will be based on the linear recharge oscillator (ReOsc) model (Jin 1997a; Burgers et al. 2005; Jansen et al. 2009). The ReOsc model is a very effective way of describing the essential elements of the ENSO dynamics, such as the SST growth rate and the coupling to the SST to the thermocline depth, which represents the delayed negative feedback leading to the observed oscillating nature of ENSO. It can be used as an effective diagnostic tool to estimate these important dynamical elements of ENSO based on the outputs of model simulations or observations. It can further be used to understand how changes in important dynamical aspects, such as the wind-SST feedback affect ENSO statistics. Vijayeta and Dommenget (2018) has illustrated in a recent study that the ReOsc model describes the ENSO dynamics and statistics in the diverse CMIP ensembles very well.

This chapter is organized as follows: the next Section 4.2 introduces the CMIP model data, the ReOsc model equations and how it is used to estimate the ENSO dynamics. It also discusses some of the limitations in this approach. Section 4.3 presents the main results of this study, starting with analysis of the thermocline depth, some simple ENSO statistics followed by an analysis of the ReOsc dynamics, which is the main focus of this study. The section will be concluded with a look at possible changes in the predictability. The last section 4.4 provides a summary and discussion.

4.2 Data, models and methods

4.2.1 CMIP5 model simulations

The analysis is based on CMIP5 model simulation of the historical and the RCP8.5 scenario (Moss et al. 2010; Taylor et al. 2012). We use all model simulations that have all variables available needed for this analysis. These are 25 model simulations, see Table 4.1. The historical scenario over the period from 1881 to 1980 is considered as the control climate. The RCP8.5 from 2051 to 2100 is considered for the climate change period. All data is linearly detrended and anomalies relative to the mean seasonal cycle are defined.

4.2.2 The recharge oscillator model

The linear ENSO dynamics are evaluated on the basis of the ReOsc model from Burgers et al. (2005); Frauen and Dommenget (2010); Vijayeta and Dommenget (2018). This model is given by two tendency equations of the NINO3 region (150°W–90°W, 5°S–5°N) SST anomalies, T, and equatorial Pacific (130°E–80°W, 5°S–5°N) mean thermocline depth anomalies, h:

$$\frac{dT(t)}{dt} = a_{11}T(t) + a_{12}h(t) + \zeta_T \tag{4.1}$$

$$\frac{dh(t)}{dt} = a_{21}T(t) + a_{22}h(t) + \zeta_h \tag{4.2}$$

The model parameters a_{11} and a_{22} represent the growth rate (or damping) of T and h, and the parameters a_{12} and a_{21} the coupling between T and h. The two equations are forced by stochastic noise terms ζ_T and ζ_h. The parameters of the 2-dimensional model Eqs. (4.1), (4.2) are estimated for each CMIP5 model simulation by multivariate linear regression the monthly mean tendencies of T and h against monthly mean T and h, respectively, following

Table 4.1:: List of CMIP5 models used in this study, the numbers in this table refer to the numbers used in the figures

Model
1. ACCESS1-0
2. ACCESS1-3
3. BNU-ESM
4. CESM1-BGC
5. CESM1-CAM5
6. CMCC-CM
7. CNRM-CM5
8. CSIRO-Mk3-6-0
9. CanESM2
10. GFDL-CM3
11. GFDL-ESM2G
12. GFDL-ESM2M
13. GISS-E2-H-CC
14. GISS-E2-H
15. GISS-E2-R-CC
16. GISS-E2-R
17. IPSL-CM5A-LR
18. IPSL-CM5A-MR
19. IPSL-CM5B-LR
20. MIROC-ESM-CHEM
21. MIROC-ESM
22. MIROC5
23. MRI-CGCM3
24. NorESM1-ME
25. bcc-csm1-1

the approach in previous studies (Burgers et al. 2005; Jansen et al. 2009; Vijayeta and Dommenget 2018).

The ReOsc model approach is different from the widely used Bjerknes stability (BJ) index or similar SST heat budget analysis (Jin et al. 2006; Kim and Jin 2011; Chen et al. 2015). The terms of the BJ-index analysis can in most cases not be directly related to the parameters of the ReOsc, and it only discusses SST stability. In turn, the advantage of the ReOsc model is that the dynamical parameters of the model can be more directly linked to the ENSO variability statistics, such as standard deviation (stdv) of T, stdv(h), the power spectrum or coupling between T and h, by integrating the ReOsc model equations (Vijayeta and Dommenget 2018).

The residual of the linear regression fit for the ReOsc model can be interpreted, as the random noise forcings with the stdv of the residuals being the stdv of the noise forcings for the T and h equations (ζ_T and ζ_h). However, it also needs to be considered that this simple linear model fit does not fully represent the ENSO dynamics in the models. Mismatches between the true, more complex, dynamics and the ReOsc model fit will also project onto the residual noise terms of the model. Vijayeta and Dommenget (2018) did evaluate the goodness of fit to the CMIP model. They found that the residual noise terms fit well with the white noise assumption, but they also do show some indications of the linear ReOsc model does not fully represents the ENSO dynamics in the CMIP models, leading to some enhanced spread in the noise terms.

The thermocline depth (h) marks the depth at which the vertical temperature gradients are largest, see sketch in Fig. 4.1. It is often estimated on the basis of the depth of 20 °C isotherm (Z20), because this is a more robust approximation when the data is of coarse resolution (Meyers 1979; Kessler 1990; Smith 1995; Yang and Wang 2009). Studies of future climate change simulations often used the maximum in the temperature gradients to

estimate the thermocline depth (Vecchi and Soden 2007; Yeh et al. 2009). Previous studies with the ReOsc model used Z20 to estimate the thermocline depth (h) (Burgers et al. 2005; Jansen et al. 2009; Vijayeta and Dommenget 2018).

However, this poses a problem when studying climate change, because a uniformly warming temperature profile will not change the thermocline depth, but will lead to deeper Z20 (Yang and Wang 2009), see sketch in Fig. 4.1. This may potentially lead to artificial changes in the ReOsc model dynamics, even though nothing may have changed in the dynamics. To address this problem, we evaluate the ENSO dynamics and the ReOsc model parameters on the basis of both, a Z20 and a maximum gradient (maxgrad) estimate of the thermocline. Both estimates are based on high-resolution (0.1 m) spline fits of the CMIP5 simulation temperature profiles. In the following analysis, we will use the maxgrad estimate for the thermocline depth if not otherwise noted.

The growth rate of T (a_{11}) in the ReOsc model can be split into an atmospheric (a_{11A}) and oceanic contribution (a_{11O}) following the approach of (Frauen and Dommenget 2010; Vijayeta and Dommenget 2018):

$$a_{11} = a_{11A} + a_{11O} \tag{4.3}$$

The atmospheric growth rate of T (a_{11A}) is estimated as a linear combination of atmospheric heat flux feedback (C_{fT}), the wind-stress (Bjerknes) feedback ($C_{\tau T}$):

$$a_{11A} = a_{12}\lambda C_{\tau T} + \frac{C_{fT}}{\gamma} \tag{4.4}$$

$C_{\tau T}$ is the linear regression of zonal wind stress, τ_x, in the central Pacific region (160°E–140°W, 6°S–6°N) and T, and C_{fT} is the linear regression of net atmospheric heat

flux in the NINO3 region and T. λ is a positive free coupling parameter and the ocean mixed layer depth that are assumed to be constant for all simulations (Vijayeta and Dommenget 2018). a_{11O} is estimated as the residual growth rate:

$$a_{11O} = a_{11} - a_{11A} \tag{4.5}$$

Vijayeta and Dommenget (2018) provided a proof of concept, illustrating this ReOsc model approach. They found, for instance, that the ReOsc model is capable in reproducing the CMIP model simulations stdv(T) with correlation of 0.99 by integrating Eqs. (4.1),(4.2) with the estimated model parameters. Similarly, other important statistics, such as stdv(h), the cross correlation between T and h or the power spectral slope (see section below for a definition) are also reproduced very well (correlation > 0.8) with this approach. However, the model does have some limitations and it does make some simplifications. Some notable limitations are, as discussed in Vijayeta and Dommenget (2018): The power spectral distribution of variance is wider in the CMIP model simulations than it is simulated in the ReOsc fitted to the CMIP models. The cross-correlation between T and h is slightly overestimated in the fitted ReOsc models, and, as mentioned above, the residual noise forcing terms are not just white noise forcings, but do partly reflect more complex dynamics that are not captured by this linear ReOsc model approach.

Important simplifications of the ReOsc model: It is a linear approach and therefore does not consider non-linearity in the ENSO dynamics or state dependent noise forcings. Further, the model describes ENSO in a one-dimensional SST index (T), therefore neglecting ENSO diversity in respect to regional differences in the ENSO amplitudes (e.g., central Pacific vs. east Pacific events).

4.2.3 Estimation of sensitivities with the recharge oscillator model

The sensitivity of ENSO statistics to changes in the ReOsc model parameters can be estimated by integrating the ReOsc model with white noise forcing (Vijayeta and Dommenget 2018). We therefore integrate the ReOsc model for 1000 years with all parameters set to the mean values of the historical simulations. Based on the resulting T and h time series we compute the control ENSO statistics. In a second integration, we use the same white noise forcings, but change one or all of the ReOsc model parameters to the mean values of the RCP8.5 simulations. Based on the resulting T and h time series we compute the RCP8.5 ENSO statistics, and the differences to the control simulations provides us an estimate of the sensitivity to the parameter changes. Given that we used the same white noise forcings in both integrations, these estimates have no statistical uncertainties from the integrations.

4.2.4 The power spectral slope

The spectral power slope is a non-dimensional characteristic of a power spectrum that effectively captures the time scale behaviour. Following the approach of Vijayeta and Dommenget (2018) we estimated the slope (in log-scale) from 1 to 7 years period to capture the range of the power spectrum in which the variance is strongly increasing with period (decreasing with frequency) and where the ENSO variance peaks. Simulations with a more pronounced interannual peak tend to have steeper slopes (more negative), and those with a less pronounce interannual peak or a shift towards low-frequencies tend to have a less steep slope (less negative). The spectral power slope therefore captures changes in the time scale behaviour or periodicity relatively well. This is in particular true for a damped oscillation as described by the ReOsc model.

We tested this approach in a wide range of different CMIP simulations and ReOsc models (Eqs. (4.1),(4.2)) integrated with different parameters and found this metric to be the best fit to describe variations of the peak of the power spectrum. An increased (less step or more flat) slope in these simulations corresponds, in statistical average, to a shift in the peak towards lower frequencies. In turn, a decreased (stepper or less flat) corresponds, in statistical average, to a shift in the peak towards higher frequencies. However, it needs to be noted that it is only one parameter describing a power spectrum that has more than one degree of freedom. Therefore, changes in the power spectrum can occur that are no capture by this parameter.

4.2.5 Estimates of uncertainties

In the following analysis, we will estimate uncertainties in the ENSO statistics and the ReOsc model parameters in two ways: First, we will provide a confidence interval for the statistical significance in changes from the historical to the RCP8.5 simulation for each individual model. Second, we will provide a confidence interval for changes in the ensemble mean values.

The 95% confidence interval for all parameters based on regressions (e.g., ReOsc model parameters and power spectral slope), are estimated for each model for the 50 years period of the RCP8.5 simulations. However, instead of presenting the confidence interval for each individual simulation we only show the mean 95% confidence interval of the ensemble in reference to the one-to-one line (e.g. see Figs. 4.5, 4.6, 4.7). This effectively illustrates if individual model parameters have changed from the historical to the RCP8.5 simulations. For uncertainties in the standard deviations, we followed a Chi squared distribution approach and assumed that the confidence interval is proportional to the expectation value (e.g. see Fig. 4.5a). The ensemble mean uncertainties are presented by 95% confidence interval of a Students t test, assuming that each simulation represents an independent

sample (e.g., see red line in Fig. 4.5a).

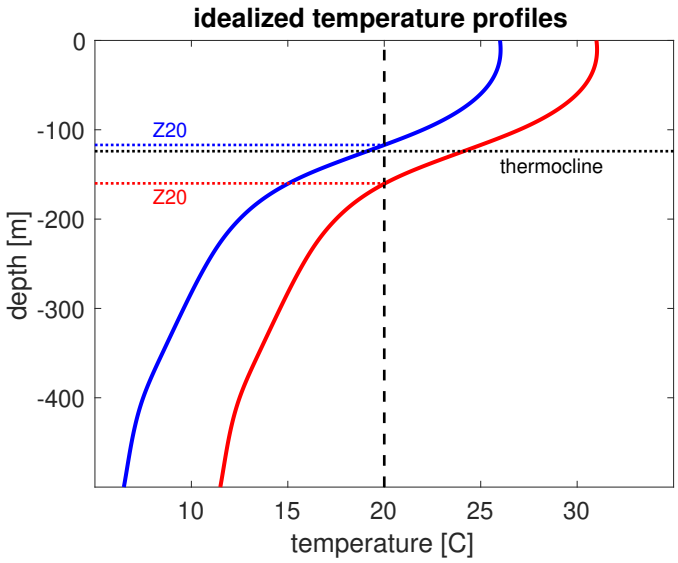

Figure 4.1: Sketch of idealised temperature profiles, Z20 and thermocline depth (maxgrad). The blue and red temperature profiles are identical with the only difference of a constant off set of 3 °C. The thermocline depth is the same for both profiles, but Z20 is deeper in the warmer profile

4.3 Results

4.3.1 Thermocline depth changes

The thermocline depth is one of the two dynamical variables of the ReOsc model, representing a proxy of upper ocean heat content. Mean state changes in the thermocline depth can affect the dynamics of ENSO, but potentially will also affect the estimation of the thermocline depth by Z20 (see sketch in Fig. 4.1). It is therefore a good starting point for the analysis of the dynamical changes of ENSO.

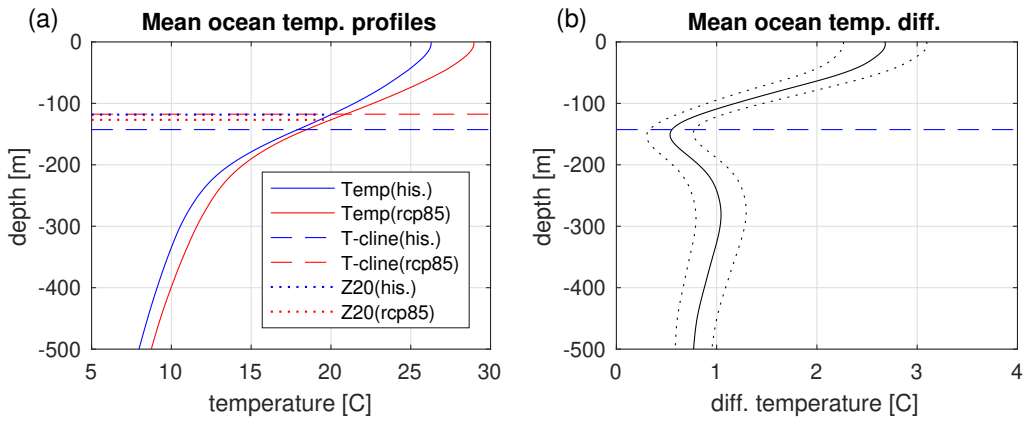

Figure 4.2: (a) CMIP5 equatorial Pacific mean (150°E–80°W, 5° S-5°N) temperature profiles of the historical (blue) and RCP8.5 (red) scenario. Estimates of the thermocline depth (maxgrad) and Z20 are shown as well. (b) Difference in the temperature profiles. The dotted lines mark the 95% confidence interval

Figure 4.2 shows the mean temperature profiles of the equatorial Pacific for the historical and RCP8.5 CMIP5 ensemble mean together with thermocline depth estimates. The temperature profile warms on all levels, but the warming is not uniform with depth, see Fig. 4.2b. The strongest warming is at the surface and the least amount of warming is very close to the mean thermocline depth of the historical simulations,followed by stronger warming in deeper layers. This profile is very different from what may have been expected from a transient or equilibrium warming (Manabe et al. 1991; Yoshimori et al. 2016). It suggests a dynamical adjustment of the upper equatorial Pacific, which leads to reduced warming at the thermocline depth.

The thermocline depth becomes shallower in the RCP85 scenario, which is due to the fast warming at the surface layers. This is consistent with the results of previous studies of simulated future thermocline depth changes (Vecchi and Soden 2007; Yeh et al. 2009; Kim and Jin 2011; Chen et al. 2015). In turn, Z20 does deepen, but not as much as one may have expected from a homogenous warming. This is due to the minimum of warming at

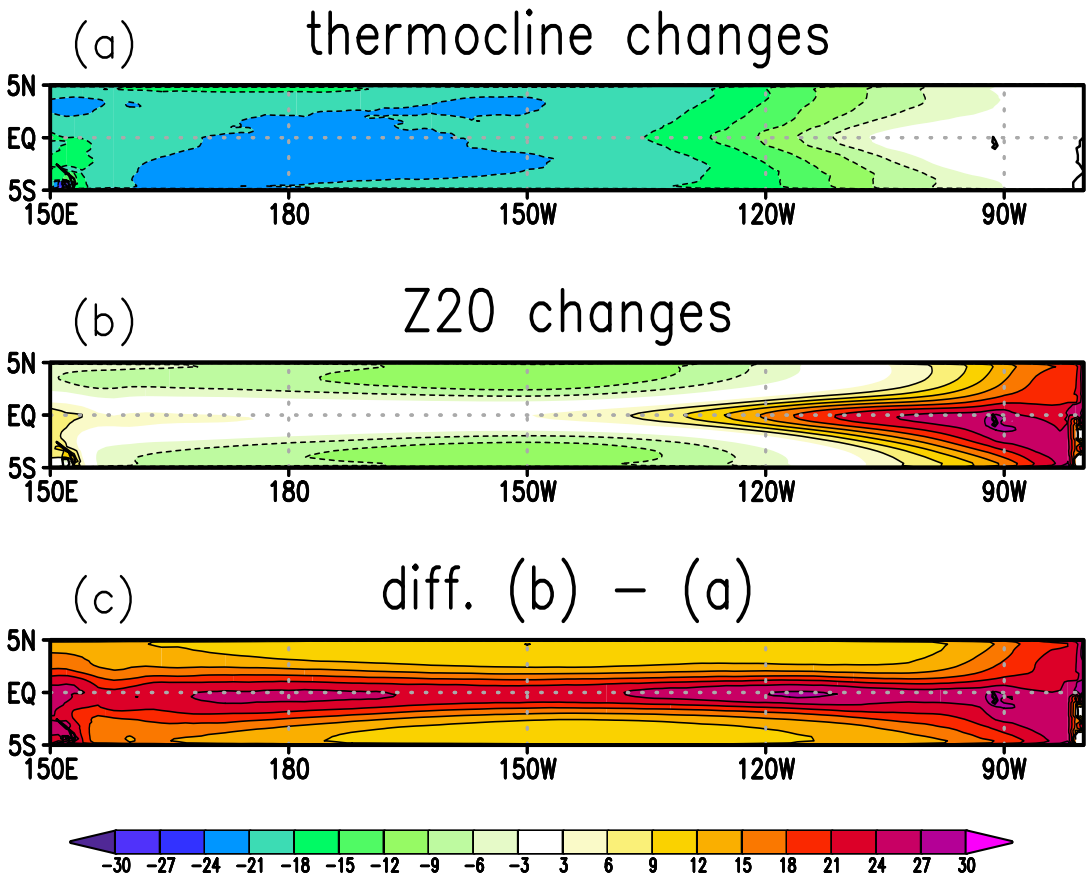

Figure 4.3: Mean changes in (a) the thermocline depth (maxgrad)and (b) Z20 for CMIP RCP8.5 minus historical simulations over the equatorial Pacific domain. (c) Is the difference of b–a. Negative values indicate shallower thermocline depth in the RCP8.5 simulations. Values are in m

the thermocline, which counteracts the deepening of Z20.

The different behaviour of the thermocline depth and Z20 is also reflected in the regional changes of the equatorial Pacific, see Fig. 4.3. The thermocline depth decreases relatively uniformly, but more in the central and west Pacific, and less in the east Pacific. Z20 shows a fairly different behaviour. It strongly deepens in the eastern Pacific and slightly along the equator. Off the equator Z20 becomes shallower, in contrast to what you would expect from a warming temperature profile. Upper layers (above Z20) of the off-equatorial

central Pacific cool (not shown), leading to a shallowing of Z20. This suggests a strong dynamical rearrangement of the upper equatorial Pacific: warm upper ocean off-equatorial water shifts into the equatorial region.

These changes in the thermocline depth also affect the cross-correlation between T and h (Fig. 4.4). In the historical CMIP5 simulations T and h (Z20) have a very clear out-of phase relation, with a strong positive correlation when h leads T and a roughly equally strong negative correlation when T leads h at about the same lead time of 5–8 months (Fig. 4.4a). This does change significantly in the future RCP8.5 simulations for Z20 estimates. The cross-correlation shifts upwards between the lags 12 to + 8 months, leading to a now significant positive instantaneous (lag = 0) correlation (Fig. 4.4a). It further leads to a change of the peak crosscorrelation at positive lead times, with a shift to smaller lead times and an overall increase in correlation at the peak.

These changes are qualitatively similar in the maxgrad estimates, but are much weaker. A notable difference to the Z20 estimate can be seen in the mean cross-correlation of the

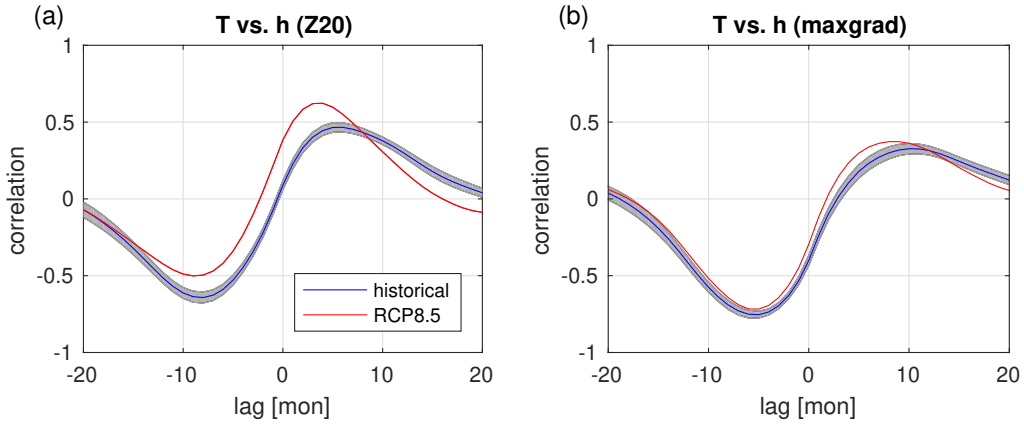

Figure 4.4: The cross-correlation of T vs. h for (a) the Z20 and (b) the maxgrad estimates. The blue lines are the historical ensemble mean values and the grey shaded area mark the standard error for a t-test. The red lines are the RCP8.5 ensemble mean values. Positive lag times indicate the time evolution of h leads T

historical simulations. The maxgrad estimates has a quite significant negative instantaneous (lag = 0) cross-correlation and the cross-correlation peak for negative lead times (T leads h) is much larger than the one for positive lead times. The different characteristics of the thermocline depth estimates as discussed in this subsection indicate that they can potentially affect the ReOsc model parameters and therefore the dynamics of ENSO as estimates by the ReOsc model.We will therefore, in the following analysis section, consider both thermocline estimates.

4.3.2 Changes in statistics of ENSO variability

Before we start analysing changes in the ENSO dynamics, it is instructive to look at changes in the overall statistics of ENSO variability. Similar analysis has been done in previous studies, and we therefore will keep this discussion short to focus more on the dynamical changes.

Figure 4.5 shows statistics of T and h variability. In addition to the standard deviation of T, Z20 and the thermocline depth, an estimate of the spectral power of T and its slope is shown (see Sect. 4.2 for details). The standard deviation of T (Fig. 4.5a) is essentially unchanged in most models. However, some models do show quite significant changes (e.g., models 14 or 5). The power spectrum of T varies from model to model, but the historical and RCP8.5 scenario spectra are nearly identical in ensemble mean, with some reduction in variance on the lower frequencies in the RCP8.5 scenario (Fig. 4.5b). The reduction in decadal variability in the RCP8.5 scenario may be related to the missing external forcings such as volcanoes or variations in aerosols (Maher et al. 2014). The reduction in decadal variance is reflected in slightly, but statistically not significant, flatter slope in the interannual variability (see Fig. 4.5b, c). This suggests no significant change in the periodicity of ENSO is present in the CMIP5 simulations. Some models, however, do show some changes in opposite directions (e.g., models 5 and 22; Fig. 4.5c).

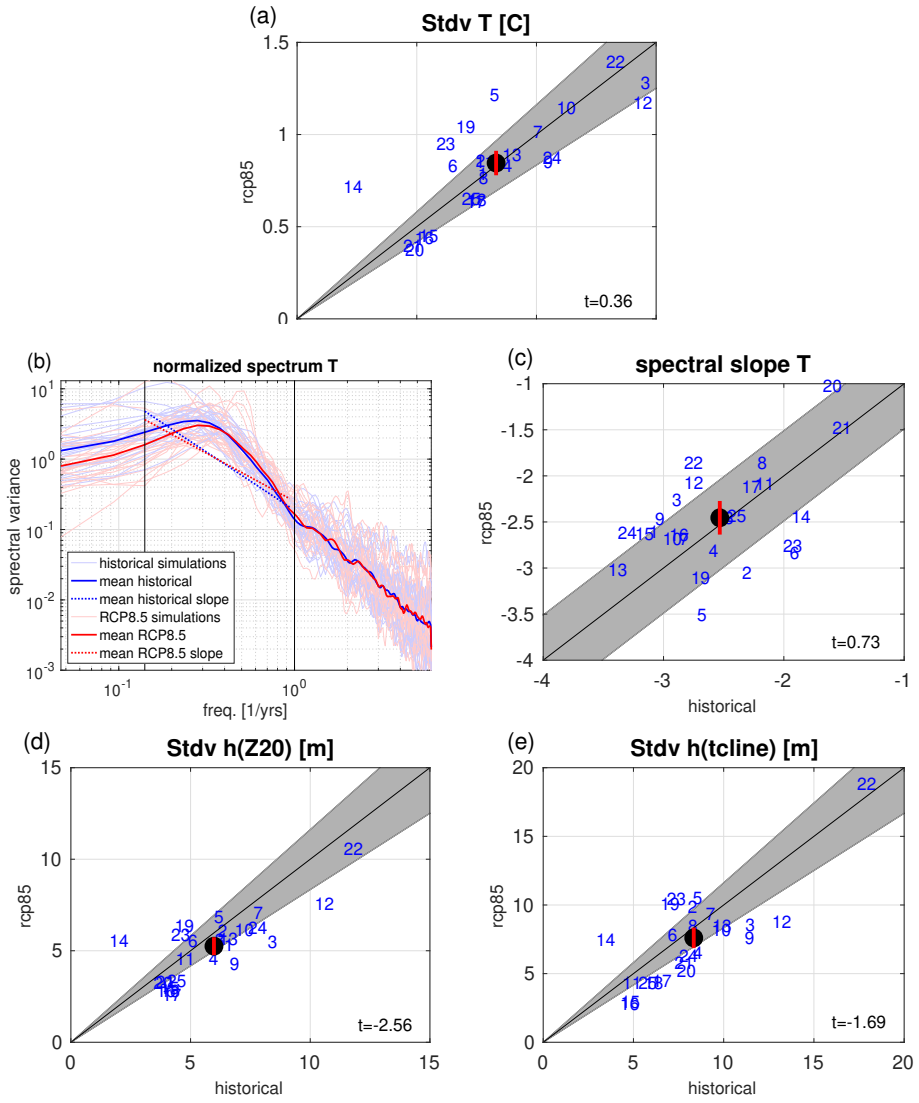

Figure 4.5: Statistics of ENSO variability: (a) stdv(T), (b) power spectral slope of T variability, (c) stdv(h) for the Z20 estimate and (d) stdv(h) for the maxgrad estimate. Each blue number marks a different model (see Table 4.1). Ensemble mean values are marked be the black circle with the red line marking the 95% confidence interval. The shaded area around the one-to-one line mark the mean 95% confidence interval for the individual models (see methods for details). The t-values for the ensemble mean differences are shown in lower left corner of each panel. An absolute t-value $>$ 2.0 passes the 95% confidence interval. Supplemental Table S4.1 lists all model values shown in this figure.

The standard deviation of h slightly decreases for both, the Z20 and the maxgrad estimates. Indeed, the changes in standard deviation of h highly correlate within the CMIP5

ensemble (correlation 0.9 between the Z20 and maxgrad estimates). However, the changes are more significant in the Z20 estimate. Overall, the variability statistics show very little changes, neither in the ensemble mean nor for most individual models. Despite missing changes in the ENSO statistics, we cannot conclude that the dynamics of ENSO have not changed, as we will illustrate in the following subsections.

4.3.3 Changes in the recharge oscillator dynamics

The ReOsc model parameters give a good first guess estimate of the linear ENSO dynamics. Thus, changes in these dynamics provide a good first guess of changes in the linear ENSO dynamics. Figure 4.6 shows the ReOsc model parameters and how they change for both thermocline depth estimates (Z20 and maxgrad). A comparison of the Z20 and maxgrad estimates of the ReOsc model highlights some significant difference in the mean parameters (see Fig. 4.6 left vs. right column).

In the historical simulations, the Z20 estimates of the ReOsc model finds a negative growth rate (damping; a_{11}) for all models, whereas the maxgrad estimates finds values centred around zero. Somewhat the opposite holds for the growth rates of h. It is beyond the scope of this study to further explore these differences in the mean ENSO dynamics resulting from the Z20 and maxgrad estimates. However, future studies should address the implications of such differences for the understanding of ENSO dynamics and the role of the thermocline estimates.

Focusing on the changes in the parameters, we can find a significant decrease in the growth rate of T (a_{11} ; Fig. 4.6a, b). This is more strongly so in the Z20 estimate, but still present in the maxgrad estimates too. In the Z20 estimates it decreases in every single model simulation, which for most models suggest an increase in the damping (negative growth rate) of T by more than a 100%. This is most striking considering that increased

damping of T should reduce stdv(T), but this is not simulated in the CMIP5 simulations (Fig. 4.5a). This apparent mismatch will be discussed further in Sect. 4.2.4, when we

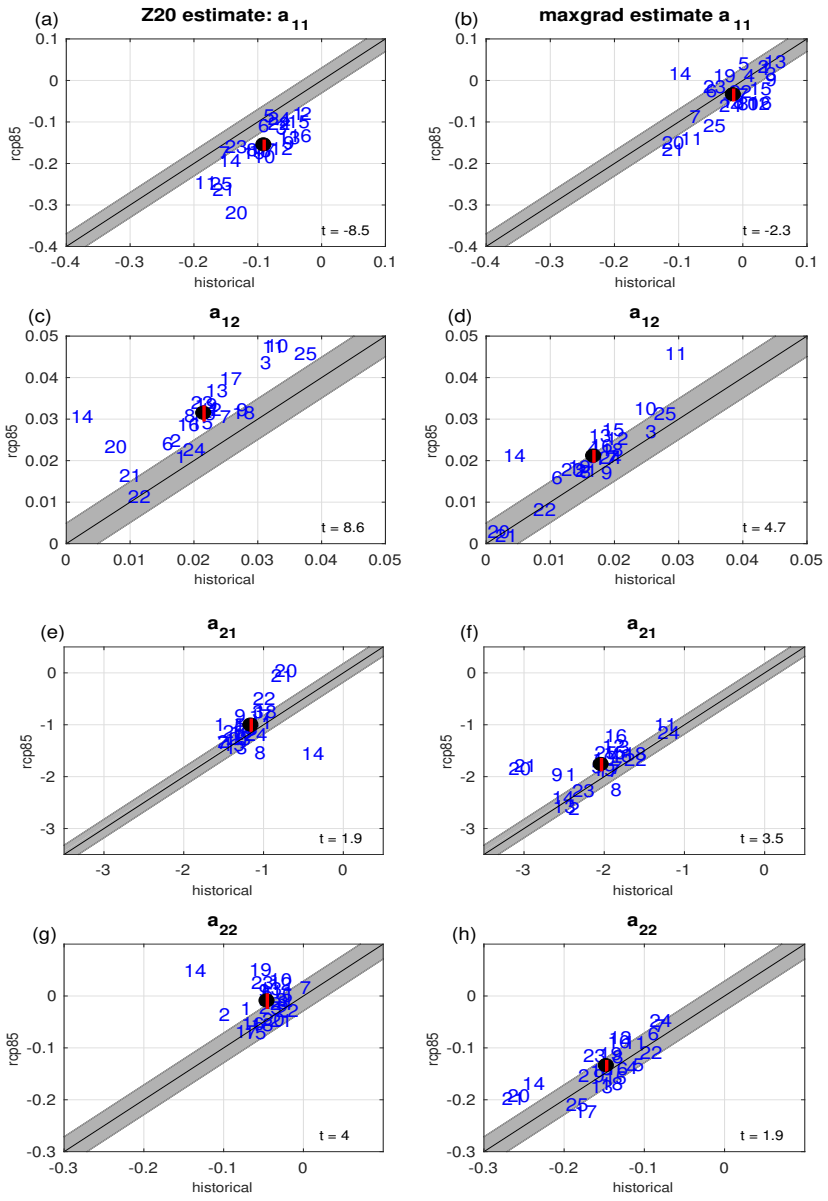

Figure 4.6: ReOsc model parameters: left column for the Z20 estimate and right column for the maxgrad estimates. Growth rate of T (a_{11}; upper row), coupling of T to h (a_{12}; second row from top), coupling of h to T (a_{21}; third row from top) and growth rate of h (a_{22}; lowest row). Details as in Fig. 4.5. Supplemental Table S4.2 and S4.3 lists all model values shown in this figure.

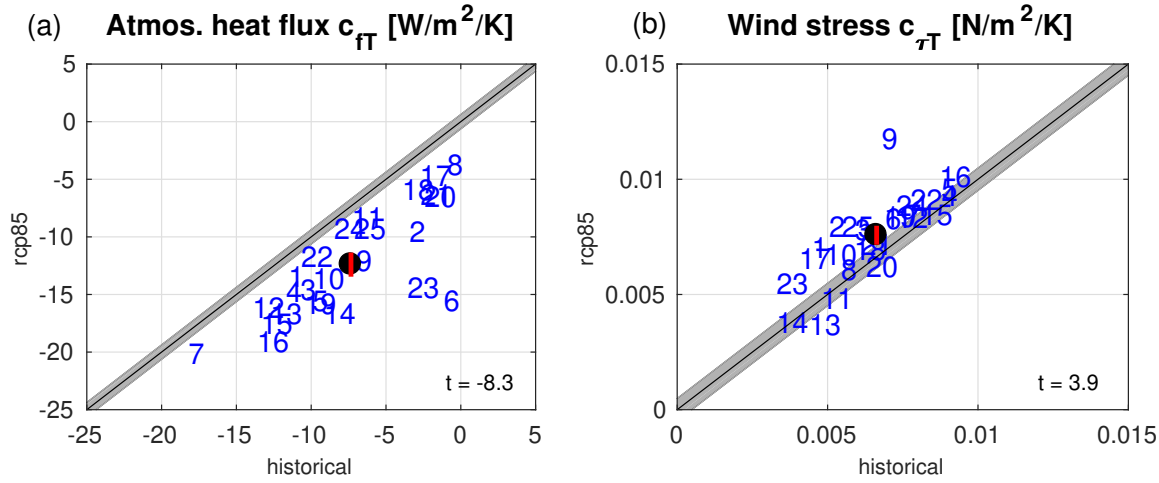

Figure 4.7: (a) Atmospheric net heat flux feedback (C_{fT}) and (b) wind-stress feedback ($C_{\tau T}$). Details as in Fig. 4.5. Supplemental Table S4.4 lists all model values shown in this figure.

discuss the sensitivity of the ENSO statistics to the dynamical changes.

The coupling of T to h (a_{12}; Fig. 4.6c, d) increases significantly in nearly all models and in the ensemble mean. This indicates that T is becoming more sensitive to variations in h. This may be a reflection of the shallower and more pronounced thermocline depth (maxgrad) in the RCP8.5 scenario (Fig. 4.2a). In turn, the coupling of h to T (a_{21}; Fig. 4.6e, f) also increases slightly. However, this change suggests that h is becoming less sensitive to T, since a_{21} is negative. This change is more pronounced in the maxgrad estimate of h. The growth rate of h (a_{22}; Fig. 4.6c, d) increases significantly for the Z20 estimates and slightly, but not statistically significant, for the maxgrad estimates. This increase in growth rate would suggest an increase in stdv(h), but the CMIP5 simulations show a small decrease (Fig. 4.5c, d).

In addition, to the ReOsc model parameters, the strength of the noise forcings can change [T and h in Eqs. (4.1),(4.2)]. However, changes in stdv(T) and stdv(h) are small

and not statistically significant (not shown). The changes in both stdv(T) and stdv(h), even though not strong, are highly correlated (0.9) in the CMIP5 ensemble members between the Z20 and maxgrad estimates. This suggest that changes in the forcing strength of Z20 and the thermocline (maxgrad) behave similarly. The growth rate of T (a_{11}) can be split into a number of atmospheric and ocean processes to further gain insight in the changes of ENSO dynamics [see Eqs. (4.3)-(4.5)]. The atmospheric feedbacks are a combination of the net heat flux feedback (C_{fT}) and the wind-stress (Bjerknes) feedback ($C_{\tau T}$). Both of these feedbacks show significant changes, see Fig. 4.7.

The atmospheric net heat flux feedback becomes more negative in every single model simulation with an average increase in the negative feedback for each model by a factor of 3 (Fig. 4.7). The change in C_{fT} is consistent with the increased overall damping of T (a_{11}). This change in C_{fT} is consistent with the increased thermodynamical damping in the BJ-index analysis of Kim and Jin (2011). The Bjerknes feedback ($C_{\tau T}$) increases slightly ($\sim$ 15%), but still statistically significant. This increase counteracts the increased overall damping of T (a_{11}).

The combined contribution of C_{fT} and $C_{\tau T}$ to the overall damping of T (a_{11}) can be summarized to an atmospheric damping of T (a_{11A}) and the residual contribution to a_{11} as an oceanic feedback [a_{11O} ; see Eq. (4.5)]. Figure 4.8 shows the distribution of a_{11} and a_{11O} in the historical and RCP8.5 scenario simulations. The atmospheric feedbacks (a_{11A}) are positive in all model simulations and become even more so in the RCP8.5 scenario. The increase in a_{11A} illustrates that the slight increase in $C_{\tau T}$ overcompensates the decrease in C_{fT}. Similarly, but with revised sign, the oceanic feedbacks (a_{11O}) are negative in all model simulations and become even more so in the RCP8.5 scenario, which, combined with the changes in a_{11A}, gives a shift in the distribution to the upper left in Fig. 4.8. The overall increased damping of T (a_{11}) is a combination of increased ocean and atmospheric net heat flux damping and counteracting increased positive Bjerknes feedback.

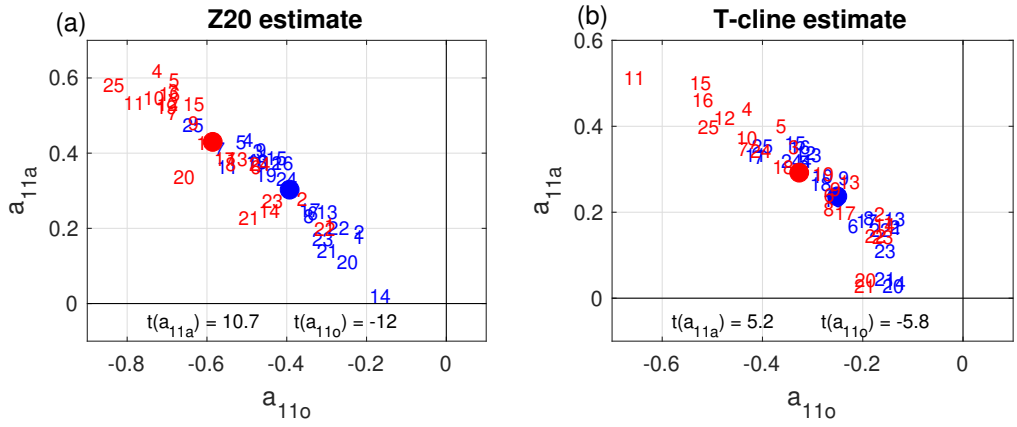

Figure 4.8: Atmospheric (a_{11A}) and oceanic a_{11O} contributions to the growth rate of T for (a) the Z20 and (b) maxgrad estimates. Historical ensemble mean values are marked by the blue circles and RCP8.5 values in red circles. The t-values for the ensemble mean differences are shown in upper right corners of each panel. An absolute t-value > 2.0 passes the 95% confidence interval. Supplemental Table S4.4 lists all model values shown in this figure.

In summary, we found stronger and more significant changes in the ENSO dynamics (Figs. 4.4, 4.6, 4.7, 4.8) than in the statistics of the ENSO variability (Fig. 4.5). All of these dynamical changes are qualitatively similar in the Z20 and maxgrad estimates of h, but in most of them are more pronounced in the Z20 estimates. The qualitative agreement in the Z20 and maxgrad estimates suggests that these results are robust, independent of how the thermocline depth variability (h) is estimated. The significant changes in the dynamics in the absence of equally significant changes in the statistics of the ENSO variability suggests that the changes in the dynamics must have counteracting effects on the ENSO variability. This will be explored further in the following subsection.

4.3.4 Sensitivity of ENSO variability to the changes in the dynamics

We can use the ReOsc model to evaluate how the changes in the ENSO dynamics would affect the ENSO variability (see Sect. 4.2 for details).

Figure 4.9 shows the sensitivities for stdv(T), stdv(h), the slope of the T power spectrum and the cross-correlation between T and h. Here we focus on the Z20 estimates and do not discuss the maxgrad estimates, as they are qualitatively similar.

We can first of all note that the changes in the statistics of the ENSO variability in the CMIP5 simulations are very well captured by the integrations of the ReOsc model with changes in the parameters, for all four statistics of the ENSO variability (compare CMIP5 with all in Fig. 4.9a–c). Thus, the ReOsc model is a good approximation of how these changes in ENSO statistics relate to changes in the ENSO dynamics.

The sensitivity to the individual ReOsc parameters shows some clear counteracting effects for the different ENSO statistics. The stdv(T) has overall very little change, resulting from a compensation of decreased variability due to the increased damping of T (a_{11}) and an increased variability due to the decreased damping of h (a_{22}; Fig. 4.9a). The stdv(h) behaves similarly, but with opposite signs for sensitivities in a_{11} and a_{22}. In addition, the increased coupling of T to h and, to a lesser extent, the decreased coupling of h to T reduces the variability in h (Fig. 4.9a).

The sensitivity of the power spectral slope of T variability is anti-correlated to the sensitivity of stdv(T) (Fig. 4.9b), suggesting that increased T variability goes along with a more strongly negative slope in the power spectrum of T. The latter is, in statistical average, an indication of a more pronounced interannual variability (peak). Subsequently, the decreased damping of h increased the interannual variability (peak), and in turn the increased

damping of T decreased it, combined leading to essentially no change in the power spectral slope. The cross-correlation between T and h is mostly shifting upwards between the lags -10 to + 8 months (Fig. 4.4a). This difference in cross-correlation is well captured by the ReOsc model integration (Fig. 9c). It results from a combination of changes in mostly a_{11} and a_{22}. The increased damping in T essentially reduces the cross-correlation between T and h, since the changes (Fig. 4.9c) are roughly the opposite of the mean cross-correlation

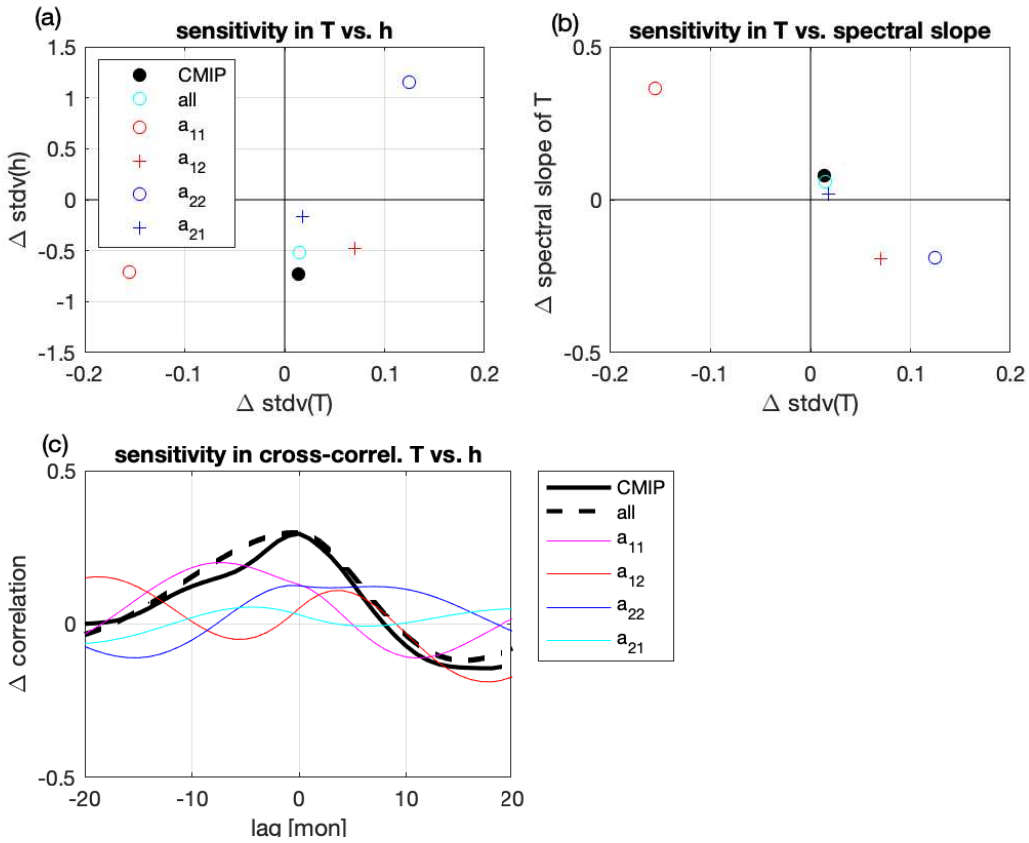

Figure 4.9: Changes in statistics of ENSO variability due to changes in the ReOsc parameters: (a) differences in stdv(T) vs. stdv(h), (b) differences in stdv(T) vs. spectral slope of T and (c) the differences in cross-correlation of T vs. h. CMIP model ensemble mean changes are marked by "CMIP" and changes in the ReOsc model integrations due to changes in one or all parameters are marked by the coloured markers or lines. Positive changes in all statistics imply larger values in the RCP8.5 simulations relative to the historical. Positive lag times indicate the time evolution of h leads T. Supplemental Table S4.1 lists all model values shown in this figure.

(Fig. 4.4a). The decreased damping in h is somewhat opposing the effect of increased damping in T for longer lag/lead times. However, the instantaneous (lag = 0) correlation is increased by both changes in a_{11} and 22. This results in the future RCP8.5 cross-correlation being now much more in-phase, rather than a clear out-of-phase relation.

The changes in the coupling of T to h have a somewhat weaker, but still relevant impact on the cross-correlation. They show a somewhat higher frequency oscillation (red line in Fig. 4.9c) than the overall cross-correlation (Fig. 4.4a) with the same signs for shorter lag/lead times as the overall cross-correlation. This suggests a shift of the peaks of the overall cross-correlation (at about -8 and + 6 months; see Fig. 4.4a) towards shorter lag/lead times (as seen in Fig. 4.4a). The changes in coupling of h to T (a_{21}), in turn, contribute very little to the changes in the cross-correlation.

4.3.5 Sensitivity of ENSO predictability to the changes in the dynamics

The changes of the ENSO dynamics we described above have the potential to affect the predictability of ENSO. The CMIP5 simulations do not give any indication of predictability of ENSO or changes thereof, as the ensemble does not include forecast runs. We can use the ReOsc model integrations to approximate the predictability of ENSO in the CMIP5 simulations based on the model parameters and changes thereof. This, however, should only be considered with some caution, as it does not fully reflect the dynamics and predictability of ENSO in the CMIP models. Thus, it is an outlook to motivate further studies on change in the predictability of ENSO. Again, we will focus on the Z20 estimates and do not discuss the maxgrad estimates, as they are qualitatively similar but weaker.

We conduct a long ReOsc model control integration with the mean model parameters from the CMIP5 historical simulations. We then start forecast runs at 400 different initial

conditions from the control run, each being 5 years apart from each other. In the forecast runs the noise forcings of the ReOsc model is chosen to be different from the control run, creating a new independent realization of the T to h evolution. The forecast skill is evaluated by the correlation between the control and forecast run at different lead times, see Fig. 4.10a. We repeat these simulations with the same noise values, but with the mean model parameters from the CMIP5 RCP8.5 simulations (Fig. 4.10a). The difference in the forecast correlation skill between the historical and the RCP8.5 simulation result purely from the difference in the model parameters. Since the noise forcings are identical in these

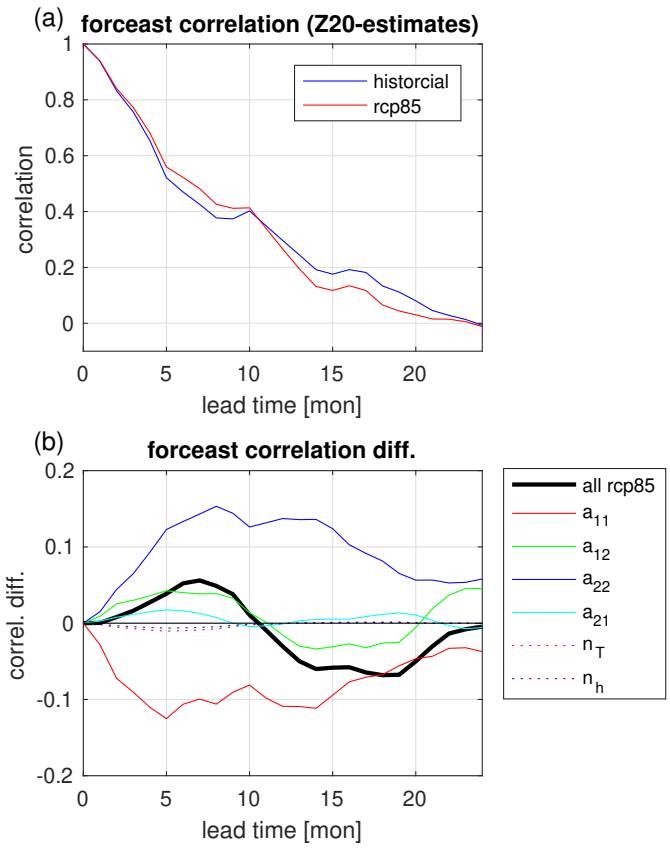

Figure 4.10: (a) Anomaly correlation skill in the ReOsc forecast integrations for historical (blue) and RCP8.5 (red) CMIP ensemble mean model parameters. (b) Changes in the correlation skill in the ReOsc forecast integrations due to changes in the individual ReOsc parameters. See text for details.

runs there are no statistical uncertainties in the differences between the runs resulting from the random noise.

We can first of all note that the correlation skill scores of the CMIP5 historical runs are decreasing relatively fast, if compared to published ENSO forecast skills (Jin et al. 2008). This mostly reflects the limited skill of the ReOsc model, but does not suggest that the CMIP5 have lower ENSO predictability than state-of-the-art forecast models. We therefore have to take these results with a grain of caution, as the true ENSO predictability in the CMIP5 model simulations is likely to be significantly larger than presented in these ReOsc model runs.

The RCP8.5 runs show a clear change in forecast correlation skill relative to the historical run, with larger forecast skill for shorter ($<$ 10 months) lead times and smaller forecast skill for longer lead times (Fig. 4.10a, b). We can evaluate the sensitivity of these changes in the forecast skills to the individual ReOsc model parameters by repeating these simulations with the same noise values, but with the mean model parameters from the CMIP5 historical simulations and a single parameter from the RCP8.5 simulations (Fig. 4.10b).

The changes in the parameters a_{11} and a_{22} have the largest impact on the predictability. The increased damping of T (a_{11}) results into decreased forecast correlation skill on all lead times. In turn, the decreased damping of h (a_{22}) results into increased forecast correlation skill on all lead times, mostly compensating the changes from a_{11} . The changes in the coupling of T to h (a_{12}) most closely follow the overall change in the correlation skill (Fig. 4.10b), suggesting that they contribute significantly to the overall shift in forecast skill.

4.4 Summary and discussion

In this study, we analysed the changes in the linear ReOsc model dynamics, as they are simulated in CMIP5 simulations for the RCP8.5 scenario relative to the historical control

simulation. The primary focus in this study was on the growth rate of T and h, the coupling between the two and the noise forcing driving the ENSO variability. We further focused on the feedbacks controlling the growth rate of T, namely the Bjerknes wind-SST, the atmospheric net heat flux and the residual oceanic feedback. The CMIP5 ensemble shows fairly significant changes in nearly all of these important elements of the ENSO dynamics, despite the fact that the ensemble shows very little changes in the overall ENSO variability strength or periodicity (time scale behaviour of the power spectrum).

The growth rate of T weakens in nearly all simulations, reflecting more strongly damped ENSO dynamics. This results from a combination of changes in the main feedbacks. The atmospheric net heat flux feedbacks become more strongly damped in all simulations, supporting the overall decrease in growth rate of T. However, this is overcompensated by an increased Bjerknes wind-SST in most simulations. The increased Bjerknes feedback leads to an increased growth rate of T, which in combination with the also increased negative net heat flux feedbacks still leads to an overall atmospheric growth rate change that is positive. The residual oceanic feedbacks are becoming more negative and therefore lead to the overall decrease in growth rate of T. Other notable changes in the ENSO dynamics are an increase in the growth rate of h in most simulations, leading to a less damped h variability. The coupling of T to h is also increasing in most simulations, reflecting a T variability that is more strongly influenced by variation in h. In turn, the coupling of h to T is becoming weaker (less negative), indicating that h becomes slightly less sensitive to T. The strength in noise forcings on T or h shows little to no changes.

The ReOsc model framework allows us to estimate the sensitivity of ENSO variability to these dynamical changes. It can also explain why there is essentially no changes in ENSO variability, while there are significant changes in the ENSO dynamics. The strength of the ENSO variability (T) is not changing due to compensating effects of the decrease in growth rate of T that is concurrent with an increase in growth rate of h. Similarly,

the periodicity or time scale behaviour of ENSO is not changing due to compensating effects. The decreases in the growth rates of T alone, would reduce the interannual ENSO oscillations, which would be reflected in an increase in the spectral slope (slope flattens). This is, however, compensated by the increase in the growth rates of h and by the increased coupling of T to h, leading effectively to no changes in spectral slope.

It is difficult to compare these findings in changes of ENSO dynamics with previous studies based on the BJindex stability or SST heat budget analysis, due to the inherently different approaches taken and due to the different set of models analysed (Kim and Jin 2011; Chen et al. 2015). However, we think that there is some agreement between these studies. Reported changes in atmospheric feedbacks (C_{fT} and $C_{\tau T}$) and mean thermocline depth are largely consistent. Compensating effects in different dynamics leading to no overall changes in stability found in Kim and Jin (2011) appears to be consistent with our findings. Further studies should, however, combine the ReOsc modelling approach with the BJ-index stability analysis to gain better understanding of the process controlling the ENSO dynamics in a changing climate.

While the above described dynamical changes may effectively not change the overall ENSO variability statistics, they can potentially affect the predictability of ENSO. The CMIP5 ensemble does not allow to directly evaluate the predictability of ENSO, but the ReOsc model framework can be used to get some approximation of predictability changes in the CMIP5 simulations. The ReOsc model analysis indicates that the predictability of ENSO increases for shorter lead times (< 9 months), but decreases on longer lead times. This of T, and an increased predictability due to the increased growth rate of h. The shift towards higher predictability at shorter lead times and lower predictability longer lead times is linked to the increased coupling strength of T to h. This is also reflected in the changes in cross-correlation between T and h, which shifts to shorter lead times when h leads T. However, we have to keep in mind that we used the ReOsc model as surrogate model of

the CMIP simulations. Further, more in-depth studies using CMIP models are required to address the predictability changes in more detail.

The CMIP5 ensemble also shows significant changes in the mean thermocline depth, which are likely to contribute to the dynamical changes found. Here it does matter whether thermocline depth is estimated by Z20 isotherm or by maxgrad. The latter should be more appropriate for climate change studies, as it is not affected by the mean temperature of the profile, but it does reflect the 'true' thermocline depth. The changes in temperature profile show a remarkable minimum change at the depth that coincides with the historical mean thermocline depth. This suggest a significant dynamical adjustment of the upper equatorial Pacific that is not just a reflection of a transient warming with more warming at the surface and less warming in deeper layers.

It is beyond the scope of this study to fully analysis why we observe the dynamical changes described above. However, some indications may be given from the analysis presented here. The increased negative net heat flux feedback and the increased positive Bjerknes feedback are both likely to be related to the El Niño like mean state changes. At least this would be consistent with some previous findings: first it was shown before that the CMIP5 ensemble has a mean cold tongue bias in the SST and too weak net heat flux and positive Bjerknes feedback (Bellenger et al. 2014; Vijayeta and Dommenget 2018). It was further shown that these two feedbacks are indeed related to the mean sst biases (Lloyd et al. 2012; Bayr et al. 2018). If we further consider that the CMIP5 ensemble has an El Niño like mean state changes in the RCP8.5 scenario (Collins et al. 2010; Liu et al. 2005), then the mean SST in the RCP8.5 scenarios is effectively reducing the CMIP5 ensemble mean state cold tongue biases. Subsequently, the negative net heat flux and the positive Bjerknes feedback are both expected to increase too.

The increase in the growth rate of the thermocline, the reduced overall variability of h

and the changes in the coupling between T and h is likely to partly result from the shallower mean thermocline depth with a sharper temperature gradient in the RCP8.5 scenario. Since thermocline depth is a positive definite number, it is likely that its variability is proportional to its mean value, if no other dynamical changes occur. Thus, a shallower mean h would go along with a reduced variability of h. The sharper temperature profile in the RCP scenario can potentially support less damped variability of h, and therefore supports an increased growth rate. However, the picture is more complex with different behaviours in the mean Z20 and maxgrad estimates, with additional different regional changes and other dynamical changes occurring.

The linear ReOsc model approach presented here, neglects non-linearities in the ENSO dynamics and therefore cannot make any statements on how non-linear ENSO dynamics may change in the future climate change. It further also does not consider regional shifts in ENSO, such as shifts towards more east or central Pacific events. However, non-linear dynamics or regional patterns of ENSO are important aspects of ENSO dynamics and studies have shown that they can potentially change (Yeh et al. 2009; Boucharel et al. 2011; Cai et al. 2015a). It is therefore interesting to see how this ReOsc modelling approach could be used to address such problems. This will be addressed in future studies.

Finally, we have to give some caveat note about this CMIP5 ensemble result.

Although, we find highly significant changes in the dynamics of ENSO in the CMIP5 ensemble this does not necessarily imply that the real world will respond in the same way. The CMIP5 ensemble has substantial common biases in the ENSO dynamics discussed here and in its mean state (Bellenger et al. 2014; Vijayeta and Dommenget 2018). Furthermore, the CMIP5 ensemble does have a significant spread in its mean state, the mean ENSO dynamics and how it responses in the RCP8.5 scenario. Combined, these common model biases and spread undermine the reliability of these results. It also illustrates that ENSO

in a climate system with slightly different mean states and slightly different mean ENSO dynamics, as simulated in individual CMIP5 models, can respond differently to climate change. It thus requires better understanding of the underlying processes and resolving the common model bias issues to gain more confidence about future changes in ENSO dynamics.

Supplementary Table S4.1: Statistical values for all models shown in Figure 4.5. First statistical value in each column is the historical run and second is the RCP8.5 run.

Model	stdv(T)		spec. slope T		stdv(Z20)		stdv(t-cline)	
#1	0.78	0.79	-3.07	-2.6	6.6	5.3	8.5	7.6
#2	0.77	0.86	-2.3	-3.05	6.4	6.1	8.3	9.9
#3	1.46	1.28	-2.88	-2.26	8.5	5.5	11.5	8.6
#4	0.88	0.83	-2.57	-2.81	6	4.6	8.6	6.5
#5	0.83	1.22	-2.67	-3.5	6.2	6.9	8.6	10.6
#6	0.66	0.83	-1.9	-2.83	5.1	5.6	7.2	7.8
#7	1.01	1.02	-2.82	-2.68	7.9	7.1	9.3	9.4
#8	0.78	0.77	-2.17	-1.85	6.3	5.6	8.4	8.5
#9	1.05	0.85	-3.02	-2.46	6.9	4.3	11.5	7.6
#10	1.13	1.15	-2.92	-2.68	7.3	6.2	9.9	8.2
#11	0.79	0.85	-2.15	-2.08	4.8	4.6	5	4.4
#12	1.45	1.18	-2.74	-2.07	10.6	7.6	13.3	8.8
#13	0.9	0.89	-3.37	-3.01	6.6	5.7	10	8.5
#14	0.24	0.72	-1.85	-2.44	2.1	5.6	3.5	7.5
#15	0.55	0.46	-3.15	-2.62	4.2	3	4.9	3
#16	0.54	0.44	-2.86	-2.63	4	2.8	4.8	2.8
#17	0.75	0.64	-2.26	-2.11	4.3	2.6	6.6	4.5
#18	0.76	0.65	-2.49	-2.45	4.2	2.8	6.2	4.4
#19	0.71	1.05	-2.68	-3.1	4.8	6.4	7.1	10.1
#20	0.5	0.38	-1.59	-1.02	3.9	3.3	8	5.2
#21	0.49	0.4	-1.51	-1.48	4	3.4	7.9	5.8
#22	1.33	1.4	-2.74	-1.86	11.8	10.6	18	18.8
#23	0.63	0.95	-1.92	-2.75	4.6	5.9	7.4	10.5
#24	1.07	0.88	-3.29	-2.61	7.8	6.3	8.1	6.3
#25	0.73	0.65	-2.38	-2.43	4.5	3.4	5.9	4.3

Supplementary Table S4.2: ReOsc model parameters for all models shown in Figure 4.6 for the Z20 estimates. First statistical value in each column is the historical run and second is the RCP8.5 run.

Model	a_{11}		a_{12}		a_{21}		a_{22}		stdv(ξ_T)		stdv(ξ_h)	
#1	-0.04	-0.08	0.018	0.021	-1.54	-0.98	-0.071	-0.024	0.22	0.21	1.67	1.63
#2	-0.02	-0.08	0.017	0.025	-1.5	-1.31	-0.098	-0.035	0.25	0.24	1.55	1.57
#3	-0.06	-0.11	0.031	0.044	-1.06	-0.74	-0.027	-0.007	0.34	0.33	1.96	1.66
#4	-0.06	-0.1	0.023	0.033	-1.12	-0.97	-0.045	-0.012	0.22	0.21	1.77	1.4
#5	-0.08	-0.08	0.023	0.031	-1.29	-1	-0.02	0.001	0.2	0.23	1.82	1.74
#6	-0.09	-0.11	0.016	0.024	-1.14	-1.06	-0.045	0.008	0.24	0.23	1.56	1.52
#7	-0.15	-0.17	0.025	0.031	-1.51	-1.34	0.003	0.016	0.36	0.35	2.42	2.24
#8	-0.11	-0.17	0.019	0.031	-1.04	-1.54	-0.025	-0.013	0.27	0.31	1.91	1.65
#9	-0.05	-0.15	0.028	0.032	-1.29	-0.82	-0.048	0.011	0.27	0.28	1.65	1.5
#10	-0.09	-0.18	0.033	0.048	-1.34	-1.27	-0.028	0.032	0.29	0.33	1.96	1.8
#11	-0.18	-0.25	0.033	0.048	-1.02	-0.94	-0.025	0.008	0.32	0.34	1.89	1.75
#12	-0.06	-0.16	0.023	0.032	-1.24	-1.18	-0.028	0.024	0.37	0.37	2.45	2.18
#13	-0.05	-0.14	0.024	0.037	-1.34	-1.43	-0.04	0.015	0.21	0.21	1.63	1.63
#14	-0.14	-0.19	0.003	0.031	-0.37	-1.55	-0.135	0.049	0.12	0.19	1.01	1.71
#15	-0.04	-0.1	0.021	0.029	-1.37	-1.38	-0.06	-0.069	0.14	0.15	1.07	1.09
#16	-0.03	-0.13	0.019	0.029	-1.27	-1.13	-0.062	-0.053	0.14	0.15	1.05	1.18
#17	-0.09	-0.17	0.026	0.04	-1.03	-0.81	-0.071	-0.069	0.3	0.28	1.3	1.19
#18	-0.1	-0.17	0.028	0.032	-0.97	-0.75	-0.051	-0.054	0.28	0.29	1.3	1.25
#19	-0.1	-0.17	0.022	0.034	-1.22	-1.02	-0.053	0.052	0.26	0.29	1.64	1.81
#20	-0.13	-0.32	0.008	0.023	-0.71	0.05	-0.037	-0.044	0.24	0.2	1.05	0.96
#21	-0.15	-0.26	0.01	0.016	-0.76	-0.04	-0.027	-0.047	0.25	0.23	1.04	1.13
#22	-0.07	-0.1	0.012	0.011	-0.98	-0.49	-0.019	-0.028	0.4	0.52	2.82	3.19
#23	-0.13	-0.16	0.021	0.034	-1.29	-1.25	-0.05	0.025	0.26	0.29	1.69	1.73
#24	-0.07	-0.09	0.02	0.023	-1.09	-1.18	-0.027	-0.013	0.25	0.22	2.26	1.9
#25	-0.16	-0.25	0.038	0.046	-1.36	-1.12	-0.041	-0.022	0.29	0.31	1.53	1.45

Supplementary Table S4.3: ReOsc model parameters for all models shown in Figure 4.6 for the maxgrad estimates. First statistical value in each column is the historical run and second is the RCP8.5 run.

Model	a_{11}		a_{12}		a_{21}		a_{22}		stdv(ξ_T)		stdv(ξ_h)	
#1	0.04	0.03	0.017	0.018	-2.41	-1.96	-0.16	-0.144	0.22	0.21	2.06	1.97
#2	0.03	0.03	0.015	0.018	-2.37	-2.62	-0.175	-0.153	0.25	0.24	1.87	2.07
#3	0.04	0.02	0.026	0.027	-1.75	-1.42	-0.145	-0.139	0.34	0.33	2.71	2.38
#4	0.01	0.01	0.017	0.023	-1.86	-1.59	-0.115	-0.138	0.22	0.21	2.25	2.03
#5	0	0.04	0.017	0.021	-2.08	-1.8	-0.107	-0.132	0.2	0.24	2.22	2.4
#6	-0.05	-0.02	0.011	0.016	-1.72	-1.58	-0.088	-0.071	0.24	0.23	1.98	1.77
#7	-0.07	-0.09	0.02	0.021	-1.84	-1.81	-0.08	-0.057	0.36	0.35	2.91	2.71
#8	0	-0.06	0.016	0.017	-1.85	-2.24	-0.132	-0.117	0.27	0.32	2.44	2.42
#9	0.04	0	0.019	0.017	-2.58	-1.96	-0.156	-0.153	0.26	0.28	2.49	1.98
#10	0.01	-0.05	0.025	0.033	-2	-1.65	-0.131	-0.088	0.3	0.32	2.71	2.35
#11	-0.08	-0.14	0.03	0.046	-1.23	-0.99	-0.111	-0.09	0.32	0.33	1.78	1.85
#12	0.03	-0.05	0.021	0.025	-1.88	-1.39	-0.129	-0.079	0.37	0.37	3.22	2.62
#13	0.05	0.05	0.018	0.026	-2.49	-2.57	-0.152	-0.175	0.21	0.21	2.19	2.26
#14	-0.1	0.02	0.005	0.021	-2.51	-2.4	-0.237	-0.168	0.12	0.19	1.59	2.43
#15	0.03	-0.02	0.02	0.028	-1.86	-1.53	-0.135	-0.157	0.14	0.15	1.18	1
#16	0.03	-0.05	0.018	0.024	-1.85	-1.21	-0.134	-0.139	0.14	0.16	1.11	1.17
#17	-0.01	-0.03	0.019	0.021	-1.94	-1.87	-0.172	-0.222	0.3	0.29	1.86	1.36
#18	-0.01	-0.05	0.02	0.023	-1.61	-1.55	-0.14	-0.167	0.28	0.29	1.74	1.32
#19	-0.03	0.01	0.015	0.019	-2	-1.86	-0.141	-0.11	0.26	0.28	2.11	2.25
#20	-0.11	-0.15	0.002	0.003	-3.04	-1.83	-0.256	-0.191	0.25	0.21	3.82	2.43
#21	-0.11	-0.16	0.003	0.002	-2.98	-1.78	-0.263	-0.197	0.25	0.23	3.92	2.83
#22	0	-0.03	0.009	0.008	-1.6	-1.66	-0.091	-0.108	0.39	0.51	4.89	5.7
#23	-0.04	-0.01	0.014	0.018	-2.25	-2.26	-0.161	-0.115	0.26	0.29	2.82	2.96
#24	-0.02	-0.06	0.019	0.021	-1.19	-1.14	-0.079	-0.048	0.25	0.22	2.38	1.96
#25	-0.04	-0.11	0.028	0.031	-1.97	-1.53	-0.183	-0.209	0.29	0.31	2.29	2.21

Supplementary Table S4.4: Reosc feedback and model parameters for all models shown in in Figure 4.7 and 4.8. First statistical value in each column is the historical run and second is the RCP8.5 run.

					Z20 estimate				maxgrad estimate			
Model	c_{fT}		$c_{\tau T}$		a_{11A}		a_{11B}		a_{11A}		a_{11B}	
#1	-10.96	-13.4	0.005	0.007	0.18	0.21	-0.22	-0.29	0.16	0.18	-0.13	-0.15
#2	-2.87	-9.54	0.005	0.008	0.19	0.28	-0.22	-0.36	0.17	0.2	-0.13	-0.16
#3	-10.15	-14.52	0.006	0.008	0.41	0.57	-0.47	-0.68	0.33	0.35	-0.29	-0.34
#4	-11.1	-14.68	0.009	0.009	0.44	0.62	-0.49	-0.72	0.32	0.44	-0.31	-0.43
#5	-9.36	-15.53	0.009	0.01	0.43	0.6	-0.51	-0.68	0.32	0.4	-0.31	-0.36
#6	-0.57	-15.48	0.007	0.008	0.24	0.37	-0.33	-0.47	0.17	0.24	-0.22	-0.26
#7	-17.64	-20.1	0.008	0.008	0.41	0.51	-0.56	-0.68	0.33	0.35	-0.4	-0.44
#8	-0.35	-3.71	0.006	0.006	0.23	0.37	-0.34	-0.54	0.19	0.21	-0.19	-0.27
#9	-6.44	-12.04	0.007	0.012	0.41	0.48	-0.46	-0.63	0.28	0.25	-0.24	-0.25
#10	-8.77	-13.58	0.005	0.007	0.38	0.55	-0.47	-0.73	0.29	0.37	-0.28	-0.43
#11	-6.15	-8.26	0.005	0.005	0.36	0.53	-0.55	-0.78	0.33	0.51	-0.41	-0.65
#12	-12.81	-16.14	0.008	0.008	0.37	0.53	-0.44	-0.7	0.34	0.42	-0.31	-0.47
#13	-11.59	-16.59	0.005	0.004	0.25	0.38	-0.3	-0.52	0.19	0.27	-0.13	-0.22
#14	-8.03	-16.61	0.004	0.004	0.02	0.25	-0.16	-0.44	0.04	0.17	-0.13	-0.15
#15	-12.24	-17.45	0.009	0.008	0.39	0.53	-0.42	-0.63	0.36	0.5	-0.33	-0.52
#16	-12.49	-19.04	0.009	0.01	0.37	0.56	-0.41	-0.69	0.35	0.46	-0.32	-0.52
#17	-1.62	-4.67	0.005	0.007	0.25	0.39	-0.34	-0.55	0.18	0.2	-0.19	-0.23
#18	-2.8	-5.83	0.006	0.007	0.38	0.43	-0.47	-0.6	0.27	0.31	-0.28	-0.36
#19	-9.33	-15.72	0.007	0.008	0.34	0.53	-0.45	-0.7	0.23	0.29	-0.26	-0.28
#20	-1.31	-6.49	0.007	0.006	0.11	0.34	-0.24	-0.65	0.03	0.04	-0.14	-0.19
#21	-1.57	-6.29	0.007	0.007	0.14	0.23	-0.29	-0.49	0.05	0.03	-0.15	-0.19
#22	-9.55	-11.69	0.008	0.009	0.2	0.2	-0.27	-0.3	0.16	0.15	-0.16	-0.17
#23	-2.45	-14.36	0.004	0.005	0.17	0.28	-0.31	-0.43	0.11	0.14	-0.15	-0.16
#24	-7.34	-9.27	0.008	0.009	0.33	0.37	-0.4	-0.46	0.32	0.34	-0.34	-0.4
#25	-6	-9.23	0.006	0.008	0.48	0.58	-0.63	-0.83	0.35	0.4	-0.4	-0.51

Chapter 5

Epilogue

5.1 Summary and Conclusions

This chapter provides a summary of the three previous results chapter which are presented as three subsections below, followed by future research questions that could be addressed using the results of our analysis.

5.1.1 Chapter 2

In this chapter, we introduced the linear recharge oscillator model as a diagnostic tool to evaluate the representation of ENSO dynamics in the CMIP model database. We presented a proof of concept analysis that illustrated that ENSO-statistics and their diversity within the CMIP5 ensemble are well represented with the linear recharge oscillator model diagnostics. Starting with the simple statistics of the variability in T and h we found that the CMIP ensembles mean can be represented reasonably well, but the model ensemble spread is relatively large, suggesting that many models are not consistent with the observed values.

Among the six ReOsc parameters, three parameters showed relatively large spread

within the CMIP ensemble and significant biases. T damping (a_{11}) was ≈ 0 for some models and twice as much damping then the ensemble mean for others. Damping of h (a_{22}) was too strong and too weak stochastic noise forcing on h for most models.

On splitting up the growth rate (damping) of T (a_{11}) into atmospheric and oceanic feedbacks, we found that the atmospheric feedbacks (Bjerknes wind–SST feedback, $C_{\tau T}$, and atmos. heat flux feedback, C_{fT}) are primarily underestimated, which is consistent with previous studies (Lloyd et al. 2009; Bellenger et al. 2014). We found that a_{11} was mostly unbiased while the three individual elements Bjerknes wind-SST feedback, $C_{\tau T}$, atmos. heat flux feedback, CfT, and oceanic damping of T, a_{11O} were strongly underestimated in the CMIP ensemble. We concluded this is due to strong compensating errors in the atmospheric and oceanic components, which is too weak atmospheric growth rates (a_{11A}) compensated with too weak oceanic damping (a_{11O}).

The reason for the compensating effect of atmospheric feedbacks (a_{11A}) and oceanic feedbacks (a_{11O}) in the CMIP ensemble could either be because C andC_{fT} are dynamically linked by the position of the Walker circulation or that the CGCM models are tuned to produce the observed ENSO statistics, which by default tunes errors into the atmospheric and oceanic dynamics that compensate each other nearly ultimately thus producing useful ENSO simulations for the wrong reasons. The combination of errors we find in the CMIP models suggests that the relative importance of ocean dynamics for the simulated ENSO SST variability is underestimated. This results from underestimated oceanic processes, which is consistent with the findings of Kim et al. (2014). We find an under representation of ENSO oceanic processes in the models such as noise forcing for h, ocean coupling of h to T(a_{21O}) and too strong damping of h. We also find that CMIP models underestimate atmospheric damping allowing models to create ENSO variability with realistic amplitudes. Thus, it appears that the relative importance of atmospheric processes in the CMIP models is larger than observed.

We then used the ReOsc model to estimate the sensitivity of the ENSO statistics to each model parameter and arranged the parameters from most to least significant as follows: $C_{\tau T}$,C_{fT}, and a_{11O}, and to a lesser extent in the noise forcing and damping of h. In terms of CMIP ensemble spread, the same parameters contribute to the ENSO statistics uncertainty, but in addition, the growth rate of T (a_{11}) is essential too. Based on the sensitivities, we calculated a normalized root mean square in the model parameters, called a dynamic skill score. All CMIP models exhibit bad bias scores relative to observed uncertainties, which is due to the compensating errors in the dynamics. Leaving out the less essential parameters does not improve the scores. Ranking the CMIP models show no substantial improvement from CMIP3 to CMIP5. The best models in this skill score are the family of models from NCAR/UCAR (CCSM4, CESM1-BGC, CESM1-CAM5, CESM1-FASTCHEM).

Our results have implications for ENSO studies with CGCMs as compensating errors could affect future SST evolution prediction skill of the models. Models producing realistic ENSO statistics with existing compensating errors could potentially affect seasonal, interannual forecasting and future climate change projections. ENSO changes in the future strongly depend on the right sensitivity of the tropical Pacific region to the different forcings (e.g., heat fluxes and winds), and significant systematic biases in the CGCM ENSO dynamics undermines model ensemble mean predictions about future (frequent extreme El-Nino).

5.1.2 Chapter 3

In this chapter, we investigated the accuracy of using the 20°C isotherm (Z20) as a thermocline depth proxy for ENSO studies instead of using the original definition of maximum gradient of temperature (maxgrad). We started our analysis by looking at the differences in the mean Pacific thermocline depths when calculated using Z20 and maxgrad estimates.

Our results indicated that the maxgrad and Z20 estimates have similarity as well as differences while representing the thermocline depths. In some models Z20 estimates is incapable of capturing the effect of ocean warming on thermocline depths. The analysis was further focused on the thermocline depth variability and we found that stdv(h) slightly increases while the mean 4-8 months correlation decreases for maxgrad estimates as opposed to Z20 estimates in both observations and all CMIP5 models. The thermocline depths estimated using maxgrad approach exhibited more variability than Z20 estimates.

For the power spectrum analysis of thermocline depth, we found that for longer timescales the Z20 and maxgrad estimates evolve similarly with maxgrad estimates having higher variance for both observations and individual CMIP5 models. For shorter time scales the maxgrad estimates have greater variance which means they are more noisier and this correlates with the higher standard deviation of maxgrad estimates. We then investigated the correlation between SST and h and found that observed time evolution of h leads that of SST by about 5–6 months (peak of cross-correlation) for the Z20 estimates and about 7-8 months for the maxgrad estimates. The observed SST and h (Z20) correlation have a more pronounced out of phase relationship as compared to the observed SST and h (maxgrad) correlation. This is evident in the historical CMIP5 simulations as well where SST and h (Z20) have a very clear out-of-phase relation, with a strong positive correlation when h leads SST and a roughly equally strong negative correlation when T leads h at about the same lead time of 5–8 months and overall increase in correlation at the peak. This indicated that the ENSO recharge and discharge mechanism is different between the two estimation techniques, which is the fundamental basis of the ReOsc model.

Using the ReOsc model, we next diagnosed ENSO dynamics for both cases and found that Z20 estimates have stronger SST damping, stronger h influence on SST, weaker h damping and weaker SST influence on h in comparison to maxgrad. The differences in the dynamical parameters and the change in the atmospheric and ocean parameter compensa-

tion indicated substantial differences in the ENSO dynamics diagnosis representation for the two h estimation techniques. Furthermore, the larger standard deviation of h for maxgrad also manifests in the SST-h phase relationships with the Z20 estimates being more similar to the theoretical recharge oscillator and the maxgrad SST-h phase diagrams are more asymmetric with SST leading thermocline depths. The main conclusion was that there is substantial differences in the ENSO dynamics representation diagnosis when using the two thermocline estimation techniques, and when using maxgrad estimates it was clear that thermocline may not have that much of a stronger influence on driving SST as suggested by current literature.

5.1.3 Chapter 4

In this chapter, we evaluated the simulated changes in future ENSO dynamics in the framework of the linear ReOsc model dynamics, by analysing the RCP8.5 scenario relative to the historical control simulation. We focused on the growth rate of T and h, the coupling between the two and the noise forcing driving the ENSO variability and feedbacks controlling the growth rate of T (Bjerknes wind-SST, the atmospheric net heat flux and the residual oceanic feedback).

The CMIP5 Ensemble showed very little changes in the overall ENSO variability strength but shows fairly significant changes in nearly all of these important elements of the ENSO dynamics. In all simulations ENSO dynamics is strongly damped due to weakened growth rate of T which in turn is due to changes in the atmospheric feedbacks. In most simulations net heat flux feedback become more strongly damped, increased Bjerknes wind-SST feedback resulting in overall decrease in growth rate of T. Increased negative net heat flux feedbacks still leads to an overall atmospheric growth rate change that is positive.

The residual oceanic feedbacks were becoming more negative and therefore lead to the overall decrease in growth rate of T. Other notable changes in the ENSO dynamics were an increase in the growth rate of h in most simulations, leading to a less damped h variability. The coupling of T to h is also increased in most simulations, reflecting a T variability that is more strongly influenced by variation in h. The coupling of h to T is became weaker (less negative), indicating that h becomes slightly less sensitive to T. The strength in noise forcings on T or h showed little to no changes.

We looked at the sensitivity of ENSO variability to dynamical changes and found no changes in ENSO variability, while there are significant changes in the ENSO dynamics. The strength of the ENSO variability (T) does not change due to compensating effects of the decrease in growth rate of T and increase in growth rate of h. The time scale behaviour of ENSO was found to not change due to compensating effects. The decrease in the growth rate of T reduces the inter-annual ENSO oscillations increasing spectral slope (slope flattens) which in turn is compensated by the increase in the growth rates of h and by the increased coupling of T to h, leading effectively to no changes in spectral slope.

We then analysed predictability changes in the CMIP5 simulations and found that the predictability of ENSO increased for shorter lead times ($<$ 9 months), but decreased on longer lead times. The shift towards higher predictability at shorter lead times and lower predictability at longer lead times is linked to the increased coupling strength of T to h. This is also reflected in the changes in cross-correlation between T and h, which shifted to shorter lead times when h leads T.

The CMIP5 ensemble also showed significant changes in the mean thermocline depth, which are likely to contribute to the dynamical changes found. The increased negative net heat flux feedback and the increased positive Bjerknes feedback are both likely to be related to the El Niño like mean state changes. We showed that CMIP5 ensemble has

a mean cold tongue bias in the SST and too weak net heat flux and positive Bjerknes feedback and these two feedbacks are related to the mean SST biases. Considering CMIP5 ensemble has an El Niño like mean state changes in the RCP8.5 scenario, the mean SST in the RCP8.5 scenarios is effectively reducing the CMIP5 ensemble mean state cold tongue biases. Subsequently, the negative net heat flux and the positive Bjerknes feedback are both expected to increase too. The increase in the growth rate of the thermocline, the reduced overall variability of h and the changes in the coupling between T and h is likely to partly result from the shallower mean thermocline depth with a sharper temperature gradient in the RCP8.5 scenario. Since thermocline depth is a positive definite number, it is likely that its variability is proportional to its mean value, if no other dynamical changes occur. Thus, a shallower mean h would go along with a reduced variability of h. The sharper temperature profile in the RCP8.5 scenario can potentially support less damped variability of h, and therefore supports an increased growth rate. However, the picture is more complex with different behaviours in the mean Z20 and $maxgrad$ estimates, with additional different regional changes and other dynamical changes occurring.

5.2 Future work

The three studies in this thesis have improved understanding of the ENSO dynamics in the framework of the linear ReOsc model and the interplay/compensation between the different atmospheric and oceanic feedback errors. Secondly, we showed that the thermocline depth may not have that much of a stronger influence on driving SST as suggested by current literature when using $maxgrad$ estimates, where $maxgrad$ is defined as the depth of maximum gradient of temperature. Also that the in a changing climate scenario, dynamical changes may not effectively lead to overall ENSO variability, but is likely to affect ENSO predictability.

From the analysis and results presented in Chapter 2,3 and 4 we identify the following research objectives for future work:

1. In Chapter 2 our results show the CGCMs tend to underestimate the oceanic damping of SST. The bias in ocean component of damping parameter reveal errors in the ocean models and further analysis is needed to determine if it is due to excessive upwelling or a shallow mixed layer. We would also like to illustrate physical representation of the "h damping", and reason for overestimation of the parameter in models.

   In Sec. 2.4.3 and Table 2.4 we present some of the interesting and significant inter parameter correlations. Although Wengel et al. (2018) proposed physical interpretations of some correlations and anti correlation, still some significant correlations are unanswered. A detailed analysis of the origin of these co-variations is needed. For example, the T noise parameter is correlated with a_{21} coupling parameter and anti-correlated with the Bjerknes feedback strength. The atmospheric component of SST damping a_{21a} is anti correlated with Bjerknes feedback strength $C_{\tau t}$. One hypothesis for this could be that the "weaker cold tongue" models that appropriately place their deep convection, convective non-linearity, wind coupling, and westerly wind events farther east, also tend to have stronger recharge/discharge dynamics — due to their eastward-shifted and meridionally-wider wind responses to SST, which results in longer Rossby wave delays and a slower delayed negative feedback onto equatorial SST (Capotondi et al. 2006).

   We estimated the ReOsc model noise parameters by multivariate regression, where the residuals were primarily white noise. Further exploration of the residuals of the regression fits to identify the extent to which deterministic non-linearity and/or multiplicative noise are important. The residuals turn out to be critical forcings for the ReOsc (accounting for most of the variance, Fig. 2.4), so it is important to more

thoroughly assess the validity of the white noise assumption.

While using the linear ReOsc model approach presented here, we neglect non-linearities in the ENSO dynamics and therefore cannot make any statements on how non-linear ENSO dynamics may change in the future. Our analysis also does not consider regional shifts in ENSO, such as shifts towards more east or central Pacific events. However, non-linear dynamics or regional patterns of ENSO are important aspects of ENSO dynamics and studies have shown that they can potentially change (Yeh et al. 2009; Boucharel et al. 2011). This is one potential area of future research, to investigate whether the non-linear feedback parameters influence the ENSO dynamics. Nonlinearity can play a particularly crucial role at the onset of the strongest and most impactful El Niño events (Vecchi et al. 2006; Gebbie et al. 2007; Thual et al. 2018), and may also play a key role in the ENSO response to climate change.

For calculating the sensitivities in eq. (2.8) we made a first order linear approximation but the ENSO statistics in the ReOsc model are in general not a linear function of the parameters. We would like to derive the same analytically in terms of simple nonlinear functions.

The main result of Chapter 2 was to highlight existence of compensating atmospheric and oceanic errors, but for future work we intend to look at the physics and pattern biases underlying the identified dynamical biases, and propose initial hypotheses and possible next steps for identifying and addressing the biases.

2. Chapter 3 highlighted a key challenge in conceptual modeling – how to map conceptual large-scale parameters onto real-world features and detailed physical processes. As formulated, the ReOsc seems conceptually better suited to the $maxgrad$ definition of thermocline depth, rather than Z20. The thermocline only coincidentally falls along Z20 for the recent historical observations. The large inter-model spread of

$maxgrad$ and Z20 relationships (Fig. 3.7) is intriguing and it would be interesting to re-examine results of Chapter 2 with $maxgrad$, rather than Z20, and test if we would have qualitatively similar results. Figs. 3.10 and 3.14 actually suggest that $maxgrad$ stratifies the models better than Z20, so there is a chance that using $maxgrad$ could have better identified the model biases and differences.

Post 1999 the predictability of the ENSO has been shown to decrease (Meinen and McPhaden 2000). The Z20 isotherm is still being used as proxy for thermocline depths for ENSO studies. We would like to analyse using both Z20 and $maxgrad$ estimates if the thermocline depth differences have an effect on ENSO predictability. We have shown in our preliminary analysis that both estimates are influenced by seasonality and they differ in the SST - h leadlag correlation patterns. We would also examine the relationship between $maxgrad$ and other more frequently used measures of upper-ocean heat, such as the heat content (vertically-averaged temperature, say over the top 300 m) and warm water volume.

3. In chapter 4 there is much scope for a number of future research objectives. Fig. 4.9 indicates that reduced damping of h (a_{22}) has a huge impact on the projected ENSO amplitude, completely counteracting the increased damping of T (a_{11}). We would be interested in examining the physical processes that lead to this reduced damping of h.

   In Fig. 4.10b we intend to address the physical reasons for the changes in predictability. The shift of predictability toward shorter leads could be due to enhanced zonal-advective and Ekman feedbacks at short leads, and reduced recharge/discharge signals at long leads.

   Section 4.4 presents opportunities to interpret the dynamical changes in terms of the underlying physical processes, and to relate the ReOsc results to those from other

conceptual frameworks. In Chapter 4 we present that projected changes toward a more El Niño-like mean climate would effectively reduce the models biases relative to the historically observed climate, leading to stronger SST-wind coupling and surface heat flux damping. This also implies that the model sensitivity may depend on the model bias, and how near the model (or reality) is to the nonlinear limits of these changes – e.g. to a state with no cold tongue or upwelling at all (like a strong El Niño), or an outcropped east Pacific thermocline (like a strong La Niña), or a very deep equatorial thermocline (as hypothesized for some paleoclimates, and realized in some low-resolution CGCMs). We intend to extend framework of this study to include such nonlinear situations and also investigate if these non-linearities only appear during a particular season or phase of the ENSO cycle.

We also intend to discuss the impacts of model biases on the projected ENSO sensitivities to climate change. For example, most of the models generate historical simulations with an excessive cold tongue, which inhibits convective cloud feedbacks near the equator. This could leave too much room in the future for increases in simulated equatorial convective cloud, resulting in an excessive increase in surface heat flux damping in most models. As a possible emergent constraint for future ENSO changes, it would be interesting to assess whether the models with more-realistic historical simulations (both in terms of background mean state, and ENSO dynamics metrics as described in Chapter 2) project future changes that are significantly different from the less-realistic models.

4. In terms of the use of ReOsc model for ENSO analysis, there is a scope of future work to incorporate metrics developed in this thesis into community frameworks for model evaluation, such as the ENSO metrics package recently developed by Planton et al. (2020).

   The results of the thesis (Chapter 2) illustrate the large biases in feedback parameters

and negligible improvement from CMIP3 to CMIP5 in terms of ENSO representation in CMIP models. The use of the ReOsc model provides an opportunity for modellers to investigate extent of the individual feedback errors and improve their simulations.

References

K. Achuta Rao and K. R. Sperber. Simulation of the El Niño Southern Oscillation: Results from the Coupled Model Intercomposition Project. *Climate Dynamics*, 19(3-4):191–209, 2002. ISSN 24521094. doi: 10.1016/j.adro.2016.02.002.

K. Achuta Rao and K. R. Sperber. ENSO simulation in coupled ocean-atmosphere models: Are the current models better? *Climate Dynamics*, 27 (1):1–15, 2006. ISSN 09307575. doi: 10.1007/s00382-006-0119-7.

R. M. Adams, C.-C. Chen, B. A. McCarl, and R. F. Weiher. The economic consequences of ENSO events for agriculture . *Climate Research*, 13(3): 165–172, 1999. URL https://www.int-res.com/abstracts/cr/v13/n3/p165-172/.

S.-I. An and F.-F. Jin. Nonlinearity and Asymmetry of ENSO*. *Journal of Climate*, 17(12):2399–2412, jun 2004. ISSN 0894-8755. doi: 10.1175/1520-0442(2004)017⟨2399:NAAOE⟩2.0.CO;2. URL http://journals.ametsoc.org/doi/abs/10.1175/1520-0442{%}282004{%}29017{%}3C2399{%}3ANAAOE{%}3E2.0.CO{%}3B2.

R. B. Aronson, W. F. Precht, I. G. Macintyre, and T. J. T. Murdoch. Coral bleach-out in Belize. *Nature*, 405(6782):36, 2000. ISSN 1476-4687. doi: 10.1038/35011132. URL https://doi.org/10.1038/35011132.

M. A. Balmaseda, D. L. T. Anderson, and M. K. Davey. ENSO prediction using a dynamical ocean model coupled to statistical atmospheres, 1994. ISSN 16000870.

D. S. Battisti and A. C. Hirst. Interannual Variability in a Tropical Atmosphere–Ocean Model: Influence of the Basic State, Ocean Geometry and Nonlinearity. *Journal of the Atmospheric Sciences*, 46(12):1687–1712, 1989. ISSN 0022-4928. doi: 10.1175/1520-0469(1989)046⟨1687:IVIATA⟩2.0.CO;2. URL http://journals.ametsoc.org/doi/abs/10.

1175/1520-0469{%}281989{%}29046{%}3C1687{%}3AIVIATA{%}3E2.0.CO{%}3B2.

T. Bayr, D. Dommenget, T. Martin, and S. B. Power. The eastward shift of the Walker Circulation in response to global warming and its relationship to ENSO variability. *Climate Dynamics*, 43(9-10):2747–2763, 2014. ISSN 14320894. doi: 10.1007/s00382-014-2091-y.

T. Bayr, M. Latif, D. Dommenget, C. Wengel, J. Harlaß, and W. Park. Mean-state dependence of ENSO atmospheric feedbacks in climate models. *Climate Dynamics*, 50(9-10):3171–3194, 2018. ISSN 14320894. doi: 10.1007/s00382-017-3799-2.

L. Bejarano and F.-F. Jin. Coexistence of Equatorial Coupled Modes of ENSO*. *Journal of Climate*, 21(12):3051–3067, 06 2008. ISSN 0894-8755. doi: 10.1175/2007JCLI1679.1. URL https://doi.org/10.1175/2007JCLI1679.1.

H. Bellenger, E. Guilyardi, J. Leloup, M. Lengaigne, and J. Vialard. ENSO representation in climate models: From CMIP3 to CMIP5. *Climate Dynamics*, 42(7-8):1999–2018, 2014. ISSN 14320894. doi: 10.1007/s00382-013-1783-z.

J. Bjerknes. Atmospheric Teleconnections from the Equatorial Pacific. *Monthly Weather Review*, 97(3):163–172, 1969. ISSN 0027-0644. doi: 10.1175/1520-0493(1969)097⟨0163:ATFTEP⟩2.3.CO;2. URL http://journals.ametsoc.org/doi/abs/10.1175/1520-0493{%}281969{%}29097{%}3C0163{%}3AATFTEP{%}3E2.3.CO{%}3B2.

J. Boucharel, B. Dewitte, Y. du Penhoat, B. Garel, S.-W. Yeh, and J.-S. Kug. ENSO nonlinearity in a warming climate. *Climate Dynamics*, 37(9):2045–2065, 2011. ISSN 1432-0894. doi: 10.1007/s00382-011-1119-9. URL https://doi.org/10.1007/s00382-011-1119-9.

J. N. Brown and A. V. Fedorov. Mean energy balance in the tropical Pacific Ocean. *Journal of Marine Research*, 66(1):1–23, 2008. ISSN 00222402. doi: 10.1357/002224008784815757. URL http://openurl.ingenta.com/content/xref?genre=article{&}issn=0022-2402{&}volume=66{&}issue=1{&}spage=1.

G. Burgers, F. F. Jin, and G. J. van Oldenborgh. The simplest ENSO recharge oscillator. *Geophysical Research Letters*, 32(13):1–4, 2005. ISSN 00948276. doi: 10.1029/2005GL022951.

W. Cai, M. Lengaigne, S. Borlace, M. Collins, T. Cowan, M. J. McPhaden, A. Timmermann, S. Power, J. Brown, C. Menkes, A. Ngari, E. M. Vincent, and M. J. Widlansky. More extreme swings of the South Pacific convergence zone due to greenhouse warming. *Nature*, 488(7411):365–369, 2012. ISSN 1476-4687. doi: 10.1038/nature11358. URL https://doi.org/10.1038/nature11358.

W. Cai, A. Santoso, G. Wang, S. W. Yeh, S. I. An, K. M. Cobb, M. Collins, E. Guilyardi, F. F. Jin, J. S. Kug, M. Lengaigne, M. J. Mcphaden, K. Takahashi, A. Timmermann, G. Vecchi, M. Watanabe, and L. Wu. ENSO and greenhouse warming, 2015a. ISSN 17586798.

W. Cai, G. Wang, A. Santoso, M. J. McPhaden, L. Wu, F.-F. Jin, A. Timmermann, M. Collins, G. Vecchi, M. Lengaigne, M. H. England, D. Dommenget, K. Takahashi, and E. Guilyardi. Increased frequency of extreme La Niña events under greenhouse warming. *Nature Climate Change*, 5(2): 132–137, 2015b. ISSN 1758-6798. doi: 10.1038/nclimate2492. URL https://doi.org/10.1038/nclimate2492.

A. Capotondi and P. D. Sardeshmukh. Is El Niño really changing? *Geophysical Research Letters*, 44(16):8548–8556, aug 2017. ISSN 0094-8276. doi: 10.1002/2017GL074515. URL https://doi.org/10.1002/2017GL074515.

A. Capotondi, A. Wittenberg, and S. Masina. Spatial and temporal structure of Tropical Pacific interannual variability in 20th century coupled simulations. *Ocean Modelling*, 15(3-4):274–298, 2006. ISSN 14635003. doi: 10.1016/j.ocemod.2006.02.004.

L. Chen, T. Li, and Y. Yu. Causes of Strengthening and Weakening of ENSO Amplitude under Global Warming in Four CMIP5 Models. *Journal of Climate*, 28(8):3250–3274, feb 2015. ISSN 0894-8755. doi: 10.1175/JCLI-D-14-00439.1. URL https://doi.org/10.1175/JCLI-D-14-00439.1.

L. Chen, T. Li, Y. Yu, and S. K. Behera. A possible explanation for the divergent projection of ENSO amplitude change under global warming. *Climate Dynamics*, 49(11-12):3799–3811, 2017. ISSN 14320894. doi: 10.1007/s00382-017-3544-x.

K. Y. Choi, G. A. Vecchi, and A. T. Wittenberg. ENSO transition, duration, and amplitude asymmetries: Role of the nonlinear wind stress coupling in a conceptual model. *Journal of Climate*, 26(23):9462–9476, 2013. ISSN 08948755. doi: 10.1175/JCLI-D-13-00045.1.

M. Collins, S.-I. An, W. Cai, A. Ganachaud, E. Guilyardi, F.-F. Jin, M. Jochum, M. Lengaigne, S. Power, A. Timmermann, G. Vecchi, and A. Wittenberg. The impact of global warming on the tropical Pacific Ocean and El Niño. *Nature Geoscience*, 3(6):391–397, 2010. ISSN 1752-0894. doi: 10.1038/ngeo868. URL http://www.nature.com/doifinder/10.1038/ngeo868.

M. Davey, M. Huddleston, K. Sperber, P. Braconnot, F. Bryan, D. Chen, R. Colman, C. Cooper, U. Cubasch, P. Delecluse, D. DeWitt, L. Fairhead, G. Flato, C. Gordon, T. Hogan, M. Ji, M. Kimoto, A. Kitoh, T. Knutson, M. Latif, H. Le Treut, T. Li, S. Manabe, C. Mechoso, G. Meehl, S. Power, E. Roeckner, L. Terray, A. Vintzileos, R. Voss, B. Wang, W. Washington, I. Yoshikawa, J. Yu, S. Yukimoto, and S. Zebiak. STOIC: a study of coupled model climatology and variability in tropical ocean regions. *Climate Dynamics*, 18(5):403–420, 2002. ISSN 1432-0894. doi: 10.1007/s00382-001-0188-6. URL https://doi.org/10.1007/s00382-001-0188-6.

D. P. Dee, S. M. Uppala, A. J. Simmons, P. Berrisford, P. Poli, S. Kobayashi, U. Andrae, M. A. Balmaseda, G. Balsamo, P. Bauer, P. Bechtold, A. C. Beljaars, L. van de Berg, J. Bidlot, N. Bormann, C. Delsol, R. Dragani, M. Fuentes, A. J. Geer, L. Haimberger, S. B. Healy, H. Hersbach, E. V. Hólm, L. Isaksen, P. Kållberg, M. Köhler, M. Matricardi, A. P. Mcnally, B. M. Monge-Sanz, J. J. Morcrette, B. K. Park, C. Peubey, P. de Rosnay, C. Tavolato, J. N. Thépaut, and F. Vitart. The ERA-Interim reanalysis: Configuration and performance of the data assimilation system. *Quarterly Journal of the Royal Meteorological Society*, 137(656):553–597, 2011. ISSN 00359009. doi: 10.1002/qj.828.

M. Dilley and B. N. Heyman. Enso and disaster: Droughts, floods and el niño/southern oscillation warm events. *Disasters*, 19(3):181–193, 1995. doi: 10.1111/j.1467-7717.1995.tb00338.x. URL https://onlinelibrary.wiley.com/doi/abs/10.1111/j.1467-7717.1995.tb00338.x.

P. N. DiNezio, B. P. Kirtman, A. C. Clement, S.-K. Lee, G. A. Vecchi, and A. Wittenberg. Mean Climate Controls on the Simulated Response of ENSO to Increasing Greenhouse Gases. *Journal of Climate*, 25(21):7399–7420, may 2012. ISSN 0894-8755. doi: 10.1175/JCLI-D-11-00494.1. URL https://doi.org/10.1175/JCLI-D-11-00494.1.

D. Dommenget. The slab ocean El Niño. *Geophysical Research Letters*, 37 (20):n/a–n/a, oct 2010. ISSN 00948276. doi: 10.1029/2010GL044888. URL http://doi.wiley.com/10.1029/2010GL044888.

D. Dommenget, S. Haase, T. Bayr, and C. Frauen. Analysis of the Slab Ocean El Nino atmospheric feedbacks in observed and simulated ENSO dynamics. *Climate Dynamics*, 42(11-12):3187–3205, 2014. ISSN 14320894. doi: 10.1007/s00382-014-2057-0.

M. H. England, S. Mcgregor, P. Spence, G. A. Meehl, A. Timmermann, W. Cai, A. S. Gupta, M. J. Mcphaden, A. Purich, and A. Santoso. Recent intensification of wind-driven circulation in the Pacific and the ongoing warming hiatus. *Nature Climate Change*, 4(3), 2014. ISSN 17586798. doi: 10.1038/nclimate2106.

A. V. Fedorov and S. G. Philander. A stability analysis of tropical ocean-atmosphere interactions: Bridging measurements and theory for El Niño. *Journal of Climate*, 14(14):3086–3101, 2001. ISSN 08948755. doi: 10.1175/1520-0442(2001)014⟨3086:ASAOTO⟩2.0.CO;2.

P. C. Fiedler. Comparison of objective descriptions of the thermocline. *Limnology and Oceanography: Methods*, 8(6):313–325, jun 2010. ISSN 1541-5856. doi: 10.4319/lom.2010.8.313. URL `https://doi.org/10.4319/lom.2010.8.313`.

C. Frauen and D. Dommenget. El Niño and la Niña amplitude asymmetry caused by atmospheric feedbacks. *Geophysical Research Letters*, 37(18):1–6, 2010. ISSN 00948276. doi: 10.1029/2010GL044444.

C. Frauen and D. Dommenget. Influences of the tropical Indian and Atlantic Oceans on the predictability of ENSO. *Geophysical Research Letters*, 39(2): n/a–n/a, jan 2012. ISSN 00948276. doi: 10.1029/2011GL050520. URL `http://doi.wiley.com/10.1029/2011GL050520`.

G. Gebbie, I. Eisenman, A. Wittenberg, and E. Tziperman. Modulation of Westerly Wind Bursts by Sea Surface Temperature: A Semistochastic Feedback for ENSO. *Journal of the Atmospheric Sciences*, 64(9):3281–3295, 09 2007. ISSN 0022-4928. doi: 10.1175/JAS4029.1. URL `https://doi.org/10.1175/JAS4029.1`.

P. W. Glynn and W. H. De Weerdt. Elimination of two reef-building hydrocorals followingthe 1982-83 el niño warming event. *Science*, 253(5015): 69–71, 1991. ISSN 0036-8075. doi: 10.1126/science.253.5015.69. URL `https://science.sciencemag.org/content/253/5015/69`.

F. S. Graham, J. N. Brown, A. T. Wittenberg, and N. J. Holbrook. Reassessing conceptual models of ENSO. *Journal of Climate*, 28(23):9121–9142, 2015. ISSN 08948755. doi: 10.1175/JCLI-D-14-00812.1.

C. Guan and M. J. McPhaden. Ocean Processes Affecting the Twenty-First-Century Shift in ENSO SST Variability. *Journal of Climate*, 29(19):6861–6879, jul 2016. ISSN 0894-8755. doi: 10.1175/JCLI-D-15-0870.1. URL https://doi.org/10.1175/JCLI-D-15-0870.1.

E. Guilyardi. El Niño-mean state - Seasonal cycle interactions in a multi-model ensemble. *Climate Dynamics*, 26(4):329–348, 2006. ISSN 09307575. doi: 10.1007/s00382-005-0084-6.

E. Guilyardi, A. Wittenberg, A. Fedorov, M. Collins, C. Wang, A. Capotondi, G. J. van Oldenborgh, and T. Stockdale. Understanding El Niño in ocean-atmosphere general circulation models: Progress and challenges. *Bulletin of the American Meteorological Society*, 90(3):325–340, 2009. ISSN 00030007. doi: 10.1175/2008BAMS2387.1.

J. W. Hansen, A. W. Hodges, and J. W. Jones. ENSO Influences on Agriculture in the Southeastern United States*. *Journal of Climate*, 11(3):404–411, 03 1998. ISSN 0894-8755. doi: 10.1175/1520-0442(1998)011⟨0404:EIOAIT⟩2.0.CO;2. URL https://doi.org/10.1175/1520-0442(1998)011<0404:EIOAIT>2.0.CO;2.

D. E. Harrison and G. A. Vecchi. El Niño and La Niña-equatorial Pacific thermocline depth and sea surface temperature anomalies, 1986-98. *Geophysical Research Letters*, 28(6):1051–1054, mar 2001. ISSN 00948276. doi: 10.1029/1999GL011307. URL http://doi.wiley.com/10.1029/1999GL011307.

M. F. Jansen, D. Dommenget, and N. Keenlyside. Tropical atmosphere - Ocean interactions in a conceptual framework. *Journal of Climate*, 22(3):550–567, 2009. ISSN 08948755. doi: 10.1175/2008JCLI2243.1.

J. H. Jiang, H. Su, C. Zhai, V. S. Perun, A. Del Genio, L. S. Nazarenko, L. J. Donner, L. Horowitz, C. Seman, J. Cole, A. Gettelman, M. A. Ringer, L. Rotstayn, S. Jeffrey, T. Wu, F. Brient, J. L. Dufresne, H. Kawai, T. Koshiro, M. Watanabe, T. S. Lécuyer, E. M. Volodin, T. Iversen, H. Drange, M. D. Mesquita, W. G. Read, J. W. Waters, B. Tian, J. Teixeira, and G. L. Stephens. Evaluation of cloud and water vapor simulations in CMIP5 climate models Using NASA "A-Train" satellite observations. *Journal of Geophysical Research Atmospheres*, 117(14), 2012. ISSN 01480227. doi: 10.1029/2011JD017237.

E. K. Jin, J. L. Kinter, B. Wang, C.-K. Park, I.-S. Kang, B. P. Kirtman, J.-S. Kug, A. Kumar, J.-J. Luo, J. Schemm, J. Shukla, and T. Yamagata. Current status of ENSO prediction skill in coupled ocean–atmosphere models. *Climate Dynamics*, 31(6):647–664, nov 2008. ISSN 0930-7575. doi: 10.

1007/s00382-008-0397-3. URL http://link.springer.com/10.1007/s00382-008-0397-3.

F.-F. Jin. An Equatorial Ocean Recharge Paradigm for ENSO. Part I: Conceptual Model. *Journal of the Atmospheric Sciences*, 54(7):811–829, apr 1997a. ISSN 0022-4928.

F. F. Jin. An equatorial ocean recharge paradigm for ENSO. Part II: A stripped-down coupled model. *Journal of the Atmospheric Sciences*, 54(7): 830–847, 1997b. ISSN 00224928.

F. F. Jin, S. T. Kim, and L. Bejarano. A coupled-stability index for ENSO. *Geophysical Research Letters*, 33(23):2–5, 2006. ISSN 00948276. doi: 10.1029/2006GL027221.

I.-S. Kang, S.-I. An, and F.-F. Jin. A Systematic Approximation of the SST Anomaly Equation for ENSO., 2001. ISSN 0026-1165. URL http://joi.jlc.jst.go.jp/JST.JSTAGE/jmsj/79.1?from=CrossRef.

W. S. Kessler. Observations of long Rossby waves in the northern tropical Pacific. *Journal of Geophysical Research*, 95(C4):5183–5217, 1990. ISSN 01480227. doi: 10.1029/JC095iC04p05183.

D. Kim, J.-S. Kug, I.-S. Kang, F.-F. Jin, and A. T. Wittenberg. Tropical Pacific impacts of convective momentum transport in the SNU coupled GCM. *Climate Dynamics*, 31(2):213–226, 2008. ISSN 1432-0894. doi: 10.1007/s00382-007-0348-4. URL https://doi.org/10.1007/s00382-007-0348-4.

S. T. Kim and F. F. Jin. An ENSO stability analysis. Part II: Results from the twentieth and twenty-first century simulations of the CMIP3 models. *Climate Dynamics*, 36(7):1609–1627, 2011. ISSN 09307575. doi: 10.1007/s00382-010-0872-5.

S. T. Kim and J. Y. Yu. The two types of ENSO in CMIP5 models. *Geophysical Research Letters*, 39(11):1–6, 2012. ISSN 00948276. doi: 10.1029/2012GL052006.

S. T. Kim, W. Cai, F.-F. Jin, and J.-Y. Yu. ENSO stability in coupled climate models and its association with mean state. *Climate Dynamics*, 42(11): 3313–3321, 2014. ISSN 1432-0894. doi: 10.1007/s00382-013-1833-6. URL https://doi.org/10.1007/s00382-013-1833-6.

G. Kociuba and S. B. Power. Inability of CMIP5 Models to Simulate Recent Strengthening of the Walker Circulation: Implications for Projections. *Journal of Climate*, 28(1):20–35, aug 2014. ISSN 0894-8755.

doi: 10.1175/JCLI-D-13-00752.1. URL https://doi.org/10.1175/JCLI-D-13-00752.1.

T. Kohyama, D. L. Hartmann, and D. S. Battisti. La Niña–like Mean-State Response to Global Warming and Potential Oceanic Roles. *Journal of Climate*, 30(11):4207–4225, feb 2017. ISSN 0894-8755. doi: 10.1175/JCLI-D-16-0441.1. URL https://doi.org/10.1175/JCLI-D-16-0441.1.

K. K. Kumar, B. Rajagopalan, and M. A. Cane. On the weakening relationship between the indian monsoon and enso. *Science*, 284(5423):2156–2159, 1999. ISSN 0036-8075. doi: 10.1126/science.284.5423.2156. URL https://science.sciencemag.org/content/284/5423/2156.

K. K. Kumar, B. Rajagopalan, M. Hoerling, G. Bates, and M. Cane. Unraveling the mystery of indian monsoon failure during el niño. *Science*, 314 (5796):115–119, 2006. ISSN 0036-8075. doi: 10.1126/science.1131152. URL https://science.sciencemag.org/content/314/5796/115.

M. Latif, K. Sperber, J. Arblaster, P. Braconnot, D. Chen, A. Colman, U. Cubasch, C. Cooper, P. Delecluse, D. Dewitt, L. Fairhead, G. Flato, T. Hogan, M. Ji, M. Kimoto, A. Kitoh, T. Knutson, H. Le Treut, T. Li, S. Manabe, O. Marti, C. Mechoso, G. Meehl, S. Power, E. Roeckner, J. Sirven, L. Terray, A. Vintzileos, R. Voß, B. Wang, W. Washington, I. Yoshikawa, J. Yu, and S. Zebiak. ENSIP: The El Niño simulation intercomparison project. *Climate Dynamics*, 18(3-4):255–276, 2001. ISSN 09307575. doi: 10.1007/s003820100174. URL http://www.soest.hawaii.edu/MET/Faculty/bwang/bw/paper/wang91.pdf.

T. Lee and M. J. McPhaden. Increasing intensity of El Niño in the central-equatorial Pacific. *Geophysical Research Letters*, 37(14), jul 2010. ISSN 0094-8276. doi: 10.1029/2010GL044007. URL https://doi.org/10.1029/2010GL044007.

A. F. Levine and M. J. McPhaden. The annual cycle in ENSO growth rate as a cause of the spring predictability barrier. *Geophysical Research Letters*, 42 (12):5034–5041, 2015. ISSN 19448007. doi: 10.1002/2015GL064309.

J. L. Lin. The double-ITCZ problem in IPCC AR4 coupled GCMs: Ocean-atmosphere feedback analysis. *Journal of Climate*, 20(18):4497–4525, 2007. ISSN 08948755. doi: 10.1175/JCLI4272.1.

Z. Liu, S. Vavrus, F. He, N. Wen, and Y. Zhong. Rethinking tropical ocean response to global warming: The enhanced equatorial warming. *Journal of Climate*, 18(22):4684–4700, 2005. ISSN 08948755. doi: 10.1175/JCLI3579.1.

J. Lloyd, E. Guilyardi, H. Weller, and J. Slingo. The role of atmosphere feedbacks during ENSO in the CMIP3 models. *Atmospheric Science Letters*, 10(3):170–176, jul 2009. ISSN 1530-261X. doi: 10.1002/asl.227. URL https://doi.org/10.1002/asl.227.

J. Lloyd, E. Guilyardi, and H. Weller. The Role of Atmosphere Feedbacks during ENSO in the CMIP3 Models. Part III: The Shortwave Flux Feedback. *Journal of Climate*, 25(12):4275–4293, feb 2012. ISSN 0894-8755. doi: 10.1175/JCLI-D-11-00178.1. URL https://doi.org/10.1175/JCLI-D-11-00178.1.

J. F. Lübbecke and M. J. McPhaden. Assessing the Twenty-First-Century Shift in ENSO Variability in Terms of the Bjerknes Stability Index. *Journal of Climate*, 27(7):2577–2587, dec 2013. ISSN 0894-8755. doi: 10.1175/JCLI-D-13-00438.1. URL https://doi.org/10.1175/JCLI-D-13-00438.1.

J. J. Luo, G. Wang, and D. Dommenget. May common model biases reduce CMIP5's ability to simulate the recent Pacific La Niña-like cooling? *Climate Dynamics*, 50(3-4):1335–1351, 2018. ISSN 14320894. doi: 10.1007/s00382-017-3688-8.

Y. Luo, J. Lu, F. Liu, and W. Liu. Understanding the El Niño-like oceanic response in the tropical Pacific to global warming. *Climate Dynamics*, 45 (7-8):1945–1964, 2015. ISSN 14320894. doi: 10.1007/s00382-014-2448-2. URL http://dx.doi.org/10.1007/s00382-014-2448-2.

Y. Luo, J. Lu, F. Liu, and O. Garuba. The Role of Ocean Dynamical Thermostat in Delaying the El Niño–Like Response over the Equatorial Pacific to Climate Warming. *Journal of Climate*, 30(8):2811–2827, oct 2016. ISSN 0894-8755. doi: 10.1175/JCLI-D-16-0454.1. URL https://doi.org/10.1175/JCLI-D-16-0454.1.

N. Maher, A. S. Gupta, and M. H. England. Drivers of decadal hiatus periods in the 20th and 21st centuries. *Geophysical Research Letters*, 41(16): 5978–5986, aug 2014. ISSN 0094-8276. doi: 10.1002/2014GL060527. URL https://doi.org/10.1002/2014GL060527.

S. Manabe, R. J. Stouffer, M. J. Spelman, and K. Bryan. Transient Responses of a Coupled Ocean–Atmosphere Model to Gradual Changes of Atmospheric CO2. Part I. Annual Mean Response. *Journal of Climate*, 4(8):785–818, aug 1991. ISSN 0894-8755. doi: 10.1175/1520-0442(1991)004⟨0785:TROACO⟩2.0.CO;2. URL https://doi.org/10.1175/1520-0442(1991)004{%}3C0785:TROACO{%}3E2.0.COhttp://0.0.0.2.

S. McGregor, A. Timmermann, M. F. Stuecker, M. H. England, M. Merrifield, F.-F. Jin, and Y. Chikamoto. Recent Walker circulation strengthening and Pacific cooling amplified by Atlantic warming. *Nature Climate Change*, 4 (10):888–892, 2014. ISSN 1758-6798. doi: 10.1038/nclimate2330. URL https://doi.org/10.1038/nclimate2330.

M. J. McPhaden. A 21st century shift in the relationship between ENSO SST and warm water volume anomalies. *Geophysical Research Letters*, 39(9), 2012. doi: 10.1029/2012GL051826. URL https://agupubs.onlinelibrary.wiley.com/doi/abs/10.1029/2012GL051826.

M. J. McPhaden, S. E. Zebiak, and M. H. Glantz. ENSO as an integrating concept in earth science. *Science*, 314(5806):1740–1745, 2006. ISSN 00368075. doi: 10.1126/science.1132588.

M. J. McPhaden, T. Lee, and D. McClurg. El Niño and its relationship to changing background conditions in the tropical Pacific Ocean. *Geophysical Research Letters*, 38(15):2–5, 2011. ISSN 00948276. doi: 10.1029/2011GL048275.

G. A. Meehl, C. Tebaldi, H. Teng, and T. C. Peterson. Current and future U.S. weather extremes and El Niño. *Geophysical Research Letters*, 34(20):1–6, 2007. ISSN 00948276. doi: 10.1029/2007GL031027.

C. S. Meinen and M. J. McPhaden. Observations of warm water volume changes in the equatorial Pacific and their relationship to El Nino and La Nina. *Journal of Climate*, 13(20):3551–3559, 2000. ISSN 08948755. doi: 10.1175/1520-0442(2000)013⟨3551:OOWWVC⟩2.0.CO;2. URL http://journals.ametsoc.org/doi/abs/10.1175/1520-0442(2000)013{%}3C3551:OOWWVC{%}3E2.0.CO;2.

G. Meyers. On the Annual Rossby Wave in the Tropical North Pacific Ocean. *Journal of Physical Oceanography*, 9(4):663–674, 1979. ISSN 0022-3670. doi: 10.1175/1520-0485(1979)009⟨0663:otarwi⟩2.0.co;2.

R. H. Moss, J. A. Edmonds, K. A. Hibbard, M. R. Manning, S. K. Rose, D. P. Van Vuuren, T. R. Carter, S. Emori, M. Kainuma, T. Kram, G. A. Meehl, J. F. Mitchell, N. Nakicenovic, K. Riahi, S. J. Smith, R. J. Stouffer, A. M. Thomson, J. P. Weyant, and T. J. Wilbanks. The next generation of scenarios for climate change research and assessment. *Nature*, 463 (7282):747–756, 2010. ISSN 00280836. doi: 10.1038/nature08823. URL http://dx.doi.org/10.1038/nature08823.

J. D. Neelin, D. S. Battisti, A. C. Hirst, F.-F. Jin, Y. Wakata, T. Yamagata, and S. E. Zebiak. ENSO theory. *Journal of Geophysical Research: Oceans*, 103

(C7):14261–14290, 1998. ISSN 01480227. doi: 10.1029/97JC03424. URL http://doi.wiley.com/10.1029/97JC03424.

J. Pedlosky. *A History of Thermocline Theory*, pages 139–152. Springer New York, New York, NY, 2006. ISBN 978-0-387-33152-2. doi: 10.1007/0-387-33152-2_9. URL https://doi.org/10.1007/0-387-33152-2_9.

S. G. H. Philander. The Response of Equatorial Oceans to a Relaxation of the Trade Winds. *Journal of Physical Oceanography*, 11(2): 176–189, feb 1981. ISSN 0022-3670. doi: 10.1175/1520-0485(1981)011⟨0176:TROEOT⟩2.0.CO;2. URL https://doi.org/10.1175/1520-0485(1981)011{%}3C0176:TROEOT{%}3E2.0.COhttp://0.0.0.2.

Y. Y. Planton, E. Guilyardi, A. T. Wittenberg, J. Lee, P. J. Gleckler, T. Bayr, S. McGregor, M. J. McPhaden, S. Power, R. Roehrig, J. Vialard, and A. Voldoire. Evaluating climate models with the CLIVAR 2020 ENSO metrics package. *Bulletin of the American Meteorological Society*, pages 1–57, 09 2020. ISSN 0003-0007. doi: 10.1175/BAMS-D-19-0337.1. URL https://doi.org/10.1175/BAMS-D-19-0337.1.

E. M. Rasmusson and T. H. Carpenter. Variations in Tropical Sea Surface Temperature and Surface Wind Fields Associated with the Southern Oscillation/El Niño, 1982. ISSN 0027-0644. URL http://journals.ametsoc.org/doi/abs/10.1175/1520-0493{%}281982{%}29110{%}3C0354{%}3AVITSST{%}3E2.0.CO{%}3B2.

N. A. Rayner, D. E. Parker, E. B. Horton, C. K. Folland, L. V. Alexander, D. P. Rowell, E. C. Kent, and A. Kaplan. Global analyses of sea surface temperature, sea ice, and night marine air temperature since the late nineteenth century. *Journal of Geophysical Research: Atmospheres*, 108(D14), jul 2003. ISSN 0148-0227. doi: 10.1029/2002JD002670. URL https://doi.org/10.1029/2002JD002670.

T. Reichler and J. Kim. How well do coupled models simulate today's climate? *Bulletin of the American Meteorological Society*, 89(3):303–311, 2008. ISSN 00030007. doi: 10.1175/BAMS-89-3-303.

H.-L. Ren and F.-F. Jin. Recharge Oscillator Mechanisms in Two Types of ENSO. *Journal of Climate*, 26(17):6506–6523, 08 2013. ISSN 0894-8755. doi: 10.1175/JCLI-D-12-00601.1. URL https://doi.org/10.1175/JCLI-D-12-00601.1.

T. Schoennagel, T. T. Veblen, W. H. Romme, J. S. Sibold, and E. R. Cook. Enso and pdo variability affect drought-induced fire occurrence in rocky

mountain subalpine forests. *Ecological Applications*, 15(6):2000–2014, 2005. doi: 10.1890/04-1579. URL https://esajournals.onlinelibrary.wiley.com/doi/abs/10.1890/04-1579.

N. R. Smith. An Improved System for Tropical Ocean Subsurface Temperature Analyses. *Journal of Atmospheric and Oceanic Technology*, 12(4):850–870, aug 1995. ISSN 0739-0572. doi: 10.1175/1520-0426(1995)012⟨0850:AISFTO⟩2.0.CO;2. URL https://doi.org/10.1175/1520-0426(1995)012{%}3C0850:AISFTO{%}3E2.0.COhttp://0.0.0.2.

S. Stevenson, B. Fox-Kemper, M. Jochum, R. Neale, C. Deser, and G. Meehl. Will There Be a Significant Change to El Niño in the Twenty-First Century? *Journal of Climate*, 25(6):2129–2145, 2012. ISSN 0894-8755. doi: 10.1175/JCLI-D-11-00252.1. URL http://journals.ametsoc.org/doi/abs/10.1175/JCLI-D-11-00252.1.

M. J. Suarez and P. S. Schopf. A Delayed Action Oscillator for ENSO. *Journal of the Atmospheric Sciences*, 45(21):3283–3287, nov 1988. ISSN 0022-4928. doi: 10.1175/1520-0469(1988)045⟨3283:ADAOFE⟩2.0.CO;2. URL https://doi.org/10.1175/1520-0469(1988)045{%}3C3283:ADAOFE{%}3E2.0.COhttp://0.0.0.2.

K. E. Taylor, R. J. Stouffer, and G. A. Meehl. An overview of CMIP5 and the experiment design. *Bulletin of the American Meteorological Society*, 93(4):485–498, 2012. ISSN 00030007. doi: 10.1175/BAMS-D-11-00094.1. URL http://cmip-pcmdi.llnl.gov/cmip5/docs/Taylor{_}CMIP5{_}design.pdf.

S. Thual, A. J. Majda, and N. Chen. A Tropical Stochastic Skeleton Model for the MJO, El Niño, and Dynamic Walker Circulation: A Simplified GCM. *Journal of Climate*, 31(22):9261–9282, 10 2018. ISSN 0894-8755. doi: 10.1175/JCLI-D-18-0263.1. URL https://doi.org/10.1175/JCLI-D-18-0263.1.

K. E. Trenberth and T. J. Hoar. El Niño and climate change. *Geophysical Research Letters*, 24(23):3057–3060, 1997. ISSN 00948276. doi: 10.1029/97GL03092.

G. J. Van Oldenborgh, S. Y. Philip, and M. Collins. El Niño in a changing climate: a multi-model study. *Ocean Science*, 1(2):81–95, Oct. 2005. URL https://hal.archives-ouvertes.fr/hal-00298272.

G. A. Vecchi and D. E. Harrison. Tropical Pacific Sea Surface Temperature Anomalies, El Niño, and Equatorial Westerly Wind Events. *Journal of Climate*, 13(11):1814–1830, jun 2000. ISSN

0894-8755. doi: 10.1175/1520-0442(2000)013⟨1814:TPSSTA⟩2.0.CO; 2. URL https://doi.org/10.1175/1520-0442(2000)013{%}3C1814:TPSSTA{%}3E2.0.COhttp://0.0.0.2.

G. A. Vecchi and B. J. Soden. Global Warming and the Weakening of the Tropical Circulation. *Journal of Climate*, 20(17):4316–4340, sep 2007. ISSN 0894-8755. doi: 10.1175/JCLI4258.1. URL https://doi.org/10.1175/JCLI4258.1.

G. A. Vecchi and A. T. Wittenberg. El Niño and our future climate: Where do we stand? *Wiley Interdisciplinary Reviews: Climate Change*, 1(2):260–270, 2010. ISSN 17577799. doi: 10.1002/wcc.33.

G. A. Vecchi, B. J. Soden, A. T. Wittenberg, I. M. Held, A. Leetmaa, and M. J. Harrison. Weakening of tropical Pacific atmospheric circulation due to anthropogenic forcing. *Nature*, 441(1):73–76, 2006. ISSN 14764687. doi: 10.1038/nature04744.

S. M. Vicente-Serrano, J. I. López-Moreno, L. Gimeno, R. Nieto, E. Morán-Tejeda, J. Lorenzo-Lacruz, S. Beguería, and C. Azorin-Molina. A multiscalar global evaluation of the impact of enso on droughts. *Journal of Geophysical Research: Atmospheres*, 116(D20), 2011. doi: 10.1029/2011JD016039. URL https://agupubs.onlinelibrary.wiley.com/doi/abs/10.1029/2011JD016039.

A. Vijayeta and D. Dommenget. An evaluation of ENSO dynamics in CMIP simulations in the framework of the recharge oscillator model. *Climate Dynamics*, 51(5):1753–1771, 2018. ISSN 1432-0894. doi: 10.1007/s00382-017-3981-6. URL https://doi.org/10.1007/s00382-017-3981-6.

E. M. Vincent, M. Lengaigne, C. E. Menkes, N. C. Jourdain, P. Marchesiello, and G. Madec. Interannual variability of the South Pacific Convergence Zone and implications for tropical cyclone genesis. *Climate Dynamics*, 36(9):1881–1896, 2011. ISSN 1432-0894. doi: 10.1007/s00382-009-0716-3. URL https://doi.org/10.1007/s00382-009-0716-3.

B. Wang, R. Wu, and R. Lukas. Annual adjustment of the thermocline in the tropical Pacific Ocean. *Journal of Climate*, 13(3):596–616, 2000. ISSN 08948755. doi: 10.1175/1520-0442(2000)013⟨0596:AAOTTI⟩2.0.CO;2.

W. Wang and M. J. McPhaden. The Surface-Layer Heat Balance in the Equatorial Pacific Ocean. Part II: Interannual Variability*. *Journal of Physical Oceanography*, 30(11):2989–3008, 2000. ISSN 0022-3670. doi: 10.1175/1520-0485(2001)031⟨2989:

TSLHBI⟩2.0.CO;2. URL http://journals.ametsoc.org/doi/abs/10.1175/1520-0485{%}282001{%}29031{%}3C2989{%}3ATSLHBI{%}3E2.0.CO{%}3B2.

C. Wengel, D. Dommenget, M. Latif, T. Bayr, and A. Vijayeta. What Controls ENSO-Amplitude Diversity in Climate Models? *Geophysical Research Letters*, 45(4):1989–1996, feb 2018. ISSN 19448007. doi: 10.1002/2017GL076849. URL http://doi.wiley.com/10.1002/2017GL076849.

A. T. Wittenberg, A. Rosati, T. L. Delworth, G. A. Vecchi, and F. Zeng. ENSO modulation: Is it decadally predictable? *Journal of Climate*, 27(7):2667–2681, 2014. ISSN 08948755. doi: 10.1175/JCLI-D-13-00577.1.

K. Wyrtki. El Niño—The Dynamic Response of the Equatorial Pacific Oceanto Atmospheric Forcing, 1975. ISSN 0022-3670. URL http://journals.ametsoc.org/doi/abs/10.1175/1520-0485{%}281975{%}29005{%}3C0572{%}3AENTDRO{%}3E2.0.CO{%}3B2.

K. Wyrtki. Water displacements in the Pacific and the genesis of El Nino cycles. *Journal of Geophysical Research*, 90(5):7129–7132, 1985. ISSN 0148-0227. doi: 10.1029/JC090iC04p07129.

H. Yang and F. Wang. Revisiting the Thermocline Depth in the Equatorial Pacific. *Journal of Climate*, 22(13):3856–3863, jul 2009. ISSN 0894-8755. doi: 10.1175/2009JCLI2836.1. URL https://doi.org/10.1175/2009JCLI2836.1.

S.-W. Yeh, J.-S. Kug, B. Dewitte, M.-H. Kwon, B. P. Kirtman, and F.-F. Jin. El Niño in a changing climate. *Nature*, 461(7263):511–514, 2009. ISSN 1476-4687. doi: 10.1038/nature08316. URL https://doi.org/10.1038/nature08316.

M. Yoshimori, M. Watanabe, H. Shiogama, A. Oka, A. Abe-Ouchi, R. Ohgaito, and Y. Kamae. A review of progress towards understanding the transient global mean surface temperature response to radiative perturbation. *Progress in Earth and Planetary Science*, 3(1):21, 2016. ISSN 2197-4284. doi: 10.1186/s40645-016-0096-3. URL https://doi.org/10.1186/s40645-016-0096-3.

L. Yu and R. A. Weller. Objectively analyzed air-sea heat fluxes for the global ice- free oceans (1981-2005). *Bulletin of the American Meteorological Society*, 88(4):527–539, 2007. ISSN 00030007. doi: 10.1175/BAMS-88-4-527.

Y. Yu, D. Dommenget, C. Frauen, G. Wang, and S. Wales. ENSO dynamics and diversity resulting from the recharge oscillator interacting with

the slab ocean. *Climate Dynamics*, 46(5):1665–1682, 2016. ISSN 1432-0894. doi: 10.1007/s00382-015-2667-1. URL https://doi.org/10.1007/s00382-015-2667-1.

S. E. Zebiak and M. A. Cane. A Model El Niño–Southern Oscillation. *Monthly Weather Review*, 115(10):2262–2278, oct 1987. ISSN 0027-0644. doi: 10.1175/1520-0493(1987)115⟨2262:AMENO⟩2.0.CO;2. URL https://doi.org/10.1175/1520-0493(1987)115{%}3C2262:AMENO{%}3E2.0.COhttp://0.0.0.2.

H. Zelle and H. Dijkstra. El Nifio and Greenhouse Warming: Results from Ensemble Simulations with the. *Journal of Climate*, 18:4669–4683, 2005.

H. Zelle, G. Appeldoorn, G. Burgers, and G. J. van Oldenborgh. The Relationship between Sea Surface Temperature and Thermocline Depth in the Eastern Equatorial Pacific. *Journal of Physical Oceanography*, 34(3):643–655, mar 2004. ISSN 0022-3670. doi: 10.1175/2523.1. URL http://journals.ametsoc.org/doi/abs/10.1175/2523.1.

Q. Zhang, A. Kumar, Y. Xue, W. Wang, and F. F. Jin. Analysis of the ENSO cycle in the NCEP coupled forecast model. *Journal of Climate*, 20(7):1265–1284, 2007. ISSN 08948755. doi: 10.1175/JCLI4062.1.

W. Zhang and F. F. Jin. Improvements in the CMIP5 simulations of ENSO-SSTA meridional width. *Geophysical Research Letters*, 39(23):1–5, 2012. ISSN 19448007. doi: 10.1029/2012GL053588.

M. Zhao, H. H. Hendon, O. Alves, G. Liu, and G. Wang. Weakened Eastern Pacific El Niño predictability in the early Twenty-First Century. *Journal of Climate*, 29(18):6805–6822, 2016. ISSN 08948755. doi: 10.1175/JCLI-D-15-0876.1. URL https://journals.ametsoc.org/doi/pdf/10.1175/JCLI-D-15-0876.1.

J. Zhu, A. Kumar, and B. Huang. The relationship between thermocline depth and SST anomalies in the eastern equatorial Pacific: Seasonality and decadal variations. *Geophysical Research Letters*, 42(11):4507–4515, 2015. ISSN 19448007. doi: 10.1002/2015GL064220. URL https://agupubs.onlinelibrary.wiley.com/doi/pdf/10.1002/2015GL064220.